NUMERICAL FORMULATIONS FOR ATTAINABLE REGION ANALYSIS

T G SEODIGENG

NUMERICAL FORMULATIONS FOR ATTAINABLE REGION ANALYSIS

TUMISANG GERALD SEODIGENG

A thesis submitted to the Faculty of Engineering and the Built Environment, University of the Witwatersrand, Johannesburg, in the fulfillment of the requirements for the degree of Doctor of Philosophy.

Johannesburg, 2005

DECLARATION

I declare that this thesis is my own unaided work. It is being submitted for the degree of Doctor of Philosophy in the University of the Witwatersrand, Johannesburg. It has not been submitted for any degree or examination in any other university.

Tumisang G. Seodigeng

27 January 2006

ABSTRACT

Attainable Region analysis is a chemical process synthesis technique that enables a design engineer to find process unit configurations that can be used to identify all possible outputs, by considering only the given feed specifications and permitted fundamental processes. The mathematical complexity of the attainable regions theory has so far been a major drawback in the implementation of this powerful technique into standard process design tools. In the past five years researchers focused on developing systematic methods to automate the procedure of identifying the set of all possible outputs termed the Attainable Regions.

This work contributes to the development of systematic numerical formulations for attainable region analysis. By considering combinations of fundamental processes of chemical reaction, bulk mixing and heat transfer, two numerical formulations are proposed as systematic techniques for automation of identifying optimal process units networks using the attainable region analysis. The first formulation named the recursive convex control policy (RCC) algorithm uses the necessary requirement for convexity to approximate optimal combinations of fundamental processes that outline the shape of the boundary of the attainable regions. The recursive convex control policy forms the major content of this work and several case studies including those of industrial significance are used to demonstrate the efficiency of this technique. The ease of application and fast computational run-time are shown by assembling the RCC into a user interfaced computer application contained in a compact disk accompanying this thesis. The RCC algorithm enables identifying solutions for higher dimensional and complex industrial case

studies that were previously perceived impractical to solve.

The second numerical formulation uses singular optimal control techniques to identify optimal combinations of fundamental processes. This formulation also serves as a guarantee that the attainable region analysis conforms to Pontryagin's maximum principle. This was shown by the solutions obtained using the RCC algorithm being consistent with those obtained by singular optimal control techniques.

DEDICATION

In the memory of my late Father, Seeletso and Brother, Moshe.

ACKNOWLEDGEMENTS

I would like to thank my colleague and supervisor Brendon Hausberger for dedicating most of his time into turning this work from an idea to a successful doctorate research. I am also thankful to my supervisors Professors Diane Hildebrandt and David Glasser for giving me this opportunity to work with the most innovative research group, COMPS. I am grateful for their guidance and encouragement to develop me into an independent researcher. I would also like to thank everyone at the COMPS group.

I am grateful to Professor Larry Biegler at the University of Carnegie Mellon for giving the opportunity to visit and work with his group.

I would also like to thank my wife for her consistent support throughout this work, my mother, my brothers and sister for their encouragement and believing in me.

I would like acknowledge the Mellon Mentorship Scheme and the National Research Fund for financial support.

TABLE OF CONTENTS

LIST OF FIGURES

LIST OF TABLES

CHAPTER 1

INTRODUCTION

1.1 Introduction

The procedure of reactor networks synthesis, as a subtask of chemical process synthesis, is concerned with identifying reactor types, layouts and flow configurations as well as key design parameters for given feed conditions and underlying reaction kinetics, that will optimise a specific objective function. This objective function might, for example, relate to the rate of production of a desired product(s). The objective function may include cost effectiveness, product yield and selectivity, and environmental concerns, among others.

The principal aim in reactor network synthesis is to develop a design that constitutes combinations of fundamental processes, flowsheet layouts and operation configurations that can be applied to transform a feed with specified conditions to the intended product(s). The types of fundamental processes concerned are generally reaction, mixing, separation, heating, cooling and compression. Commonly, many designs for attaining the same output are possible but there is generally only one optimal design to satisfy a specific objective.

For a steady state process, reactor network design establishes an optimal process layout with flow interconnections of material and energy between the process units. The unit operations that are considered include types of

reactors, heat transfer equipment and mass transfer equipment. In addition to the specifications for a steady state process listed above, the optimal control sequence and operation can be identified for a dynamic or transient system.

Fundamental processes are essentially necessitated by the primary transformation objective of the process that is being designed. However, it is common that a process can be required to prepare the condition of the available feed. In the case of impure feed, upstream separation may be required. Preheating is commonly necessary in many processes. In some cases, a fundamental process is dictated by preceding processes, an example of this is the separation of a product from by-products due to side reactions.

Each unit operation in the design utilises a respective fundamental process or combinations of fundamental processes. For a system where the fundamental process is reaction, batch and plug flow reactors are possible choices, for example. Distillation columns, membrane separators and flash drums are used for separation processes and heat exchangers for heating and cooling. Reactive distillation columns and membrane reactors will be considered for combinations of reaction and separation. Thus, by considering only permitted fundamental processes, it is possible to synthesise a process network that can be further interpreted as a system of interconnected unit operations with design parameters.

From a different perspective, the essence of reactor network synthesis is to determine the configuration of fundamental processes and/or combinations thereof that will optimise some objective function for the transformation of a given feed to a desired product(s). Key design parameters such as process flows, residence times, temperatures and pressures also need to be specified

for such an optimal operation. The interpretation of these specifications into interconnected unit operations becomes a simple and straightforward task, from which a complete process flowsheet arises. The Attainable Region analysis applies a systematic consideration of all feasible combinations of permitted fundamental processes to obtain a set of all possible product states for a given feed. Equipped with a set of all possible product states, termed the Attainable Region (AR), optimisation of a given objective function can be carried out with ease to obtain the optimal product. A set of interconnected processes used to attain the optimal product is then interpreted as a network of unit operations with flow configurations and key design parameters. Obtaining a set of all possible products that can be realised for a given feed by applying all feasible combinations of all permitted processes can be an exhaustive and mathematically complex exercise. This can limit the use of a potentially powerful process synthesis technique such as Attainable Region analysis to specialists only.

The advent of powerful computers has recently stimulated interest in developing automated process synthesis techniques. These techniques combine complex numerical methods with the power of fast computers to produce tools that can be made available for use by process synthesis engineers to generate optimal unit operations structures and also optimise existing processes.

1.2 Aim of the study

This research focuses on further developing attainable region analysis and formulating numerical methods to ease the complexity surrounding the

application of these methods to the design of optimal reactor networks. Combining these formulations with the increased power of computers, the research proceeds to develop algorithms that automate and speed-up the procedure of reactor network synthesis. These algorithmic tools will enhance the relevance of AR analysis to the chemical process industry. Currently, the AR analysis is limited to only a few feed and product components and fundamental processes due to the unavailability of tools that can handle computational complexities inherent in systems with multiple feed and product components and multiple fundamental processes. In this study we develop tools to remedy these drawbacks by performing tasks listed below:

- Revising the basic ideas governing AR analysis and the construction of ARs.

- Introducing a new systematic method of generating ARs and further formulating this method into an algorithmic tool.

- Demonstrating the robustness of the new algorithmic tool by studying complex systems that were previously considered impossible to solve.

- Showing how the currently known optimisation techniques can be used in AR analysis.

- Applying the newly developed tool to classical optimisation problems to validate outcomes.

- Finally, compiling the new tool into a user friendly computer software package that can be used to solve problems and teach AR analysis.

These topics will be addressed with the aid of study cases ranging from very simple ideal systems to complex well-known industrial ones. As we continue with the study of AR analysis for various process systems, exploring combinations of permitted fundamental processes, extensively intricate networks will ensue including the ones that transcend current understanding.

1.3 Thesis Outline

Chapter 2

Process synthesis literature is reviewed to provide insight on the latest progress in the development on the techniques involved. The evolution of process design is followed from exhaustive hands-on traditional approaches to the sophisticated modern techniques such as computer algorithmic tools and simulation packages. The role played by attainable region analysis in process synthesis is also highlighted with its progression tracked from its origin to the current status. The key points in the AR theory that are relevant to the focus of this thesis are then revised with additional features developed in the course of the research. Emphasis is placed on demonstrating the competence of AR analysis in generating optimal process synthesis solutions for systems of virtually any complexity.

Analytical methods that have been derived by researchers over the years are revised and their application in solving attainable regions problems is demonstrated. The key issue emphasised in this chapter is the need for

systematic techniques to automate the application of AR analysis to solving process synthesis problems by taking advantage of the power of computers.

However, this chapter does not conclude the literature survey for the entire thesis as every chapter begins with literature review specific to its focus of study.

Chapter 3

This chapter starts by demonstrating how analytical methods can be used to identify optimal process configurations by use of a simple ideal case study. The objective of the demonstration is to show that even for a simple ideal case study; the analytical methods can develop into a very intricate algebraic exercise. Once again the need for systematic algorithmic computer techniques to identify attainable regions is highlighted.

The second section reviews the literature specific to the previous development of systematic tools for AR analysis to date. The limitations and the need for improvement of these tools are also detailed. These limitations include long computational run-times and the incapability to handle higher dimensional problems.

The third section proposes a new robust and easy apply technique. The theory that supports the foundation of this new technique is revised with mathematical definitions. The recursive convex control policy (RCC) technique is then introduced by detailing its approach to solving AR problems. The first application of the RCC algorithm is demonstrated with the use of a simple case study that has previously been solved with analytical

methods. The solution obtained is shown to be spot-on with that obtained using analytical formulations. The easy plug and play solution procedure is acknowledged without the need to carry out any algebraic calculations prior to implementing the algorithm. Clear cut advancement to a four-dimensional case study is demonstrated and the results are proved to conform to the necessary conditions of optimality as required by the analytical methods derived from AR theory. Visualisation of a four-dimensional candidate AR is demonstrated using a number of lower dimensional projections. An objective function is optimised to illustrate how an optimum point that lie on the boundary of the four-dimensional AR can appear be in the interior when projected in lower dimensional space.

In conclusion, emphasis is placed on the capability of the RCC algorithm to solve higher dimensional problems that previously could only be speculated on.

Chapter 4

In this chapter the RCC algorithm is packaged as a complete AR analysis application and teaching tool with an easy to use graphic interface. User-manual style is adopted to describe the features of the user interfaced tool. The package uses a built-in theoretical example that allows the user to change parameters and identify candidate attainable regions at the click of a button. This software package is included in a compact disk attached to this thesis.

Chapter 5

The robustness of the RCC algorithm is demonstrated by application to identifying candidate attainable regions (AR^{C}s) for industrial case studies. This is achieved by solving a generic model for first order exothermic reversible reactions that has previously been studied using analytical methods. This case study considers processes of reaction, mixing and heat transfer.

In the second example the RCC algorithm is used to identify an optimal process configuration for the industrially important ammonia synthesis via attainable regions analysis. This case study has also been studied using the previously developed automated AR techniques.

Chapter 6

The optimal reactor configuration for a more complex industrial process of methanol synthesis is identified via attainable region analysis. The methanol synthesis reaction scheme and kinetics are mathematically complex and it would be impractical to attempt to identify candidate attainable regions (AR^{C}s) from analytical formulations. The geometric guidelines that have traditionally been used to identify optimal reactor networks for exothermic reversible reactions do not hold for the methanol process as more than one reaction is involved.

The RCC algorithm is applied to solve candidate attainable regions for methanol synthesis and further interpreted in terms of reactor networks with process parameters.

Chapter 7

In this chapter, classical optimisation techniques are used to identify optimal combinations of processes that outline the shape of the attainable regions. In this section, attainable regions problems are formulated as singular optimal control problems that can be solved using techniques that are based on traditional optimisation theory such as Pontryagin's maximum principle.

The classical optimisation technique is acknowledged as one of the systematic tools that can be used to automate the construction of candidate attainable regions. The water-gas shift reaction is used as an industrial case study and the results obtained using singular optimal control techniques are proven to be consistent with solutions from other automated techniques.

In conclusion emphasis is placed on demonstrating that the attainable region analysis conforms to the necessary condition of optimality as required by Pontryagin's maximum principle. This is demonstrated by the results obtained from both methods being consistent with one another.

Chapter 8

The RCC technique is applied to solve unsteady state optimisation problems that have traditionally being solved by methods based on Pontryagin's maximum principle. The main objective of the chapter is not to accurately compute the solution profiles for optimisation problems, but to indicate that the control sequence and switching times can be quickly established using the RCC algorithm.

Chapter 9

This chapter concludes the thesis by summarising the conclusions of all chapters. The contribution of this thesis to knowledge is stated and the relevance of the thesis title is verified by confirming that the objectives have been achieved. Possible areas of future research that are consequent to this study are also proposed.

CHAPTER 2

ATTAINABLE REGION ANALYSIS: BACKGROUND LITERATURE AND THEORY

2.1 Introduction

In this chapter we review the literature and theory of attainable regions relevant to the focus area of this research. We start with an introductory summary and some definitions, followed by a review of research literature in the field which is covered in the next section. The theory pertinent to this study is then presented in the third section.

As defined by Horn (1964) and subsequent researchers; Glasser *et al.*, (1987), Hildebrandt *et al.*, (1990) Glasser *et al.*, (1992) and Feinberg and Hildebrandt (1997), the Attainable Region (AR) is a set of all possible outcome states that can be realised from all or any feasible combination of all permitted fundamental processes for a given input, subject to specified constraints. The boundary of the AR sets limits to the achievable states and it is therefore of special interest as it is where the optimal operating policies are usually located (Horn 1964). The boundary of the attainable region is characterised by certain necessary conditions that ensure that there are no possible extensions pertaining to these known necessary conditions (Feinberg and Hildebrandt, 1997). It should be emphasised that there are no sufficiency conditions to guarantee that the nominated region contains all possible outcomes from all possible combinations of all of the permitted fundamental processes and that no possibilities have been excluded (Feinberg and Hildebrandt, 1997). In the light of this indeterminacy, a region that

satisfies all the known necessary conditions is termed the Candidate Attainable Regions (AR^C).

The Attainable Region analysis method can be used to identify optimal reactor types, flow configurations and key design parameters which will optimise the objective function.

2.2 Background Literature

The process synthesis procedure involves identifying optimum process specifications for a given system. The traditional methods of process synthesis were based on heuristics that are generally derived from years of practical experience (Douglas, 1985). These traditional methods use well understood behaviours of simple systems to explain higher level complex systems which are generally difficult to simplify. To design a process using these traditional methods, experts in the field propose a large number of flowsheets based on their experience. These flowsheets are then entered into a decision making procedure as potential candidates. The heuristics handle the complexity of problems by multilevel decomposition, thus, identifying promising candidate processes while eliminating unpromising ones in a hierarchical decision making procedure (Douglas, 1985). This process often results in heuristics contradicting each other as indicated by Douglas, (1985) and later Shah and Kokossis (1997).

To overcome the contradictory nature of heuristics, Shah and Kokossis (1997) proposed an idea of conceptual programming for a reactor-separator system. The authors used shortcut methods to identify possible designs, which were followed up with a mathematical program to evaluate the trade-offs between the processes.

Another process synthesis technique based on mathematical programming is the superstructure optimisation method (Kokossis and Floudas, 1990, 1991, 1994). A superstructure is a complex generalised process that comprises a number of processing units connected together by a large number of interlinking streams. By eliminating various processing units and streams, a large number of alternative process layouts can be obtained from the superstructure optimisation. A superstructure optimisation problem can be formulated as a mixed integer non-linear programming (MINLP) problem. Integer variables are used to signify the presence or absence of processing units or streams while non-linear variables are used for controls such as temperature, pressure, reactor volumes and stream flowrates. The disadvantages of this technique include the fact that it relies on the assumption that the superstructure is sufficiently general to include the optimum process layout, although that may not be the case and cannot be proven in advance.

Papalexandri and Pistikopoulos (1994, 1996) proposed an alternative method to superstructure optimisation. The structure in this case was more generalised and consisted of mass exchanger and heat exchanger modules instead of specific processing units as in the superstructure. The authors also included complete connectivity by ensuring that the feed to any particular module can be a combination of products of all modules and system feeds. Combinations of these modules were used to represent known complex structure such as distillation columns. These combinations could also result in novel processing units, but, could however not represent nor distinguish between reaction and mass transfer.

The concept of representing all possible states that can be reached by a system of reactions was first proposed by Horn (1964) four decades ago. Horn (1964) argued that the objective variables associated with a chemical reactor, formed a space

whose components can be divided into attainable and non-attainable regions. In particular, Horn described the attainable region as the set of all possible outcome states that can be realised in a reactor system. He further suggested that the optimal operating policies would generally correspond to the boundary of the attainable region. Without stating any general technique for determining the attainable region boundary, Horn pointed out a number of its important characteristics. These characteristics stated that the attainable region would not necessarily include all stoichiometrically possible compositions as it would be restricted to sets of compositions that can be realised in all possible reactor configurations.

More than two decades after Horn proposed the concept of Attainable Regions, Glasser *et al.* (1987) and Hildebrandt (1989) suggested a general technique for determining the boundary of the AR for isothermal reactor systems with constant density.   Their method represented the processes of reaction and mixing geometrically as vectors. Working from a graphical basis and using a number of examples, Hildebrandt (1989) derived a set of necessary conditions arising from geometric interpretations of the process vectors which must be satisfied by any AR[C].

Hildebrandt *et al.* (1990) further developed somewhat more general geometric techniques for finding ARs. In this case the systems were no longer restricted to isothermal or constant density. A more sophisticated contribution on these geometric techniques was made by Glasser *et al.* (1992). It was only then that clear conjectures about optimal process combinations were asserted. Though at a very intuitive level, they suggested geometric principles governing the occurrence of the optimal trajectories for combination of reaction and mixing on the AR boundary. This optimal structure, termed the differential side-stream reactor

(DSR), represents a reactor in which reaction and mixing occur simultaneously in a controlled ratio (Glasser *et al.*, 1992). It is practically possible to realise this reactor as a plug flow reactor (PFR) with mixing of fresh feed material along its length.

Love (1995) formalised the mathematical ideas governing the properties of the AR boundary in three dimensions. Godorr (1998) presented a set of application examples where the attainable regions method was used to solve chemical reactor optimisation problems. Nicol (1998) extended the AR technique to solve problems with heat transfer and also attempted to address four dimensional problems. A more general study was done by McGregor (1998) by applying attainable regions analysis to systems with reaction and mass transfer. McGregor further outlined guidelines that could be used as a systematic procedure for finding AR^Cs.

Feinberg and Hildebrandt (1997) presented a rigorous and more universal set of proofs of geometric principles of the AR boundary for reaction and mixing. In particular, the necessary conditions for the AR boundary were formally detailed and proved. A powerful result of this work, although not explicitly stated, was that optimal combinations of permitted fundamental processes provide access to regions where single processes operate on the boundary of the AR. This result is of high importance as it suggests that, for a given system, the AR^C can primarily be identified by solving optimal combinations of permitted fundamental processes. Feinberg and Hildebrandt (1997) also introduced the Complement Principle, which is a general theory of the overall mass balance that can be applied to any reactor system. This principle was instrumental in geometrically proving the completeness of the AR^C and it was not clear if it could be used beyond that.

Feinberg (2000a) derived, from the optimal geometric control ideas, the analytical equations governing the optimal control policies for trajectories of combinations of reaction and mixing. These optimal trajectories were interpreted as differential side-stream reactors (DSRs) as defined by Glasser *et al.* (1992). Feinberg demonstrated how these optimal trajectories served as precursors from which plug flow reactor curves and mixing surfaces emanated, providing final access to the boundary of the attainable regions. The analytical formulations for optimal process combinations were derived for processes of reaction and mixing. There were no stated dimensional limitations of these formulations as there were illustrations for three to six dimensions, to claim dimensional generality.

In a third paper, Feinberg (2000b) communicated special analytical equations that the continuous flow stirred tank reactors (CFSTRs) should conform to in order to occur on the attainable region boundary. These special reactors were called critical CFSTRs. Once again these were derived for a class of steady state isothermal designs involving only reaction and mixing, and the derivations showed dimensional generality. However, these analytical equations required algebraically intensive derivations resulting in complex mathematical expressions (Feinberg 2000a &b).

2.3 Background Theory

The theory of the attainable regions has been progressively assembled over the years. The most recent is the work of Feinberg and Hildebrandt (1997) and the subsequent articles by Feinberg (2000 a & b).

2.3.1 The Necessary Conditions

A candidate attainable region (AR^C) should satisfy a set of necessary conditions as detailed below, (Feinberg and Hildebrandt, 1997):

1. The AR should include all defined input states.

    The AR by definition encompasses all possible output states. Any input to the system is a possible output if neither process nor combinations thereof are applied to it.

2. No permitted fundamental process vectors on the boundary of the AR are allowed to extend outside of the AR unless the operation of such a process beyond the boundary results in the violation of the stated system constraints.

(a)   (b)
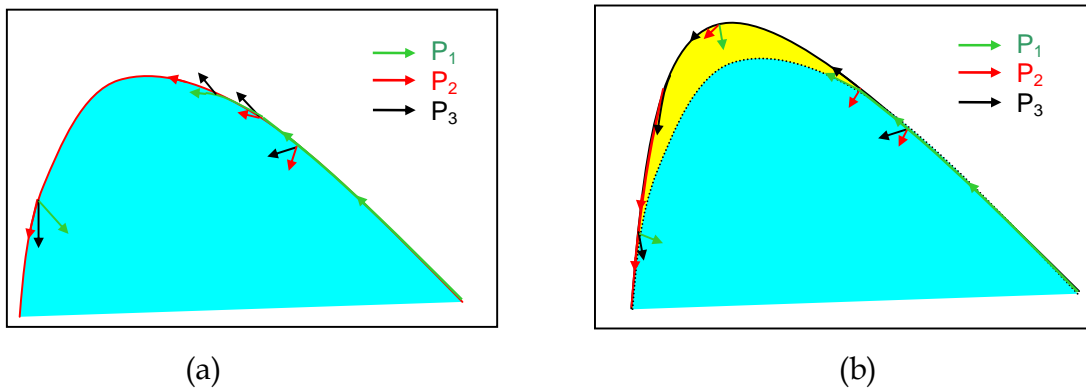
Figure 2.1:   *Illustration of boundary extension via a process vector*
pointing outwards the candidate region

To illustrate this we consider the boundary of the candidate AR shown in Figure 2.1, where processes P_1, P_2 and P_3 are permitted fundamental processes. If a point existed on the AR boundary such that the vector

describing process P_3 points out of the region (Figure 2.1 a), the existing region can be extended further by applying P_3 (Figure 2.1 b). But if the application of P_3 results in exceeding the maximum constraints placed on the system, such process cannot be undertaken due to the resulting constraint violation.

3. For systems where the variables of the construction space obey linear mixing and where mixing is also a permitted fundamental process, the AR should be convex.

<div align="center">(a)   (b)</div>
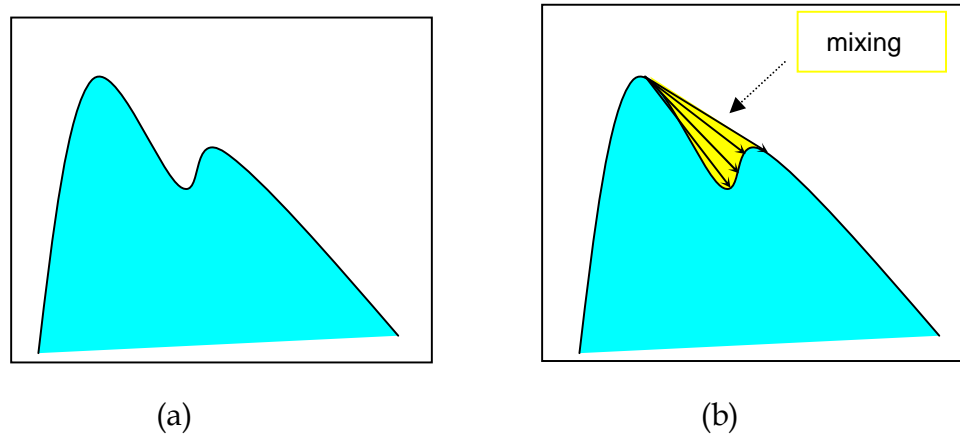
Figure 2.2:   Illustration of filling the concavities on the candidate AR boundary with mixing

This condition is a direct result of the second condition. Any concavities on the boundary (Figure 2.2 a), will result in a manifold of points from which a set of mixing vectors will emanate and to all other points on the manifold, thus filling the concavity (Figure 2.2 b).

4. No fundamental process vectors in the constrained complement of the AR boundary may intersect the AR boundary itself when negatively extrapolated.

To illustrate this we will restrict our system to consider fundamental processes of reaction and mixing only. The constrained complement of the AR is the non-attainable region and is bounded by the operational constraints. If there are such negative extensions of vectors that intersect the AR boundary, those vectors by combination with mixing could represent a point of CFSTR operation. This condition constrains the set of vectors that may be present in any steady state unit operations for systems permitting only processes of reaction and mixing.

In the absence of a sufficiency condition, the above-stated necessary conditions serve as guidelines for testing AR^cs for completeness, although it cannot be exhaustively demonstrated that regions have no possible extensions. As already defined, a region that satisfies all the necessary conditions is termed the candidate attainable region (AR^c).

2.3.2   Elements of Attainable Region Analysis

In this section we review the traditional guidelines of the AR technique. These were first detailed by Hildebrandt (1989) and later appeared in a series of publications with minor amendments (Godorr, 1998; Nicol, 1998). The most elaborate correspondence detailing these guidelines was made by McGregor (1998).

We start with the problem statement describing *the system* with its physical and mathematical descriptions. All input states, permitted fundamental processes, system constraints and objective functions are stated in the problem statement. The aim is to apply attainable regions analysis to obtain all possible outcome states in order to later find process specifications that optimise the given objective.

I. *Fundamental Processes*

The permitted fundamental processes will generally be specified in the problem statement as physical phenomena that can be applied to effect a change in the state of the system input(s). These processes can include, for reactor network synthesis; reaction, mixing, separation, heating and cooling as well as compression and decompression among others.

II. *Choice of State Variables*

The state variables are chosen to adequately describe all permitted fundamental processes and the system objective functions. Typical state variables include the system reactants and products concentrations, reaction conversions, partial pressures and temperatures. State variables that arise from the objective functions may be cost variables that are in most cases some functions of reaction residence time. It is often at this point where the geometry of the AR is determined. The number of variables that fully describes the system determines the geometric dimensionality of the problem. The geometric dimensionality of the problem dictates the dimension of the space in which the AR is going to be identified, i.e. if the AR is going to be two, three or four dimensions in Euclidian space. In most cases, it is imperative to choose state variables that obey convex mixing, such that the region to be constructed is characterised by conditions detailed in the preceding section.

III. *Mathematical Definition of the Fundamental Process Vectors*

After the fundamental processes have been selected and the state variables chosen, appropriate mathematical vector descriptions for the fundamental processes in terms of the state variables can be formulated. These vectors

represent the instantaneous state change when the processes are applied to their respective input.

For the system where isothermal reaction takes place, the reaction vector defined at concentration C is $r(C)$. This vector represents the instantaneous change in C due to the fundamental process of reaction. For exothermic adiabatic systems where the reaction takes place in the gas phase, and where there is a change in the total number of moles as given in the balanced chemical reaction equation which results in the total pressure (P_T) change, the reaction vector can be represented as $r(P, T)$ defined at the partial pressures of components, P, and temperature T.

For a system where a number of fundamental processes are permitted to occur simultaneously, the overall process vector can be described as a convex combination of all fundamental processes. Consider a system where M processes are permitted to occur. The fundamental processes (p) depend on the state of the system c, and possibly some other achievable state or combinations of achievable states within the system, c^*. The fundamental processes for this case may be represented as $p_1(c,c^*)$, $p_2(c,c^*)$..., $p_M(c,c^*)$. The overall net effect of the system due to all processes can be expressed as

$$p_{NET}(c,c^*) = \sum_{j=1}^{M} \alpha_j \, p_j(c,c^*) \qquad (2.1)$$

defining the operating control policy for the fundamental process j as α_j which specifies the degree to which the fundamental process j occurs relative to other fundamental processes. It is possible that each fundamental process depends on its individual achievable state c_j^*, in which case equation 2.1 can be accordingly modified to be as shown below:

$$\boldsymbol{p}_{NET}\left(\boldsymbol{c},\boldsymbol{c}^{*}\right)=\sum_{j=1}^{M}\alpha_{j}\,\boldsymbol{p}_{j}\left(\boldsymbol{c},\boldsymbol{c}_{j}^{*}\right) \tag{2.1 b}$$

IV. *Specifying the System Constraints*

The system constraints represent the physical restrictions placed on the system. These restrictions may be a function of the state variables and/or fundamental processes. A state variable such as temperature may be confined within the lower and upper bounds as $T^{min} \leq T \leq T^{max}$. The process operating policy may also be constrained as $\alpha_{j}^{\min} \leq \alpha_{j} \leq \alpha_{j}^{\max}$.

V. *Verification of the Necessary Conditions*

Based on the state variables, process vectors and system constraints, the applicability of the necessary conditions for the system may be verified. These conditions will be a modification of the necessary conditions stated in section 2.2.1. For example, in cases where there are system constraints such as maximum temperature, process vectors will be allowed to extend out of the AR^{C} if following such process vectors results in constraint violation.

VI. *Construction of the Attainable Region*

McGregor (1998) suggested a trial and error approach to the construction of attainable regions. The fundamental processes are applied to all system feeds and the resulting set of outcome states is checked for violations of the necessary conditions. Wherever a necessary condition is broken, fundamental processes or combinations thereof are applied to expand the region. This procedure is performed iteratively until all necessary conditions are satisfied by all state points on the candidate AR boundary. This technique of construction is a typical example of constructing the attainable regions from the *interior*, where a small

region is grown outwards by extensions arising from application of fundamental processes and/or combinations thereof.

VII. *Optimisation of the Objective Function*

The objective function is now evaluated over the region to obtain the optimum operating point.

VIII.   *Interpretation of the Boundary*

Once the optimum operating point has been established it can further be interpreted in terms of optimal operating policies. Any point on the boundary can be interpreted as a result of an application of a sequence of fundamental processes applied to achieve it from the input states. This network of processes, together with the optimal operating policies, can be further construed to represent unit operations with flow configurations and key design parameters. If the optimum operating point is in the interior of the attainable regions boundary there will be an infinite number of ways of achieving it (Glasser *et al.*, 1992).

2.4 Structure of the Attainable Region Boundary

2.4.1 Background

McGregor (1998) derived a number of postulates to simplify the exhaustive nature of the traditional trial and error method for identify candidate attainable regions. Without giving any proofs or specific guidelines, McGregor (1998) intuitively suggested that the postulates will ease the complexities surrounding the procedure of identifying and interpreting the AR^Cs. These postulates were later validated by the universal properties of the AR boundary derived by Feinberg and Hildebrandt (1997) for the specific case of steady-state systems involving the

fundamental processes of isothermal reaction and mixing. McGregor (1998) used numerous examples and Pontryagin's maximum principle to substantiate the validity of these postulates in general.

In this study the relevance of these postulates to expedite the procedure of systematic identification and interpretation of AR^Cs will be demonstrated. In conjunction with and supported by the latter work of Feinberg (2000a & b), McGregor's postulates form a foundation of this study.

2.4.2 McGregor's Postulates

Consider a system in Section 2.3 above with M permitted fundamental processes that can be represented by a net effect resultant process expressed as;

$$\boldsymbol{p}_{NET}\left(\boldsymbol{c},\boldsymbol{c}^{*}\right)=\sum_{j=1}^{M}\alpha_{j}\boldsymbol{p}_{j}\left(\boldsymbol{c},\boldsymbol{c}_{j}^{*}\right) \qquad\qquad (2.1\ b)$$

The boundary of the AR of this particular system can be generalised using the McGregor's postulates (McGregor, 1998). A summary of some of these postulates is detailed below.

Postulate 1:   *The boundary of the attainable region consists of distinct process surfaces that are a union of process trajectories where all of the control policies are common and at either their lower or upper bounds.*

This postulate was confirmed by the results of Feinberg and Hildebrandt for systems with reaction and mixing, that the AR boundary comprised reaction trajectories and mixing lines. The mixing control policy is at zero (lower bound) along the reaction surface and infinite (upper bound) along the mixing plane.

<u>Postulate 2</u>: *The junctions between various process surfaces, termed intersectors, represent either change in one or more of the control policies or termination of two different process trajectories or lines that intersect.*

The importance of the intersectors was first acknowledged by Glasser *et al.* (1992). The authors asserted that the optimal process combination intersectors played a significant role in outlining the structure of the AR boundary for systems considering processes of reaction and mixing.

Recently the work of Feinberg (2000a & b) demonstrated with mathematical proofs how the intersectors that are optimal combinations of processes outline the shape of the AR boundary from which distinct process surfaces emanate. These optimal process combination intersectors are studied in detail in Section 2.5.6. Postulate 2 can be divided into several sub-postulates that characterise different types of intersectors that may occur on the boundary of the AR.

<u>Postulate 2.1</u>: *The smooth trajectory intersectors may exist on the boundary of the AR, where one or more of the operating policies are trajectories defined by functions taking intermediate values between the upper and lower bounds.*

This type of intersectors is a union of distinct process trajectories. Consider a system with two permitted fundamental processes r and v, and a net effect process vector defined by,

$$\boldsymbol{p}_{NET} = \boldsymbol{r} + \alpha_v \boldsymbol{v}$$

A smooth trajectory intersector is a union of process r and v trajectories. Along this trajectory intersector the operating policy is defined by a function that takes

intermediate values between zero and infinity. For the case where process *r* represents reaction and *v* representing mixing, the smooth trajectory intersector that occurs on the boundary of the AR will be an optimal combination of reaction and mixing (Feinberg, 2000a) as shown in Figure 2.3. This optimal combination represents a DSR (Glasser *et al.*, 1992).
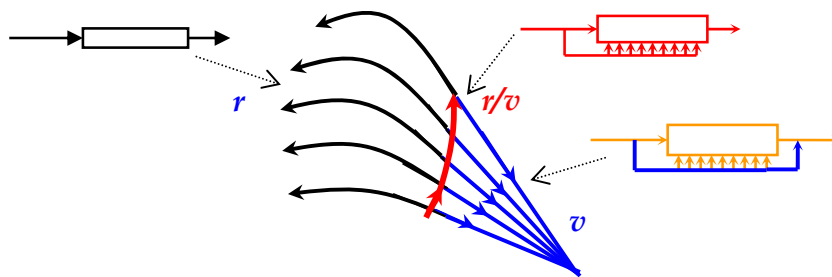
Figure 2.3: Local AR Boundary structure for the smooth trajectory intersector for a system with processes of reaction and mixing.

The smooth trajectory intersector can also occur for systems with reaction (*r*) and heat transfer (*q*). In this case the intersector represents the optimal combination of reaction and heat transfer as shown in Figure 2.4.
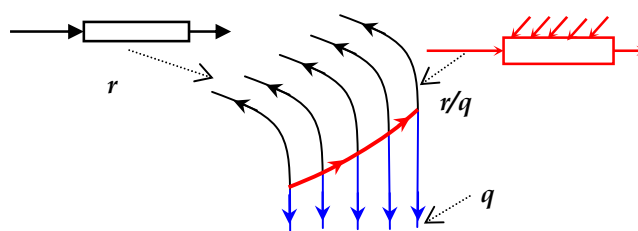
Figure 2.4: Local AR Boundary structure for the smooth trajectory intersector for a system with processes of reaction and heat transfer.

<u>Postulate 2.2</u>: *The smooth intersectors may exist on the boundary of the AR, that are not the union of trajectories. These intersectors may represent the locus of stationary points that include mixing.*

Illustrated in Figure 2.5 is an example of a smooth intersector that is a locus of stationary points that represents stationary points where reaction and mixing process vectors are collinear. This union represents a well stirred unit where reaction and mixing are combined optimally as in a CFSTR. Feinberg (2000a) demonstrated the significance of these intersectors in outlining the structure of the AR boundary. These optimal combinations of reaction and mixing are termed critical CFSTRs.
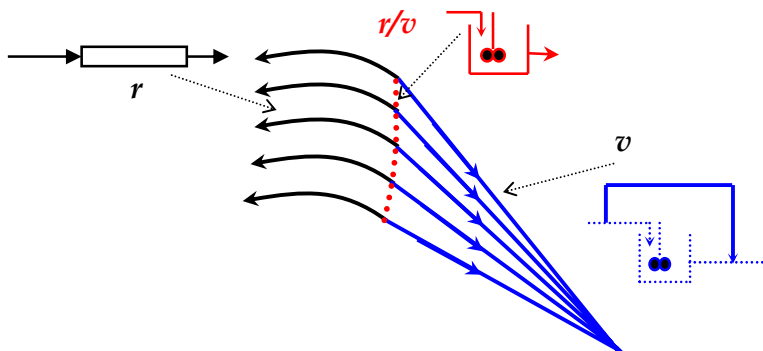
Figure 2.5: Local AR Boundary structure for the smooth intersectors that are the locus of stationary points for a system with reaction and mixing

<u>Postulate 2.3</u>: *The non-smooth intersectors may exist on the boundary of the AR that is not the union of trajectories. These intersectors may represent the union of points where two process surfaces intersect and/or terminate.*

For a system considering fundamental processes of reaction *r*, mixing *v* and heat transfer *q*, a non-smooth ridge may exists where the process surfaces of mixing and heat transfer intersect. This case may be due to the initiating of a new

trajectory on the boundary, such as the smooth trajectory intersector that is a union of reaction and heat transfer as illustrated in Figure 4.6.
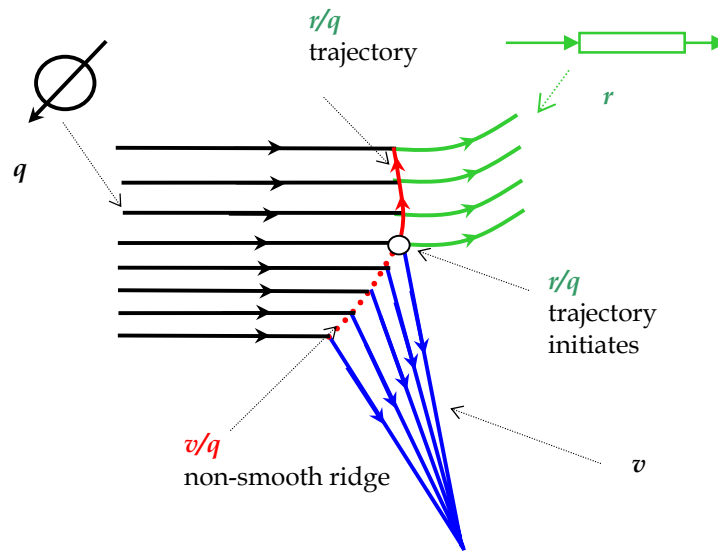
Figure 2.6: Local AR Boundary structure for the non-smooth intersectors that are ridges of the intersection of mixing and heat transfer process surfaces.

The non-smooth intersectors are essentially the intersections of two distinct process surfaces and cannot be characterised as a single process unit or combinations thereof. As these intersectors are neither trajectories nor a locus of points they do not have any mathematical description governing their occurrence on the boundary of the AR. This conjecture is asserted without any proof and will later be clarified with the use of examples (Chapters 5 and 6).

From the postulates derived by McGregor (1998), it can be suggested that the structure boundary of the attainable regions is essentially outlined by smooth intersectors that are either trajectories or stationary points from which distinct surfaces formed by the union of process trajectories emanate. The non-smooth

intersectors will be identified on the AR boundary consequent to the intersection of process surfaces.

2.5 Mathematical Models for Idealised Processes

In this section we review mathematical models used to describe fundamental processes. We further extend the theory of overall process combination vectors such as intersectors, and finally interpret the mathematical model in terms of processing units such as reactor structures and the conditions of optimality governing the occurrence of these structures on the boundary of the attainable regions.

2.5.1 The Reaction Vector

Let c represent the state of process components such as reactants and products. The state c will provide information such as concentrations, mass fractions or partial pressures. Consider a reaction vector space comprising instantaneous reaction vector at c as $r(c)$. The instantaneous change in the system state, c due to a change in the process residence time, $d\tau$ can be expressed as

$$dc = r(c)d\tau \qquad \text{(2.2 a)}$$

The reaction rate vector $r(c)$ will contain information about the kinetics of the reaction taking place. The scalar process residence time in this example is denoted by τ, which gives a measure of the duration of the application of the reaction process. For non-isothermal reactions, the process instantaneous change in the reacting system temperature T, due to the reaction process can be given as

$$dT = \frac{\Delta H_{rxn}}{Cp} r(c,T)d\tau \qquad \text{(2.2 b)}$$

The average isobaric specific heat capacity, $\overline{Cp}$ of the reaction mixture is assumed to be constant. ΔH_{rxn} is the enthalpy of reaction.

2.5.2 The Mixing Vector

If we mix state c with another achievable state c^* in a linear mixing space, the resulting state lies along the mixing vector v, described by

$$v = \left(c^* - c\right) \tag{2.3}$$

2.5.3 The External Heat Exchange Vector

External heat exchange can be carried out between material at the state of temperature T and constant temperature utility with the temperature T_c. The heat exchange process is described by a heat transfer coefficient, h_o. The process vector representing heating can be described as (Nicol, 1998);

$$w = h_o\left(T_c - T\right) \tag{2.4}$$

If we consider a heat transfer unit such as a heat exchanger with some heat transfer constant k_c, relating the residence time and the heat exchange area of the heat exchange unit. Assuming that h_o and Cp remain constant over the temperature range of interest; the rate of change of temperature in the heat exchange unit can be expressed as:

$$dT = \frac{h_o k_c}{Cp}\left(T_c - T\right)d\tau = K_c\left(T_c - T\right)d\tau \tag{2.5}$$

Cp is defined as the isobaric specific heat capacity of the material being processed.

2.5.4 The Overall Reaction, Mixing and Heating Vector

For a process unit where reaction, mixing and heating or cooling are allowed to occur as fundamental processes, the variables of interest are defined in the state characteristic vector, $c = [x, T, \tau]$, comprising the reactants and products compositions, temperature and residence time. The overall process rate vectors are defined as a controlled combination of the fundamental processes;

$$dx = r(x)d\tau + \alpha v(x, x^*)d\tau \qquad (2.6\ a)$$

$$dT = \frac{\Delta H_{rxn}}{\overline{Cp}} r(x, T)d\tau + \alpha v(x, x^*, T, T^*)d\tau + \beta w(T_c - T)d\tau \qquad (2.6\ b)$$

The process combination control policies for mixing and heat transfer are represented as α and β respectively.

2.5.5 Idealised Reactor Structures

The objective of attainable region analysis is usually to be able to interpret the boundary as a process network structure. It is therefore an essential step to review idealised mathematical models describing some reactor units in order to signify their relationship with the process vectors that outline the geometry of the AR boundary.

i.   The Plug Flow Reactor

The equation governing a plug flow reactor (PFR) is that of reaction occurring as the only process. This process vector can be derived from reaction rate vector (2.2 a) as follows.

$$\frac{d\boldsymbol{c}}{d\tau} = \boldsymbol{r}(\boldsymbol{c}) \qquad \boldsymbol{c}(\tau = 0) = \boldsymbol{c}^0 \tag{2.2 c}$$

The state space curve describing a PFR in the AR state space is a trajectory such that the reaction vector is tangential to it at each state point $\boldsymbol{c}$. The fundamentals of differential algebra define trajectories as being directional. The unique nature of the rate vector at any point means that these trajectories progress such that they cannot cross each other (Love 1995). There exists one unique PFR trajectory for any given initial feed point $\boldsymbol{c}^0$.

ii.   *Continuous Flow Stirred Tank Reactor*

In a continuous flow stirred tank reactor (CFSTR), reaction and mixing occur simultaneously, such that the reaction vector is collinear and directionally opposite to the mixing vector. A CFSTR curve is a locus of stationary points as a function of the scalar τ, satisfying equation 2.7;

$$-\boldsymbol{r}(\boldsymbol{c}) = \frac{1}{\tau}(\boldsymbol{c}^0 - \boldsymbol{c}) \tag{2.7}$$

where τ is the residence time of the reactor and $\boldsymbol{c}^0$ is the feed state.

The CFSTR locus is obtained by varying the residence time and solving for the corresponding state, $\boldsymbol{c}$.

iii.   *The Differential Sidestream Reactor*

A differential sidestream reactor (DSR) can be conceptualised as a PFR with differential feed along the length. This structure arises when reaction and mixing occur simultaneously and the relative action of the process is governed by the

equation defining the rate of controlled combination of reaction and mixing (2.6a). On the boundary of the attainable region a DSR is a smooth trajectory intersector tangential to the plane containing both fundamental process vectors of reaction and mixing at each point along the trajectory (Section 2.4);

$$\frac{d\boldsymbol{c}}{d\tau} = \boldsymbol{r}(\boldsymbol{c}) + \alpha\boldsymbol{v}(\boldsymbol{c},\boldsymbol{c}^*) \qquad c(\tau = 0) = c^0$$

The state of the mixing stream $\boldsymbol{c}^*$, may be constant in the case of a fixed mixing point or it may vary along the length of the reactor (varying with τ) in which case it is referred to as a varying mixing point, $\boldsymbol{c}^*(\tau)$. It should be noted that the DSR equation is analogous to that of the CFSTR when the rate equals zero,

$$\frac{d\boldsymbol{c}}{d\tau} = 0 \qquad \rightarrow \qquad \boldsymbol{r}(\boldsymbol{c}) = -\alpha(\boldsymbol{c}^* - \boldsymbol{c})$$

$$\rightarrow \qquad (\boldsymbol{c} - \boldsymbol{c}^*) = \frac{1}{\alpha}\boldsymbol{r}(\boldsymbol{c})$$

$$\text{with} \quad \tau = \frac{1}{\alpha}$$

iv.   Differentially Cooled Reactor

The differentially cooled reactor (DCR) arises when reaction and cooling are incorporated in the same unit. The structure can be conceptualised as a PFR with differential cooling along the length. Similar to the DSR, the curve representing a DCR is a smooth trajectory intersector such that the reaction vector and the cooling vector form a tangential plane to the trajectory at any state $\boldsymbol{c} = [x, T]$

(Section 2.4). The equations representing the rate changes of the state variable are therefore given by;

$$\frac{d\boldsymbol{x}}{d\tau} = \boldsymbol{r}(\boldsymbol{x}, T) \qquad\qquad (2.8\ a)$$

$$\frac{dT}{d\tau} = \frac{\Delta H_{rxn}}{\overline{Cp}} \boldsymbol{r}(\boldsymbol{x}, T) + \beta w (T_c - T) \qquad\qquad (2.8\ b)$$

The same argument as for the DSR holds, stating that the cooling temperature T_c may be fixed or vary along the length of the reactor. In the case where heating not cooling occurs the structure obeys the same equations and the structure is termed a differentially heated reactor (DHR).

v. *More Complex Structures*

As we continue to combine the fundamental processes, more and more reactor structures will be formed. In higher dimensional space the complexity of the AR^Cs structure increases yielding intricate geometric forms. The DSR trajectories that are tangential to surfaces comprising both reaction and mixing in three dimensions become DSR family surfaces that are tangential to hyper-planes that contain surfaces of reaction and mixing in four dimensions.

As a number of processes combined reaches three and beyond, more complex structures will arise including the ones that surpass our current practical imagination. For example we may have a structure for controlled combination of reaction, differential mixing, differential heating, and differential compression to carry out an endothermic gas phase reaction, where a reaction forming an undesirable by-product also takes place. It is important to note that a structure or

a reactor configuration arises from the solution, and not the imagination of the designer or optimiser.

2.5.6   Optimal Process Combination

Feinberg and Hildebrandt (1997) proved that the boundary of the AR consists of optimal combinations of fundamental processes that give rise to pathways to navigate to extreme points of single process operation forming the boundary of the AR. On the AR boundary these optimal combinations are smooth trajectory intersectors and smooth locus intersectors as defined in Section 2.4. Feinberg (2000a) further demonstrated this geometric property of the attainable region boundary for combined processes of reaction and mixing. The smooth trajectory intersector curve representing the controlled combination of reaction and mixing is a DSR trajectory. It was stated in the work of Glasser *et al.* (1992), that for a DSR curve to lie on the boundary of the AR, it must lie on the surface described by;

$$\varphi(c) = \left[dr(c)v(c,c^*) \right] \cdot \left[v(c,c^*) \times r(c) \right] - dv(c,c^*)r(c) = 0 \qquad (2.9)$$

where dx is the Jacobian matrix of vector x, $r(c)$ and $v(c, c^*)$ are the reaction and the mixing vectors respectively as defined earlier.

This condition is true only for a three dimensional AR for an isothermal system considering only reaction and mixing. The mixing control policy α, that ensures that the DSR (2.9) remains in the φ surface in three dimensions can therefore be computed as;

$$\alpha = \frac{-\nabla \varphi \cdot r(c)}{\nabla \varphi \cdot v(c,c^*)} \qquad (2.10)$$

Feinberg (2000a) proved these assertions from the ideas of geometric control and advanced a theory to derive conditions for higher dimensional problems. With

rigorous mathematical proofs Feinberg illustrated that, in fact, a more fundamental mathematical requirement exists for a DSR to lie on the boundary of the AR. He further proved that the DSR should lie in the φ surface that satisfies the following determinant condition;

$$\varphi = \det\{\boldsymbol{v}(\boldsymbol{c},\boldsymbol{c}^*),\boldsymbol{r}(\boldsymbol{c}),\left(d\boldsymbol{r}(\boldsymbol{c})\boldsymbol{v}(\boldsymbol{c},\boldsymbol{c}^*)-d\boldsymbol{v}(\boldsymbol{c},\boldsymbol{c}^*)\boldsymbol{r}(\boldsymbol{c})\right)\}$$ (2.11)

The required mixing control policy to ensure that the DSR remain in the φ surface was then derived as;

$$\alpha = -\frac{\det\{\boldsymbol{v},\boldsymbol{r},\left(d(d\boldsymbol{v}(\boldsymbol{r})-d\boldsymbol{r}(\boldsymbol{v}))(\boldsymbol{r})-d\boldsymbol{r}(d\boldsymbol{v}(\boldsymbol{r})-d\boldsymbol{r}(\boldsymbol{v}))\right)\}}{\det\{\boldsymbol{v},\boldsymbol{r},\left(d(d\boldsymbol{v}(\boldsymbol{r})-d\boldsymbol{r}(\boldsymbol{v}))(\boldsymbol{v})-d\boldsymbol{v}(d\boldsymbol{v}(\boldsymbol{r})-d\boldsymbol{r}(\boldsymbol{v}))\right)\}}$$ (2.12)

Feinberg (2000a) further derived the mixing control policy for higher dimensions to indicate the dimensional generality of his postulates. The derivation for a four dimensional system considering only reaction and mixing arrives at a control policy described by;

$$\alpha = -\frac{\det\{\boldsymbol{v},\boldsymbol{r},\left(d\boldsymbol{v}(\boldsymbol{r})-d\boldsymbol{r}(\boldsymbol{v})\right),\left(d(d\boldsymbol{v}(\boldsymbol{r})-d\boldsymbol{r}(\boldsymbol{v}))(\boldsymbol{r})-d\boldsymbol{r}(d\boldsymbol{v}(\boldsymbol{r})-d\boldsymbol{r}(\boldsymbol{v}))\right)\}}{\det\{\boldsymbol{v},\boldsymbol{r},\left(d\boldsymbol{v}(\boldsymbol{r})-d\boldsymbol{r}(\boldsymbol{v})\right),\left(d(d\boldsymbol{v}(\boldsymbol{r})-d\boldsymbol{r}(\boldsymbol{v}))(\boldsymbol{v})-d\boldsymbol{v}(d\boldsymbol{v}(\boldsymbol{r})-d\boldsymbol{r}(\boldsymbol{v}))\right)\}}$$

(2.13)

Feinberg (2000a) further derived the control policies for stoichiometric space in five and six dimensions to demonstrate the dimensional generality of his proofs. It should be noted that these conditions of optimality apply only if $\alpha > 0$ (Feinberg, 2000a).

In a subsequent publication, Feinberg (2000b) derived the necessary conditions required for a CFSTR output state to lie on the AR boundary. As shown in Section 2.4, the CFSTR that occur on the AR boundary is a smooth intersector that is a locus of stationary points that include mixing (McGregor, 1998).   Once again, we will emphasise that a CFSTR is a special class of the DSR. Mathematically a CFSTR is equivalent to a DSR with these properties:

- The rate vector is collinear and in opposite direction to the mixing vector.

- The overall rate vector is zero, i.e. the sum of the reaction and mixing vectors equals zero.

Using geometric optimal control derivations Feinberg (2000b) proved that for an isothermal system considering only reaction and mixing, the condition required for the effluent state of the CFSTR to occur on the AR boundary in three dimensions is described by,

$$\det\{\boldsymbol{v}, d\boldsymbol{r}(\boldsymbol{v}), d\boldsymbol{r}(d\boldsymbol{r}(\boldsymbol{v}))\} = 0 \tag{2.14}$$

For a four dimensional space the CFSTR effluent is required to conform to the condition (Feinberg (2000b),

$$\det\{\boldsymbol{v}, d\boldsymbol{r}(\boldsymbol{v}), d\boldsymbol{r}(d\boldsymbol{r}(\boldsymbol{v})), d\boldsymbol{r}(d\boldsymbol{r}(d\boldsymbol{r}(\boldsymbol{v})))\} = 0 \tag{2.15}$$

Feinberg (2000b) called these types of CFSTRs critical CFSTRs. Using these necessary conditions it is possible to evaluate the residence times and further evaluate the effluent states of such CFSTR that reside on the AR boundary.

2.6 Discussion

Attainable Region analysis background and theory have been presented, from which it is evident how significant this technique is as process synthesis tool. The theory is clearly introduced with discussion on how fundamental process networks can profile the boundary of the AR. A set of necessary conditions that are used as check points for any possible extensibility on candidate ARs have also been presented together with elements of attainable regions analysis which are essentially sequential traditional guidelines developed by previous researchers on how to identify candidate ARs. From the postulates derived by McGregor (1998), a theory was suggested to generalise the structure of the AR boundary. This theory stipulates that the AR boundary comprises mainly of distinct process surfaces formed by process trajectories that emanate from and connected by intersectors. These intersectors were interpreted as optimal combinations of permitted fundamental processes.

We further discussed how fundamental processes can be idealised for AR analysis, illustrating using fundamental processes of reaction, bulk mixing, and heat transfer as well as combinations thereof. The optimal process combinations that shape the boundary of ARs have also been asserted using analytical derivations from the work of Feinberg (2000 a & b). These analytical derivations have strong mathematical foundations based on the theory of geometric control but however have a shortcoming of being hard to solve due to imbedded algebraic complexity. It is this intricacy that limits attainable region analysis applications to reactor network synthesis. Alternative techniques to generate AR^C will greatly improve its relevance and broaden its use by giving non-specialist users access.

Throughout the background theory and literature review emphasis was placed on the fact that the boundary of the attainable regions can be established by identifying the optimal process combination intersectors that give rise to distinct process surfaces that form the final shape of the AR boundary.

In the next chapter we propose an automated systematic method of solving candidate attainable regions by identifying the optimal process combination trajectories. The method offers full automation of construction without the need for prior analytical solutions of algebraic expressions. The procedure also promises automated interpretation of the boundary in terms of reactor structures.

2.7 References

Douglas, J. M., (1985), A hierarchical decision procedure for process synthesis, *AICHE J.*, **31**, pp. 353-362.

Feinberg, M. & Hildebrandt, D., (1997), Optimal Reactor Design from a Geometric Viewpoint: I Universal Properties of the Attainable Region, *Chem. Eng. Sci.*, **52**, (10), pp. 1637-1665.

Feinberg, M., (2000 a), Optimal reactor design from a geometric viewpoint II: Critical sidestream reactors., *Chem. Eng. Sci.*, **55**, pp. 2455 – 3565.

Feinberg, M., (2000b), Optimal reactor design from a geometric viewpoint III: Critical CFSTRs, *Chem. Eng. Sci.*, **55**, pp. 3553 – 2479.

Glasser, D., Hildebrandt, D., & Crowe, C.M., (1987), A Geometric Approach to Steady Flow Reactors: The Attainable Region and Optimisation in Concentration Space, *Ind. & Eng. Chem. Research.*, **26**, pp. 1803-1810.

Glasser, B., Hildebrandt D., Glasser, D., (1992), Optimal mixing for Exothermic Reversible Reactions. *I&EC Research*, 1992, **31**, pp. 1541-1549.

Godorr, S. A. (1998). *Optimising chemical reactor structures and other systems by means of the attainable region*, PhD thesis, Republic of South Africa: University of the Witwatersrand.

Hildebrandt, D., (1989), *The Attainable Region generated by Reaction and Mixing*, PhD Thesis, University of the Witwatersrand, Johannesburg, South Africa.

Hildebrandt, D. & Glasser, D., (1990), The Attainable Region and Optimal Reactor Structures, *Chem. Eng. Sci.*, **45**, (8), pp2161-2168.

Horn, F., 1964, Attainable and non-attainable regions in chemical reaction technique, Proc. Third European Symposium on Chemical Reaction Engineering, Pergamon, New York, pp. 1-10.

Kokossis, A. C. & Floudas, C. A., (1990), Optimisation of complex reactor networks –I. Isothermal operation, *Chem. Eng. Sci.* **45** (3), pp. 595.

Kokossis, A. C. & Floudas, C. A., (1991), Synthesis of Isothermal Reactor-Separator-Recycle Systems, *Chem. Eng. Sci.* **46**, pp. 1361-1383.

Kokossis, A. C. & Floudas, C. A., (1994), Optimisation of complex reactor networks –II, Non-Isothermal operation, *Chem. Eng. Sci.* **49** (7), pp. 1037.

Love, A.D., *Mathematics of the Attainable Region*, (1995), PhD Thesis, Republic of South Africa: University of the Witwatersrand, Johannesburg.

McGregor, C. (1998). *Choosing the optimal system structure using the attainable region approach for systems involving reaction and separation*, PhD thesis, Republic of South Africa: University of the Witwatersrand.

Nicol, W. (1998). *Extending the attainable region technique by including heat exchange and addressing four dimensional problems*, PhD thesis, Republic of South Africa: University of the Witwatersrand.

Papalexandri, K. P. &, Pistikopoulos, E. N., (1994), A Multiperiod MINLP Model for the Synthesis of Flexible Heat and Mass Exchange Networks, *Comp. Chem. Eng.* **18** (11/12), pp. 1125-1139.

Papalexandri, K. P. & Pistikopoulos, E. N., (1996), Generalised Modular Representation Framework for Process Synthesis, *AICHE J.* **42** (4), pp. 1010-1032.

Shah, P. B. & Kokossis, A., (1997), Design Targets of Separator and Reactor-Separator Systems using Conceptual Programming, *Comp. Chem. Eng.* **21**, pp. S1013-S1018.

2.8 List of Symbols

Abbreviations

AR	Attainable Regions
AR^C	Candidate Attainable Regions
CFSTR	Continuous Flow Stirred Tank Reactors
DCR	Differentially Cooled Reactor
PFR	Plug Flow Reactor
DHR	Differentially Heated Reactor
DSR	Differential Side-stream Reactor
MINLP	Mixed Integer Non-Linear Programming

Symbols

α	Combination control policy for fundamental processes (mixing)
β	Combination control policy for heat transfer
c	State variable of the system
c^o	State variable of the system at the feeding point
c^*	Mixing state variable of the system
$\boldsymbol{c}$	State vector comprising all variables describing the system
C	Concentration of the reacting components
Cp	Isobaric specific heat capacity of the material
ΔH_{rxn}	Enthalpy of reaction
h_o	Heat Transfer coefficient
k_c	Heat Transfer constant
p	Fundamental processes taking place in the system
p_{NET}	Overall net effect of the system due to all processes
P	Partial pressure of the reacting components
$\boldsymbol{r}(c)$	Reaction rate vector defined at c

$r(C)$	Reaction vector defined at C
$r(P,T)$	Reaction vector defined at P and T
T	Temperature of reaction
T^*	Temperature of mixing
T_c	Cooling or Heating utility temperature
τ	Residence time
υ	Mixing vector, mixing c with c^*
w	Heat Exchange vector
x	Reactants and Products state compositions
x^*	Reactants and Products mixing compositions
$\varphi(c)$	The optimum process combination surface (phi surface)

CHAPTER 3

RCC ALGORITHM FOR ATTAINABLE REGION ANALYSIS

3.1 Introduction

A general theory such as AR analysis can handle a problem with any number of fundamental processes, feed and product components, design parameter variability, and virtually any system complexity. This is important as it allows for the consideration of complicated systems that have previously been considered impossible to be studied.

"A general theory, such as this, is required for the future development of an algorithm to automate the construction of attainable region boundaries. A computer programme that can determine attainable regions would greatly enhance the relevance of attainable region analysis to the chemical process industry." McGregor (1998)

3.2 Background

In the absence of a sufficiency condition, finding a region that contains all possible outcomes from all possible combinations of all permitted fundamental processes without exclusion of any possibility cannot be conclusively shown. The traditional methods for constructing the AR^C use the necessary conditions as guidelines (McGregor, 1998). The fundamental processes are applied to all system feeds and the resulting region of outcome states is checked for violation of the necessary conditions. Wherever a necessary condition is broken, fundamental processes or combinations thereof are applied to achieve the

identified expansion. This procedure is performed iteratively until all necessary conditions are satisfied by all output state points on the AR^C boundary. This method of construction is limited only to known necessary conditions and cannot ensure the identification of the full AR, but only a candidate subset AR^C. This traditional method suggested by McGregor (1998) constructed the AR^C from the *interior*. Thus, a region is constructed from the feed and further extended outward by application of fundamental processes until some convergence criterion is met and the *outer bounds* of the AR^C are approximated.

Recently, research work has focused on automating the construction of candidate ARs. Rooney *et al.* (2000) communicated the Iso-state Algorithm, one of the first contributions in the search for the automated techniques for construction of ARs. The AR^{C}s in this case, were also generated from the *interior* as in the traditional methods suggested by McGregor (1998). The algorithm generated 2D planes in orthogonal subspaces which are fused into higher dimensional ARs. This technique worked well for three dimensional problems with two fundamental processes, but due to its 2D plane decomposition it required long computational runtimes in higher dimensions.

Burri *et al.* (2000) proposed a method called IDEAS for automated AR construction. This method constructed two-dimensional regions using linear programming formulations based on CFSTRs, PFRs, and mixing lines. The technique arose from a relaxation of an infinite dimensional state space formulation. The problem was broken down into two phases; a distribution network and a process operator. All mixing, splitting, recycling, and bypassing occurred in the distribution network and all fundamental unit operations took place in the process operator.

Another systematic method to construct candidate ARs was the Linear Programming (LP) formulations proposed by Kauchali *et al.* (2001). This

method used what the authors called the total connectivity model, which applied all possible combinations of CFSTRs and mixing patterns to represent any known reactor structure for the fundamental processes of reaction and mixing. The authors then considered a rate vector field in concentration spaces with a large grid of points from which several LPs were derived to solve for the AR^C. This method also generated AR^{C}s from the *interior* by outward extensions.

Abraham and Feinberg (2004) proposed a method of Bounding Hyperplanes which constructed the AR^C from the *exterior*. The construction is carried out using a polygon bound by hyperplanes in composition space, within which all the attainable compositions must reside. The procedure of this technique entails progressive increment in the number of hyperplanes bounding the polygon, and eliminaton of the non-attainable compositions from the interior of the bounds. As the number of hyperplanes increases, the bounding polygon approximates the upper bound of the attainable regions. This method is different from other techniques due to its approach of approximating the AR^C boundary form the *outside*.

In this work another systematic method for automated attainable regions construction is proposed. The method constructs AR^{C}s from the *interior* by applying combinations of fundamental processes to find outward extensions on the boundary attained from application of the fundamental processes on the given feed. In the following section, we illustrate with the aid of an example, how complicated the analytical solution for optimal reactor structures that contour the boundary of the AR can be, even for a simple idealised kinetic system. The analytical computations are then followed by the introduction of a relevant theory and formulations for the proposed algorithm and the technique is then demonstrated by a number

of study cases for illustration including the one solved using analytical methods.

3.3 Example: Analytical Solution

In this section we consider an example with the intention of obtaining the AR^C via analytical methods reviewed in the preceding sections. We present a case study with Van de Vusse type kinetics for the underlying network of chemical reactions shown in Figure 3.1 with the corresponding rate expressions,

Reaction Network	Rate Expressions	Rate Constants
$A \underset{k_r=k_2}{\overset{k_f=k_1}{\leftrightarrow}} B \overset{k_3}{\to} C$	$k_1 = 1\,\text{min}^{-1}$	$r_A = -k_1 C_A - 2k_4 C_A^2 + k_2 C_B$
	$k_2 = 0.5\,\text{min}^{-1}$	$r_B = k_1 C_A - k_2 C_B - k_3 C_B$
$2A \overset{k_4}{\to} D$	$k_3 = 10\,\text{min}^{-1}$	$r_D = k_4 C_A^2$
	$k_4 = 100\,\frac{litre}{\min\,mol}$	

Figure 3.1: Van de Vusse Reaction Scheme with Kinetics

The case study is of an isothermal type and considers only reaction and bulk mixing. The reaction occurs in the liquid phase at constant density. We consider a feed of 1 mol/litre of pure A. The objective is to construct an AR^C in a three dimensional A-B-D stoichiometric space.

As discussed in Chapter 2, the procedure for generating the AR boundary is to first solve for optimal process combination trajectories that will give final access to the manifolds of extreme points that form the boundary. In this example the optimal DSR profiles will serve as precursors, giving access to manifolds of extreme PFR trajectories and mixing planes that make up the boundary of the AR. The critical CFSTRs may also need to be computed as they also play the same role as DSRs.

To solve for the optimal DSR(s) we start by deriving the optimal control policy α described from derivations of Feinberg(2000a) by (2.12),

$$\alpha = -\frac{\det\{v, r, (d(dv(r) - dr(v))(r) - dr(dv(r) - dr(v)))\}}{\det\{v, r, (d(dv(r) - dr(v))(v) - dv(dv(r) - dr(v)))\}} \qquad (2.12)$$

We start with the mathematical definition of the fundamental process vector. The state variables are determined from the dimensionality of the AR to be determined. For the 3D A-B-D stoichiometric space the state vector is denoted by,

$$c = [C_A, C_B, C_D] = [c_1, c_2, c_4] \qquad (3.1)$$

The fundamental processes have to be defined as vectors in the c space, for the processes of reaction and mixing in the vector space as in (3.1) we express,

$$r(c) = \begin{bmatrix} r_A(c) \\ r_B(c) \\ r_D(c) \end{bmatrix} = \begin{bmatrix} -k_1 c_1 - 2k_4 c_1^2 + k_2 c_2 \\ k_1 c_1 - k_2 c_2 - k_3 c_2 \\ k_4 c_1^2 \end{bmatrix} \qquad v(c, c^*) = \begin{bmatrix} c_1^* - c_1 \\ c_2^* - c_1 \\ c_4^* - c_4 \end{bmatrix} \qquad (3.2)$$

The derivation of the optimal control policy α, is an algebraically exhaustive task resulting in a complex mathematical expression given in Figure 3.2.

$$\boldsymbol{\alpha =}$$

$$
\begin{aligned}
& 5\,k4\,c1^3\,k1^2 + 2\,k4\,k2^2\,c2^3 + 10\,k4^2\,c1^4\,k1 - 2\,k4\,c1^2\,k1^2 - 4\,k4^2\,c1^3\,k1 \\
& \quad + 10\,k1\,c4\,k4\,c1^2\,k2\,c2 + 5\,k4\,c1^2\,c2^2\,k2\,k1 + 4\,k4\,c1^3\,k1\,k2\,c2 + 2\,k4\,c1^3\,k3\,c2\,k1 \\
& \quad - 6\,k4^2\,c1^5\,k1 - 3\,k4\,c1^4\,k1^2 + 8\,k3\,c2\,c4\,k4^2\,c1^3 + 8\,k2\,c2\,c4\,k4^2\,c1^3 \\
& \quad - 4\,k2^2\,c2^2\,c4\,k4\,c1 - k4\,c1^2\,k3\,c2^2\,k2 - 4\,k3\,c2^2\,c4\,k4\,c1\,k2 \\
& \quad + 4\,k3\,c2\,c4\,k4\,c1^2\,k1 + 2\,k3^2\,c4\,k4\,c1^2\,c2 + 2\,k4\,c1^3\,k2\,k3\,c2 - 2\,k4\,c1^2\,k2\,k1 \\
& \quad + 2\,k4\,c1\,k3^2\,c2 - 2\,k4\,c1^2\,k3\,k1 + 2\,k4\,k3\,c2\,k1\,c1 + 4\,k4\,c1\,k2\,k3\,c2 \\
& \quad + 2\,k4\,c1\,k2^2\,c2 - 2\,k3\,c4\,k4\,c1^3\,k1 + 4\,k4^2\,k2\,c2\,c1^2 + 4\,k4\,c1\,k1\,k2\,c2 \\
& \quad - 2\,k4\,k2^2\,c2^2 + 4\,k4^2\,k3\,c2\,c1^2 - 2\,k4\,k3\,c2^2\,k2 - 2\,k2\,c4\,k4\,c1^3\,k1 \\
& \quad + 4\,k3\,c4\,k4\,c1^2\,k2\,c2 + 2\,k2^2\,c4\,k4\,c1^2\,c2 - 4\,k4^2\,k2\,c2^2\,c1^2 + 4\,k1^2\,c4\,k4\,c1^2 \\
& \quad - 4\,k4\,c1^2\,k3\,c2\,k1 + 2\,k4\,c1\,k3\,c2^2\,k2 - 8\,k1\,c4\,k4\,c1\,k2\,c2 - 8\,c4\,k2\,c2\,k4^2\,c1^2 \\
& \quad - 4\,c4\,k3\,c2\,k4\,k1\,c1 + 4\,c4\,k3\,c2^2\,k4\,k2 - 8\,c4\,k3\,c2\,k4^2\,c1^2 - 4\,k4\,k2\,c2^2\,k1\,c1 \\
& \quad - 7\,k4\,c1^2\,k1\,k2\,c2 - 6\,k4\,c1^2\,k2\,k3\,c2 - c4\,k3\,k1\,k2\,c2 + 4\,c4\,k2\,k4\,c1^2\,k1 \\
& \quad - 8\,c4\,k2\,k4\,c1\,k3\,c2 - 4\,c4\,k2^2\,k4\,c1\,c2 + 4\,c4\,k3\,k4\,c1^2\,k1 - 4\,c4\,k3^2\,k4\,c1\,c2 \\
& \quad + 2\,k4\,c1\,k2^2\,c2^2 + 4\,k4^2\,c1^3\,c2\,k1 + 2\,k4\,c1^2\,c2\,k1^2 + 4\,c4\,k2^2\,c2^2\,k4 \\
& \quad + 8\,k1\,c4\,k4^2\,c1^3 - 12\,k1\,c4\,k4^2\,c1^4 - 6\,k1^2\,c4\,k4\,c1^3 - 8\,k4^2\,c1^3\,k3\,c2 \\
& \quad - 8\,k4^2\,c1^3\,k2\,c2 + 4\,k4^2\,c1^4\,k2\,c2 - k4\,c1^2\,k2^2\,c2^2 - 6\,k4^2\,c1^4\,c2\,k1 \\
& \quad - 3\,k4\,c1^3\,c2\,k1^2 + 4\,k4^2\,c1^3\,c2^2\,k2 - 2\,k4\,c1\,c2^3\,k2^2 + 4\,k4^2\,c1^4\,k3\,c2 \\
& \quad - c4\,k3^2\,k1\,c2 + c4\,k3\,k1^2\,c1 - 3\,k4\,c1^2\,k3^2\,c2 + 3\,k4\,c1^3\,k3\,k1 - 3\,k4\,c1^2\,k2^2\,c2 \\
& \quad + 3\,k4\,c1^3\,k2\,k1 + k4\,c1^3\,k3^2\,c2 - k4\,c1^4\,k3\,k1 + k4\,c1^3\,k2^2\,c2 - k4\,c1^4\,k2\,k1
\end{aligned}
$$

$$
\begin{aligned}
& {-}8\,c4\,k3\,c2\,k4\,c1^2 - 8\,c4\,k2\,c2\,k4\,c1^2 + 16\,c4\,k3\,c2\,k4\,c1 + 16\,c4\,k2\,c2\,k4\,c1 \\
& \quad - 2\,k4\,c1\,k1 - 10\,k4\,c1^3\,k1 + 8\,k4\,c1^2\,k1 + 2\,k4\,k2\,c2 + 2\,k4\,k3\,c2 - 2\,k4\,k2\,c2^2 \\
& \quad + 4\,k4\,c1^4\,k1 - 6\,k4\,c1^2\,c2\,k1 - 12\,k1\,c4\,k4\,c1^2 + 4\,k1\,c4\,k4\,c1 + 2\,k4\,c1\,c2\,k1 \\
& \quad + 8\,k4\,c1\,c2^2\,k2 - 10\,k4\,c1\,k2\,c2 - 10\,k4\,c1\,k3\,c2 - 4\,c4\,k2\,c2\,k4 - 4\,c4\,k3\,c2\,k4 \\
& \quad + 2\,c4\,k3\,c2\,k1 + 12\,k4\,c1^2\,k2\,c2 + 12\,k4\,c1^2\,k3\,c2 - 4\,k4\,c1^3\,k3\,c2 \\
& \quad - 4\,k4\,c1^3\,k2\,c2 - 4\,k4\,c1^2\,c2^2\,k2 + 8\,k1\,c4\,k4\,c1^3 + 4\,k4\,c1^3\,c2\,k1
\end{aligned}
$$

Figure 3.2: Optimal Control Policy for 3D A-B-D Van de Vusse Example

Using the optimal control policy, the optimal DSRs can be computed using (2.6a). Once the DSRs that reside on the AR boundary have been established, the boundary can now be completed using PFR highways and mixing lines. The candidate AR boundary for the case study is solved a depicted in Figure 3.3. The boundary is also interpreted in terms of reactor structures.
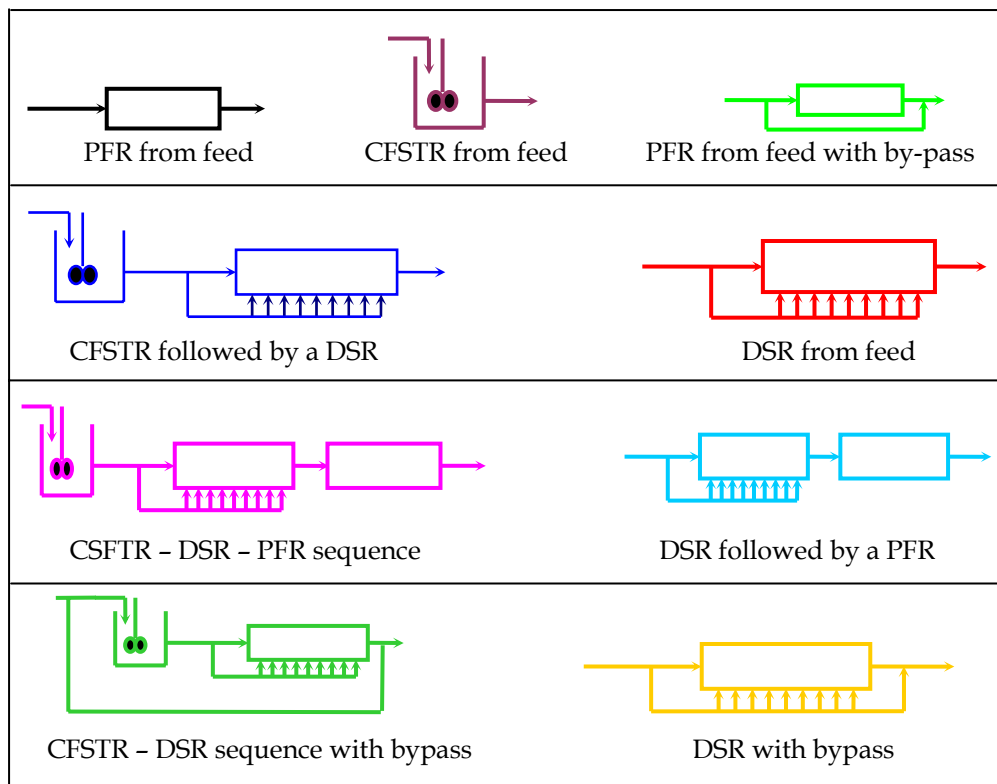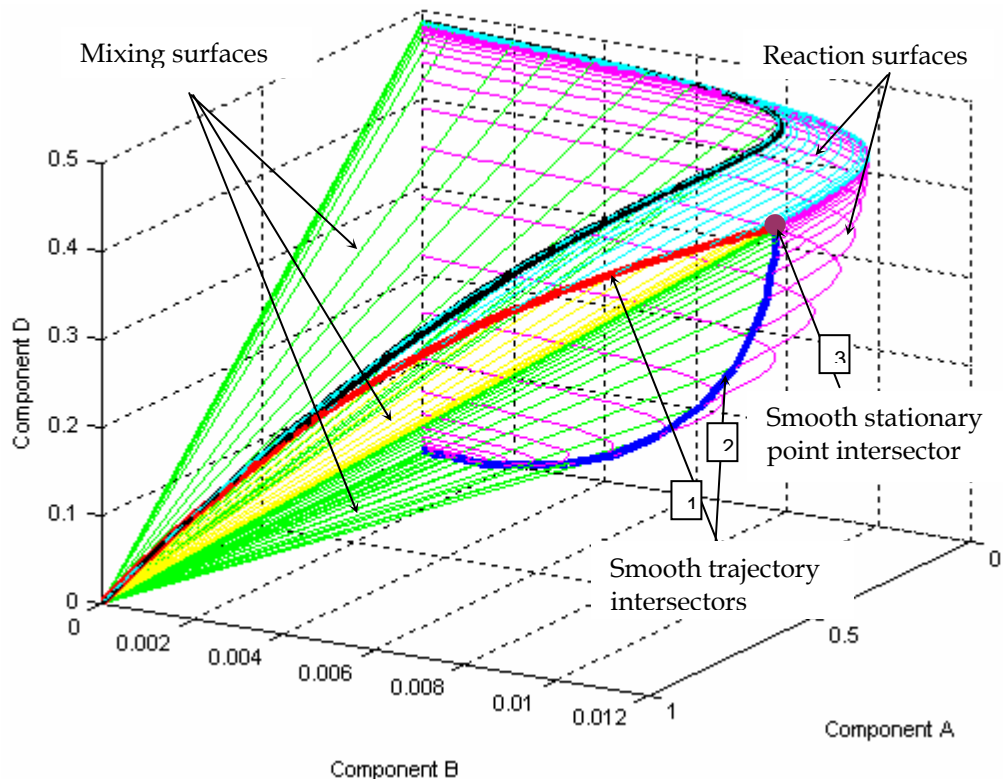
Figure 3.3: 3D ARᶜ for a Van de Vusse Example

The structure of the candidate AR boundary for this example consists of reaction and mixing process surfaces that are formed by the unions of reaction trajectories (PFRs) and mixing lines respectively. These process surfaces can be envisaged as connected by or emanating from the smooth connectors. These connectors are the optimal DSR trajectories 1 and 2, and optimal CFSTR point denoted by number 3.

3.4 Recursive Convex Control Policy (RCC) Algorithm

3.4.1 Mathematical Definitions

In this section we review some mathematical definitions pertaining to the convexity of the AR boundary. We review the points that are of special significance such as mixing points and points from which optimal process combination trajectories emanate. Some ideas discussed herein are arrived at in the light of the work of Feinberg and Hildebrandt (1997). The definitions in this section are specific and may lack some generality as they are based on finite discretised points in space.

Convexity

In the Euclidean space R^N, a set C is termed convex if and only if any two points x_1 and x_2 where $x_1, x_2 \in C$ are such that $\lambda x_1 + (1 - \lambda)x_2 \in C$ wherever $0 \leq \lambda \leq 1$. Thus, C is convex if and only if a convex combination of any two of its elements lies entirely in C. In simple geometric terms a set is convex if it contains all the line segments connecting any pair of its points (Lay, 1982).

Convex Hull

A convex hull of a set C, *conv C*, is the smallest convex set containing all points of C. In geometric terms, a convex hull in R^N is a finite convex

polytope enclosed by a finite number of hyperplanes. A convex hull in 3D is the smallest polyhedron enclosed by triangular planar facets such that all the elements lie on or in the interior of the polyhedron. In four dimensions, a convex hull is a polychoron enclosed by quadrilateral hyperplanar facets. We will call the points forming the vertices of the facets vertex points. Convexifying a set C finds the vertices of the convex hull of C. Each vertex point on a 3D convex hull is connected to a minimum of 3 other vertex points by line segments such that each vertex point serves as a vertex to at least 3 triangular facets that enclose the convex hull. In 4D a vertex point is connected to a minimum of four vertex points and this progression carries on to higher dimensions (Kelley and Weiss, 1979).

Lower Dimensional Projection

An N-dimensional convex hull when projected into M-dimensional space with $M<N$ remains a convex polytope enclosed by facets with N edges (Barvinok, 2002). However not all of the extreme points of the N-dimensional polytope will remain on the convex hull of the M-dimensional projection (Barvinok, 2002). An example of this theory is that of a three-dimensional sphere that becomes a circle when projected into two dimensions, with some of the sphere's extreme points lying in the interior of the circle.

Extreme Points

A point x is an extreme point if it is a vertex of the convex hull. An extreme point does not lie in the interior of any line segment bounding the facets of the polytope. In particular, $x \in C$ is extreme if there exists no points x_1, $x_2 \in C$, such that $\lambda x_1 + (1 - \lambda)x_2 = x$ with $0 < \lambda < 1$.

Generating Extreme Points

A generating extreme point in Euclidean space R^N, is an extreme point that forms a vertex to M facets such that M > N. In three dimensional space a generating extreme point forms a vertex to more that three triangular facets and the progression is carried on to higher dimensions (Kelley and Weiss, 1979; Manning, 1956).

3.4.2 Theory and Formulations

Consider a system with two permitted fundamental processes in some state space *c*, made up of all system state variables such as compositions and temperature. If we denote two process to be

Fundamental process one: *$p_1(c)$*

Fundamental process two: *$p_2(c, c^*)$*

The second process *p_2*, also depends on some other state *c^**, which should be attainable, thus it is a state that has already been attained or will be attained later by a fundamental process or a combination thereof.

The two processes can be combined with the use of a control policy *α*, to obtain a generalised net process vector that describes how state *c* changes with residence time as;

$$ \boldsymbol{p} = \frac{d\boldsymbol{c}}{d\tau} = \boldsymbol{p}_1(\boldsymbol{c}) + \alpha \boldsymbol{p}_2(\boldsymbol{c}, \boldsymbol{c}^*) \tag{3.3} $$

τ is the residence time of the processes.

For a given system with feed conditions *c^0*, the attainable regions can be found by obtaining the optimal combination of fundamental processes described by equation 3.3 as previously explained in Chapter 2. Once the

optimal control policies for the combinations of fundamental processes have been identified, their optimal trajectories can be used to navigate along the AR^C boundary to provide pathways to manifolds and surfaces of single process operation that make up the AR boundary such as reaction extreme high-ways, and mixing and heat exchange surfaces.

In the next section we provide a conceptually simple but powerful technique of finding optimal control policies for combinations of processes.

3.4.3 The Algorithm: Modus Operandi

The recursive convex control policy (RCC) algorithm uses non-negative scalar values for the process combination control policy, α to identify convex combinations of two processes. The novelty of this approach lies in the use of combinations of fundamental processes applied to the available feed to construct candidate attainable regions for a system with given kinetics, without the use of known necessary conditions. Also this approach interprets the structure of the AR boundary to primarily consist of optimal processes combinations, which once identified the shape of the boundary can be completed by separate process surfaces. The RCC algorithm grows the boundary of the AR^C from the *interior* as in the systematic techniques proposed by McGregor (1998), Rooney (2000), Burri (2000), and Kauchali (2001). Thus, the *lower* or *inner bounds* of the AR^C is approximated when compared to the upper bounds AR method suggested by Abraham and Feinberg (2004), where the candidate boundary was grown from the *exterior*.

The RCC algorithm uses scalar values to delineate instantaneous α values along the optimal process combination trajectories. These scalar values can be an arbitrarily chosen grid of values ranging from zero to very large

value, depending on the system. In the case where the control policy is bounded, the grid is chosen between the lower and upper boundaries. For reaction and mixing, the optimal control profile represents the differential side stream reactor (DSR). A DSR with an α value that equals zero is equivalent to a PFR and as previously stated in the preceding chapter, when the overall rate turns to zero the DSR becomes a stationary point, mathematically equivalent to a CFSTR.

The algorithm comprises steps as detailed below,

1. The initialisation stage: This stage generates the starting state points. The single process operation trajectories are generated from all system feed states and convexified to locate all extreme state points that form the convex hull and eliminate all interior state points. Convexification is carried out in the dimension which the candidate AR is targeted to be built in. From the resulting structure, a grid of extreme points is selected for use as starting points and some to use as c^* points which process p_2 in 3.1 depends on. For a case where fundamental process p_2 represents mixing, these points will be mixing points.

The class of c^* points include all feed states and all state points that are generating extreme points as defined in section 3.3.1. To illustrate this we consider process p_2 being the mixing process, the state c^* will connect all mixing vectors $v = (c^* - c)$ forming the mixing surface. As the mixing surface may contain infinitely many mixing vectors, all connecting to the mixing point, the point c^* which is a mixing point will serve as a vertex to infinitely many facets.

The optimal process combination profiles can only start from state points that satisfy conditions of optimality $\varphi = 0$ (Chapter 2 section 2.5.6 equation 2.11) as the starting points themselves must be on the profile. From the set of states generated in the initialisation stage the starting points include all points where process vectors are zero;

$p_1(c) = 0$

$p_2(c, c^*) = 0$

These points satisfy the condition for optimality, $\varphi = 0$ as can be seen that the determinant below will be fixed at zero for if the two process vectors p_1 and p_2 take zero values;

$$\varphi = \det\left\{p_2(c,c^*), p_1(c), \left(dp_1(c)p_2(c,c^*) - dp_2(c,c^*)p_1(c)\right)\right\}$$

For a combination of reaction and mixing processes, the potential starting points include all reaction equilibrium points where the reaction vector $r(c) = 0$ and all mixing points where the mixing vector $v(c,c^*) = 0$.

2.   Growth Stage: This stage generates a grid of process operation control policy values such that $\alpha = [\ 0, \alpha_1, \alpha_2, \ ... \ \alpha_{large}]$. It is also possible to define the values of the control policy such that $0 \leq \alpha \leq 1$. The control bounds should be used in cases where they are provided. From each starting point, for each control policy value using each of c^* states, a number of process combination profiles are generated. The structure is then convexified to eliminate all interior points. From all extreme points that are process combinations output states, single process trajectories are generated and the resulting data set is convexified. Only the extreme points that are output state results from combinations of

processes are stored for the next stage. In cases where the objective is evident, as in single reversible reaction processes where the AR is constructed to maximise conversion, instead of using convexification, the process combination profiles are generated to optimise the objective function. Those states where the objective function is optimal are taken as extreme points.

At this point the existence of process combination profiles on the boundary of the convex hull can be readily observed from the resulting structure. This stage serves satisfactorily for approximate calculations of finding reactor structures where accurate process parameters are not crucial or in the more usual cases where there is considerable uncertainty in the kinetic data. In the case where the growth stage results in an empty incremental set the algorithm is terminated and the candidate AR boundary comprises only single process operation regions.

3.   Iteration Stages: From each extreme point that is an output state from combinations of fundamental processes, for each in c^* class, two process combination profiles are generated. From an extreme point where the control policy is α_i, the first process combination profile should have a control policy with a value of $(\alpha_{i-1} + \alpha_i)/2$ and the second profile should have control policy with a value of $(\alpha_{i+1} + \alpha_i)/2$. This step refines using mid-point interpolation and as a result populates the control policy grid with more values. The data set is then convexified to locate all extreme state points that enclose the convex hull and eliminate all interior state points.

The iteration stage is repeated until the termination criterion is satisfied. The termination criterion cannot be generalised as it depends on the type of problem being solved. Volume percentage growth can be used for some

problems and for others it cannot be exclusively used as the volume reaches 99% of the expected candidate region after stage 2 and the growth rate drops below 0.2% for the first iteration. Standard deviation techniques can also be coupled into the termination criterion for some problems, specifically for those where the accuracy of the optimal profile is a concern. The use of different termination criteria for different cases will be illustrated with the use of case studies in subsequent chapters.

> 4.   Final Stage: From all extreme points that are output states to combinations of fundamental processes combinations output states, single process trajectories are generated to complete the AR^C. For a system where the permitted fundamental processes are reaction and mixing, the simple process trajectories will be PFR highways, reaction surfaces and mixing lines.

For a system with feed states

$$C^0 = [c^1,\ c^2\ ...c^M]$$

The permitted fundamental processes are p_1 and p_2 which can be combined to form the general process combination p defined by (3.3).

The mathematical model of the algorithm can be written out as

---

Stage 1: Initialisation Stage
  For i = 1…M
  Solve $c^i_1(\tau)$ and $c^i_2(\tau)$
    subject to

$$\frac{dc_1(\tau)}{d\tau} = p_1(c(\tau))\ \text{given } c = C^0(i),\ \tau = 0$$

$$\frac{dc_2(\tau)}{d\tau} = p_2(c(\tau))\quad \text{given } c = C^0(i),\ \tau = 0$$

  end

$$C = [c_1^1, c_2^2, \ldots c_1^M, c_2^1, c_2^1, \ldots, c_2^M]$$

$$C = C_{extreme} = conv\ (C) \qquad \text{or} \qquad C(\tau)_{Extreme} = \big(C(\tau)\big)_{optimum\_f(C)}$$

where f(c) is the objective function

$$C^* = [C^0, generating\_extreme(C)]$$

$$C^{start} = [C(p_1=0),\ C(p_2=0)]$$

Stage 2: Growth Stage

$\alpha = [\ 0,\ \alpha_1,\ \alpha_2,\ \ldots\ \alpha_{large}]$

For all α, for all C^*, for all C^{start}
        Solve c subject to

$$\frac{dc}{d\tau} = p_1(c) + \alpha p_2(c, c^*)$$

C = [all c]

$$C = C_{extreme} = conv(C) \text{ or} \qquad C(\tau)_{Extreme} = \big(C(\tau)\big)_{optimum\_f(C)}$$

where f(c) is the objective function

Stage 3: Iteration Stage

Repeat
    For all C^{start},   for all C^*
        For α = (α_{i+1}+ α_i)/2 and α = (α_{i-1}+ α_i)/2
        Solve c subject to

$$\frac{dc}{d\tau} = p_1(c) + \alpha p_2(c, c^*) \text{ using } c^0 = c_i,\ \tau^0 = \tau_i$$

C = [all c]

$$C = C_{extreme} = conv(C) \text{ or} \qquad C(\tau)_{Extreme} = \big(C(\tau)\big)_{optimum\_f(C)}$$

where f(c) is the objective function

Stage 4: Final Stage

For all C
    Solve $c^i{}_1(\tau)$ and $c^i{}_2(\tau)$
        subject to

$$\frac{dc_1(\tau)}{d\tau} = p_1(c(\tau)) \qquad c = C\ (i),\ \tau^0 = \tau_i$$

$$\frac{dc_2(\tau)}{d\tau} = p_2(c(\tau)) \qquad c = C\ (i),\ \tau^0 = \tau_i$$

To demonstrate the systematic formulation of the RCC algorithm we will consider an example we solved in section 3.3 of this chapter.

3.5 3D Example: Numerical Solution

3.5.1 Formulation

The example studied here considers fundamental processes of reaction and mixing in an isothermal system with constant density. The objective of this example is to identify a three-dimensional A-B-D candidate AR by solving a four dimensional stoichiometric A-B-C-D system. From the Van de Vusse kinetics depicted in Figure 3.1 the algorithm formulation can be detailed as follows. We first start by defining the feed state and fundamental process as shown below:

$$\text{Feed state} \qquad c^0 = \begin{bmatrix} c_A^0 \\ c_B^0 \\ c_C^0 \\ c_D^0 \end{bmatrix} = \begin{bmatrix} 1 \\ 0 \\ 0 \\ 0 \end{bmatrix}$$

$$\text{Reaction process} \qquad p_1 = r(c(\tau)) = \begin{bmatrix} r_A \\ r_B \\ r_C \\ r_D \end{bmatrix} = \begin{bmatrix} -k_1 c_A - 2k_4 c_A^2 + k_2 c_B \\ k_1 c_A - k_2 c_B - k_3 c_B \\ k_3 c_B \\ k_4 c_A^2 \end{bmatrix}$$

$$\text{Mixing process} \qquad p_2 = v(c(\tau), c^*) = \begin{bmatrix} c_A^* - c_A \\ c_B^* - c_B \\ c_C^* - c_C \\ c_D^* - c_D \end{bmatrix}$$

The formulation of the algorithm is detailed below along with the resulting structures after every stage.

Stage 1

Solve the PFR trajectory $c_1(\tau) = [c_A(\tau), c_B(\tau), c_C(\tau), c_D(\tau)]$

Subject to

$$p_1 = r(c(\tau)) \quad given \ c(\tau = 0) = c^0$$

Solve the CFSTR locus $c_2(\tau) = [c_A(\tau), c_B(\tau), c_C(\tau), c_D(\tau)]$

Subject to

$$\begin{bmatrix} c_A - c_A^0 \\ c_B - c_B^0 \\ c_C - c_C^0 \\ c_D - c_D^0 \end{bmatrix} = \tau \begin{bmatrix} -k_1 c_A - 2k_4 c_A^2 + k_2 c_B \\ k_1 c_A - k_2 c_B - k_3 c_B \\ k_3 c_B \\ k_4 c_A^2 \end{bmatrix} \quad for \ \ 0 \le \tau \le \infty$$

$$C(\tau) = [c_1(\tau), c_1(\tau), c^0]$$

$$C(\tau) = C(\tau)_{Extreme} = conv(C(\tau))$$

$$C^* = [c^0, generating\_extreme(C(\tau))]$$

$$C^{start} = [C(r(c) = 0), C(v(c, c^*) = 0)]$$

In this stage, four differential equations were solved to attain the PFR trajectory from the specified system feed. The differential equation solver method used in the RCC formulation is the MATLAB® built-in ODE45 algorithm based on explicit Runge-Kutta (4, 5) formula. The differential equations were solved over a residence time span ranging from the feed at $\tau = 0$, to the equilibrium point where all four differential equations diminished to zero. For each composition variable, 397 points were solved and the equilibrium point was approximated at $\tau = 18.19$ minutes.

For set of four non-linear equations describing the CFSTR locus was solved using the standard Newton's method to evaluate 500 logarithmically spaced points with residence time span ranging from the

feed (τ = 0) to τ = 200 minutes. The upper residence time was chosen sufficiently large to approximate the equilibrium point. In total, 897 points were solved for stage 1.

The convex hull was solved using the MATLAB® built-in convhull solver based on the Qhull algorithm (Barber *et al.*, 1996). Upon convexification the number of points was reduced to 491 extreme points.

The convex hull resulting from the convexification of the output states of the PFR and CFSTR is shown in Figure 3.4. The triangular facets forming the three dimensional convex hull can be visualised on the boundary of the structure with extreme points forming vertices to the facets. The feed point is indicated as a generating extreme point forming a vertex to more than 3 facets.
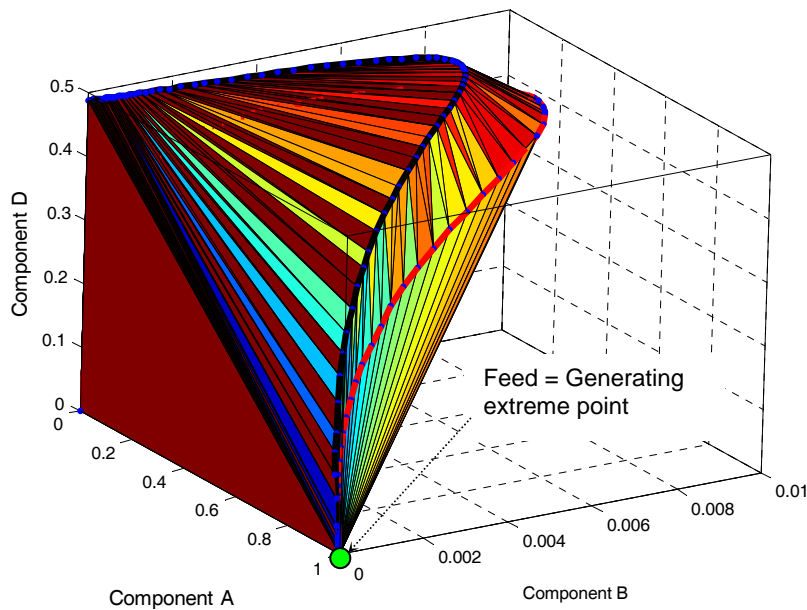
Figure 3.4: A convex hull resulting from stage 1 of the 3D AR construction

Figure 3.5 depicts and rotation of Figure 3.4 to expose the equilibrium point where the reaction vector diminishes to zero. This point is also a generating extreme point as it is a vertex to more than three facets.
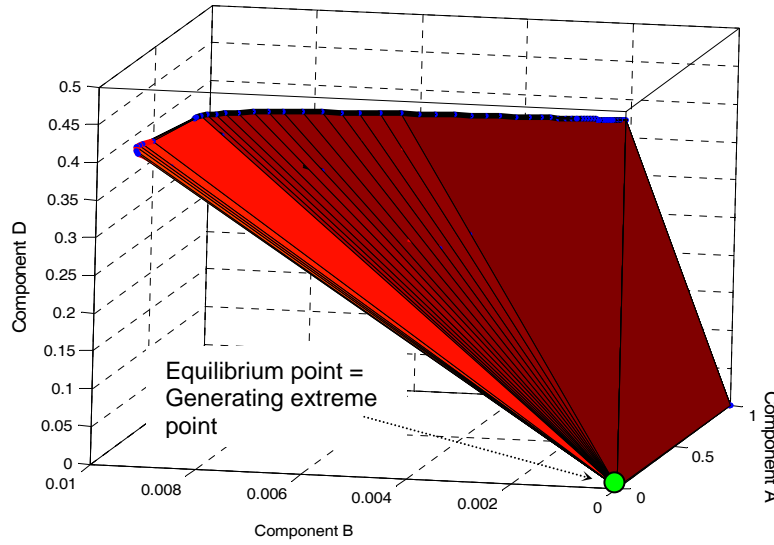
Figure 3.5: A convex hull resulting from stage 1 of the 3D AR construction

As discussed earlier the feed and equilibrium points are the potential starting points for the DSR profiles as they both satisfy the condition of optimality. These points are also generating extreme points and will therefore be considered as the DSR starting points and mixing points.

Stage 2

Solve $c(\tau) = [c_A(\tau), c_B(\tau), c_C(\tau), c_D(\tau)]$

$$\alpha = [0, \alpha_1, \alpha_2, ..., \alpha_\infty]$$

$$\left[\frac{dc(\tau)}{d\tau}\right] = r(c(\tau)) + \alpha(c(\tau), c^*)$$

$$\text{Given } c\left(\tau = \tau_i^{start}\right) = C^{start}(i)$$

$$C(\tau) = [c(\tau), C(\tau)]$$

$$C(\tau) = C(\tau)_{Extreme} = conv(C(\tau))$$

$$C^* = [c^0, generating\_extreme(C(\tau))$$

$$C^{start} = \left[C(r(c) = 0), C(v(c, c^*) = 0)\right]$$

For stage 2, 20 logarithmically spaced points between 0 and 500 were selected for the α-grid. This grid will be automatically refined and the bounds will be adjusted as may be necessary during the computation by the RCC algorithm (Section 3.4.2).

The convex hull obtained at the end of stage 2 is depicted in Figure 3.6 below. In this figure all the outputs states that remain on the boundary of the convex region are shown. Only the output states resulting from combination of reaction and mixing using the feed as the mixing point remain on the boundary of the convex hull. The output states resulting from the combination of reaction and mixing using the equilibrium point lie in the interior. At this stage the equilibrium point is omitted as a potential mixing point even though it is still a generating extreme point of the convex hull as it does not result in the extension of the boundary.
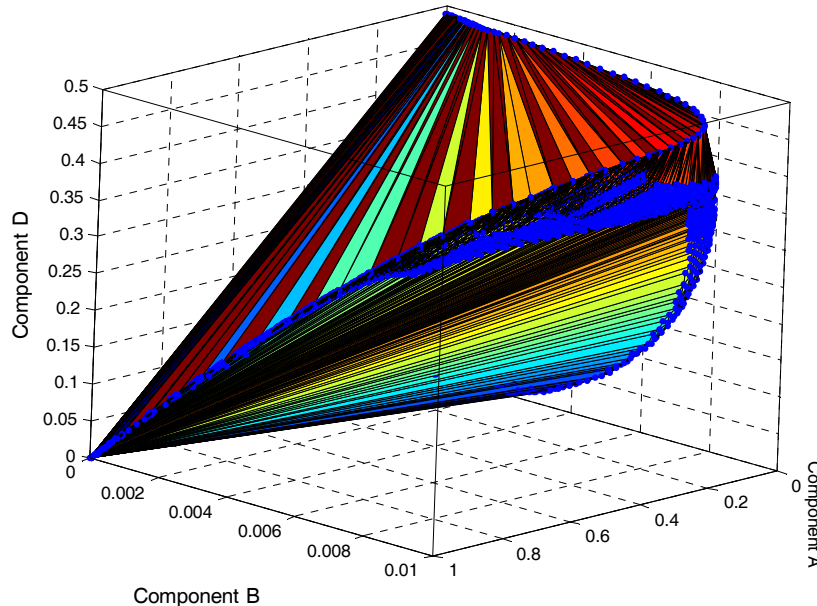
Figure 3.6: A convex hull resulting from stage 2 of the 3D AR construction

Figure 3.7 shows only the output states from the combinations of reaction and mixing that are extreme points of the convex hull.
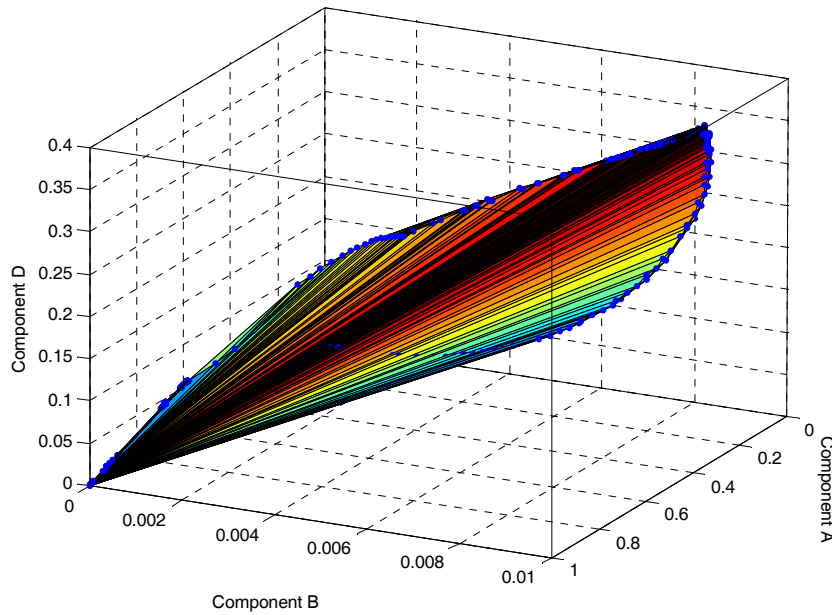
Figure 3.7: A DSR convex hull resulting from stage 2 of the 3D AR construction

At this stage it can be noted that the DSR structure is clearly identifiable and resembles that solved used analytical methods.

Using the feed point as the mixing point and the equilibrium and feed points as DSR starting points, the iteration stage can be started and the final candidate AR be obtained once the termination criteria are satisfied.

For this example the convex hull volume growth rate is used as the stopping criterion. The algorithm iteration step is terminated when the volume growth rate drops below a value of 0.1% of the total volume. The above RCC formulations were implemented in MATLAB® to solve the candidate AR in the A-B-D space.

3.5.2 Results

The candidate AR generated using the AR algorithm is shown in Figure 3.8. The AR^C boundary matches the one obtained via analytical methods in section 3.3, showing the same reactor structures.
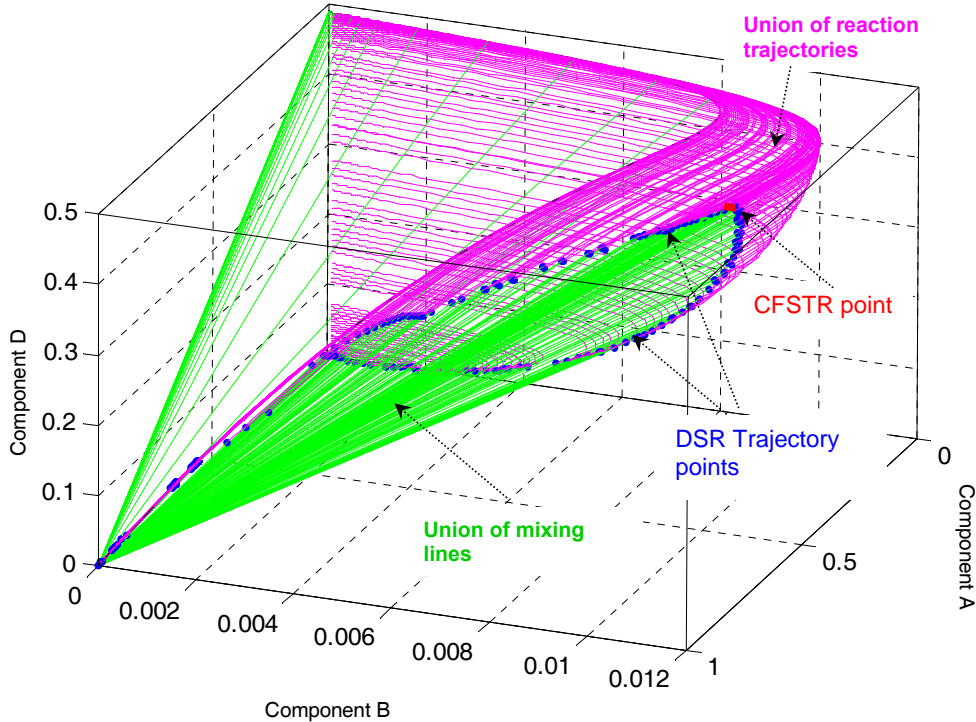
Figure 3.8: 3D Van de Vusse AR^C Constructed with the RCC Algorithm

The optimal trajectory for combination of reaction and mixing, i.e. the optimal DSR trajectory is delineated by points as indicated in Figure 3.8. The optimal CFSTR is also identified on the candidate AR boundary as was the case with the analytical computations.

Figure 3.9 shows how the RCC results approximate the analytical computation for optimal DSR profiles. The RCC algorithm returns a smooth approximate DSR profile with no scattered points.

Alpha vs Component A
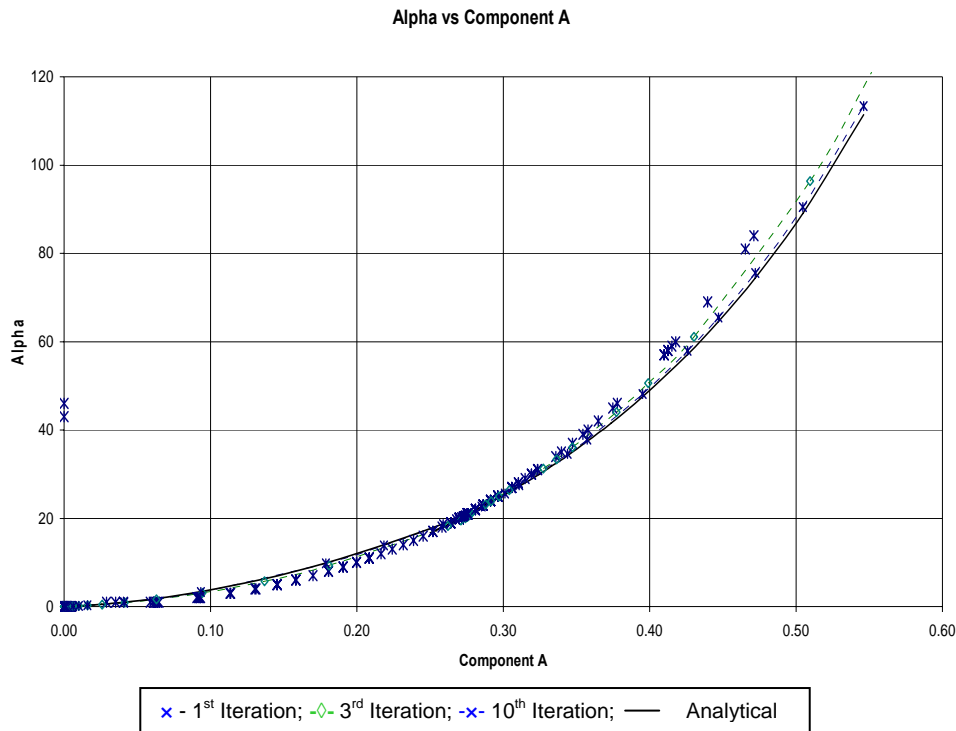
Figure 3.9: Optimal DSR Profile: Comparison of Techniques

For this example the algorithm run-time on a Pentium 4 2.5 GHz Intel computer with 256MB RAM is broken down as follows:

- Initialisation stage and Growth stage – 7 seconds
- First Iteration - 8 seconds
- Second Iteration - 15 seconds
- Third – Tenth Iteration – 4 min
- Polish Stage – 6 seconds

The AR^C volume growth rate dropped below 0.1% after the fifth iteration (2 minutes run-time). More iterations were performed to improve the accuracy of the DSR delineation and the results for ten iterations are shown in Figure 3.9. To quantify the deviation of the approximate optimal DSR profile from the analytical optimal profile, the percentage deviation error method was applied. The method uses the equation below to calculate the deviational error.

$$\%Error = \sum_{i=1}^{i=N_i} \frac{\left| \alpha_{anal}(\boldsymbol{C}) - \alpha_{approx}(\boldsymbol{C}) \right|}{\alpha_{anal}(\boldsymbol{C})} \times \frac{100}{N_i} \qquad (3.4)$$

Figure 3.10 shows how the value of the percentage deviational error diminishes with an increasing number of iterations. The error rapidly reduces in the early stages of the algorithm run and asymptotes to a low value of about 1% as the number of iterations increases further.
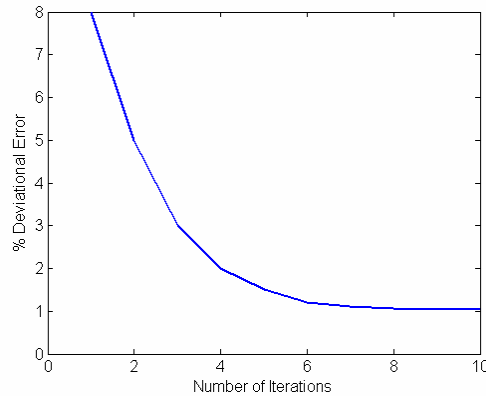
Figure 3.10: Algorithm Accuracy with Number of Iterations

3.6   4D Example

3.6.1   Background and Kinetics

In this example we demonstrate the straightforward application of the RCC algorithm to higher dimensional problems. This is illustrated using a four dimensional Van de Vusse type kinetics. The reaction scheme considered in this example is shown in Figure 3.11.

Reaction Network	Rate Expressions	Rate Constants
$A \underset{k_r=k_2}{\overset{k_f=k_1}{\leftrightarrow}} B \overset{k_3}{\to} C$		$k_1 = 1\,\text{min}^{-1}$
	$r_A = -k_1 C_A - 2k_4 C_A^2 + k_2 C_B$	$k_2 = 0.5\,\text{min}^{-1}$
$2A \overset{k_4}{\to} D$	$r_B = k_1 C_A - k_2 C_B - k_3 C_B - k_5 C_B + k_6 C_E$	$k_3 = 0.2\,\text{min}^{-1}$
	$r_D = k_4 C_A^2$	$k_4 = 20\,\frac{litre}{\min \cdot mol}$
$B \underset{k_r=k_6}{\overset{k_f=k_5}{\leftrightarrow}} E$	$r_E = k_5 C_B - k_6 C_E$	$k_5 = 0.3\,\text{min}^{-1}$
		$k_6 = 1.5\,\text{min}^{-1}$

Figure 3.11: 4D Van de Vusse reaction scheme with kinetics

Attainable regions analysis in four dimensions has so far been a research area that could only be speculated on. Nicol (1998) made some conjectures on the structure of four dimensional AR boundaries. Using the results from the quadrilateral hyper-planar facets of a four dimensional convex hull, Nicol (1998) stipulated that the CFSTR locus will lie entirely on the boundary of the AR. Feinberg (2000a & b) derived some groundbreaking analytical formulations for higher dimensional ARs. Feinberg (2000b) demonstrated with mathematical proofs that only special types of CFSTRs lie on the AR boundary. However due to the difficulty associated with starting different optimal DSR trajectories from a known stationary point, Feinberg (2000a & b) could not demonstrate graphically how the unions of optimal DSR trajectories formed hyper-surfaces in four or higher dimensions. The relationship between critical CFSTRs and unions of DSR trajectories could also not be asserted.

3.6.2 RCC Formulation Modifications

A convex hull four-dimensional space is enclosed by quadrilateral hyper-planar facets with four vertices. Each extreme point is connected to at least four other extreme points. Thus every extreme point forms a vertex to a minimum of four facets. The generating extreme points form vertices to more than four quadrilateral facets.

In four dimensions unions or families of smooth trajectory intersectors that are optimal process combination trajectories are expected to form hyper-surfaces from which four dimensional manifolds of reaction and mixing emanate. In this case, the RCC algorithm is expected to return a surface of points that demarcate families of optimal process combination trajectories not single trajectory curves as was for the three-dimensional example.

The algorithm formulation for this example is clear-cut and analogous to that of a three dimensional example studied in section 3.5. The intended AR is to be constructed in a four dimensional A-B-D-E space. Using the kinetic information in Figure 3.11 the algorithm was formulated and implemented in MATLAB®.

3.6.3 Results

In four-dimensional space the structure of the AR boundary can only be visualised by projecting into three dimensions. The 4D AR^C is visualised using four three-dimensional projections namely, A-B-D, A-B-E, A-D-E and B-D-E. From the properties of the AR boundary it is known that the 4D A-B-D-E structure has to be convex and the laws of convexity state that all four 3D projections of a 4D polychoron have to be convex polyhedrons (Barvinok, 2002). A three dimensional A-B-D projection of the candidate 4D A-B-D-E AR is shown in Figure 3.12.
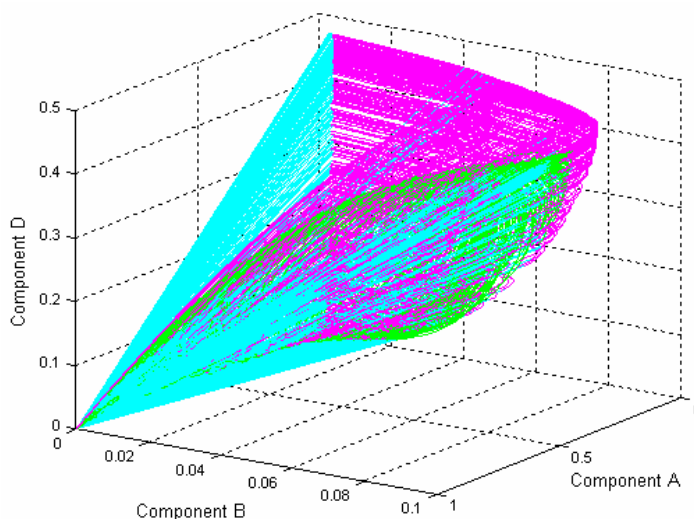
Figure 3.12: A Three Dimensional A-B-D Projection of the 4D A-B-D-E AR^C

The optimal DSR of this four dimensional example is not a single trajectory as is for a three dimensional example. In this case a family of curves forming a surface is observed in three dimensional projections. However in three dimensional projections most of this family of curves lie in the interior of the AR^C. Only specific curves of the family appear on the boundary as single trajectories connecting the mixing and the reaction surfaces.

The 3D A-B-E projection of the AR^C is depicted in Figure 3.13. This structure is convex as expected and also shows single trajectories of the 4D DSR family on the boundary, smoothly connecting the reaction and mixing surfaces. The A-D-E projection shown in Figure 3.14 and B-D-E projection in Figure 3.15 also exhibit the same properties.
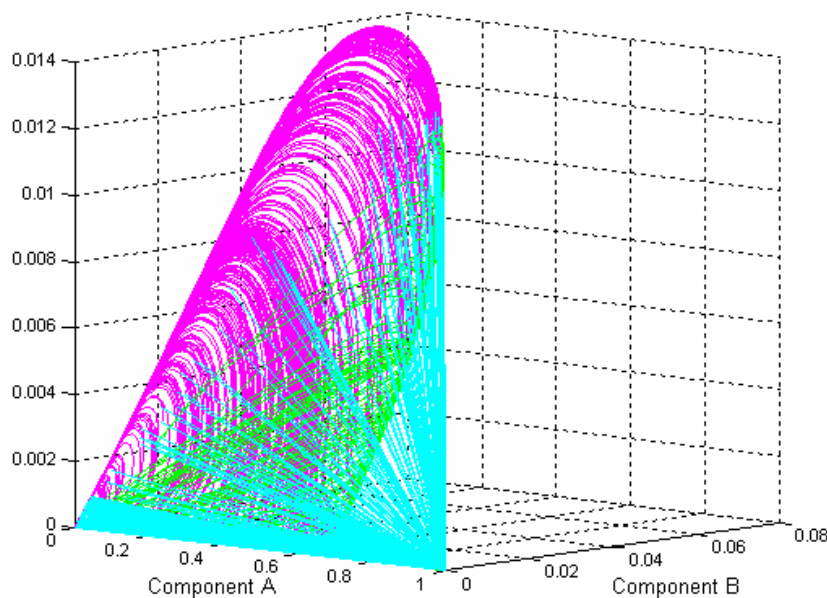
Figure 3.13: A Three Dimensional A-B-E Projection of the 4D A-B-D-E AR^C
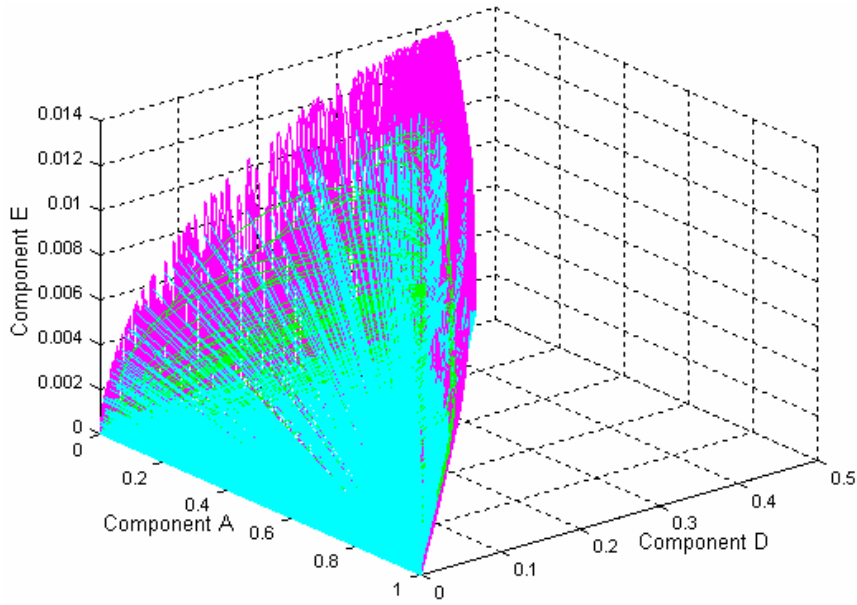
Figure 3.14: A Three Dimensional A-D-E Projection of the 4D A-B-D-E AR^C
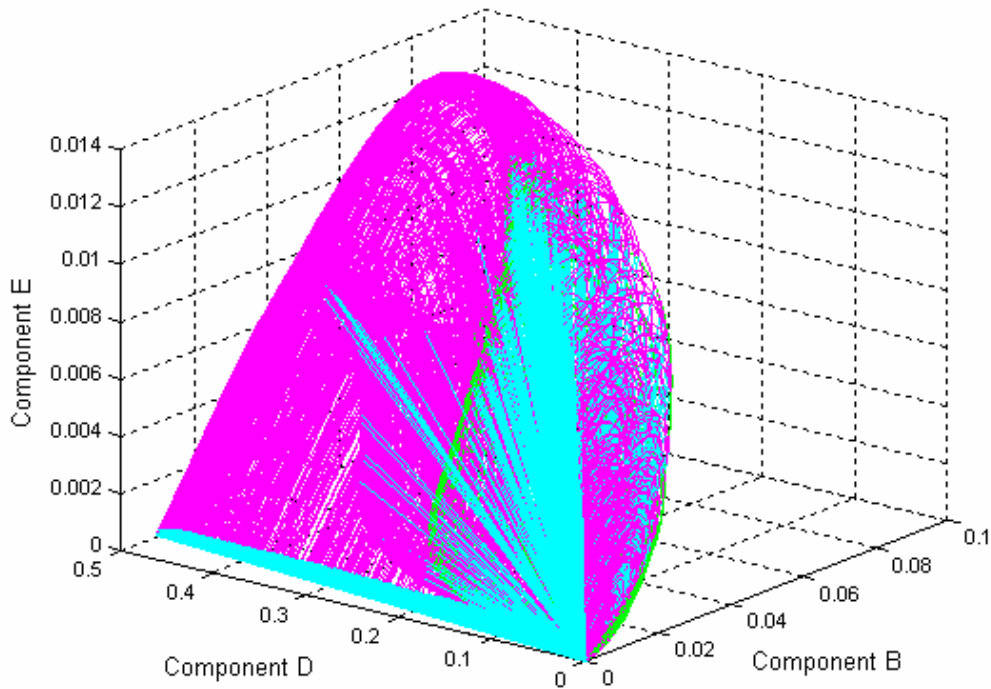
Figure 3.15: A Three Dimensional B-D-E Projection of the 4D A-B-D-E AR^C

For this example the occurrence of critical CFSTRs on the boundary of the AR^C is observed in four occasions corresponding to [C$_A$ (mol/l), τ (min)] = [0, τ^∞]; [0.11, 1.55]; [0.22, 0.35] and [1, 0]. The point $\tau = 0$ is simply the system feed which is also used as the mixing point and $\tau = \tau^\infty$ is the infinite

residence time CFSTR. This is indicated by the fact that the value of the determinant of the eigenvectors of the Jacobian matrix of the process vectors takes a zero value (equation 2.14 in section 2.5). This behaviour is displayed in Figure 3.16 where the determinant is evaluated along the locus of CFSTR stationary point and plotted against the concentration of component A.

These critical CFSTRs do not all appear on the boundary of the 3D AR^C projections. For example, the critical CFSTR labelled M in Figure 3.16 does not appear on the boundary of the A-B-D projection as it lies interior to the boundary of this projection. However, the critical CFSTR M lies on the boundary of the B-D-E projection.
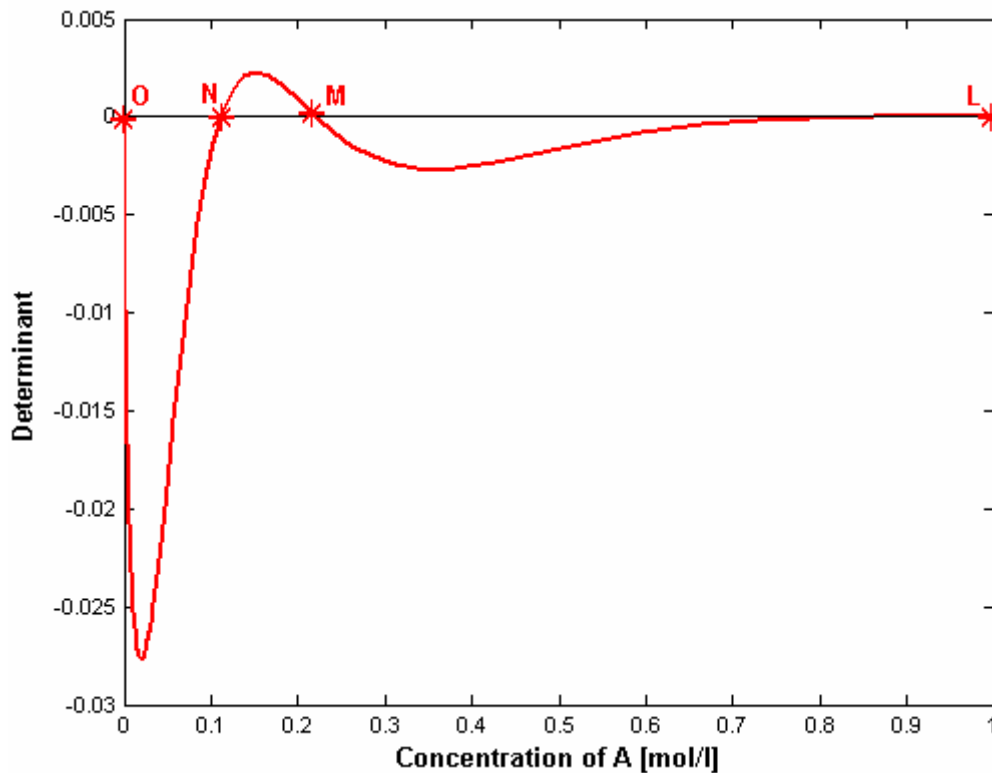
Figure 3.16: The Determinant Value along the CFSTR locus.
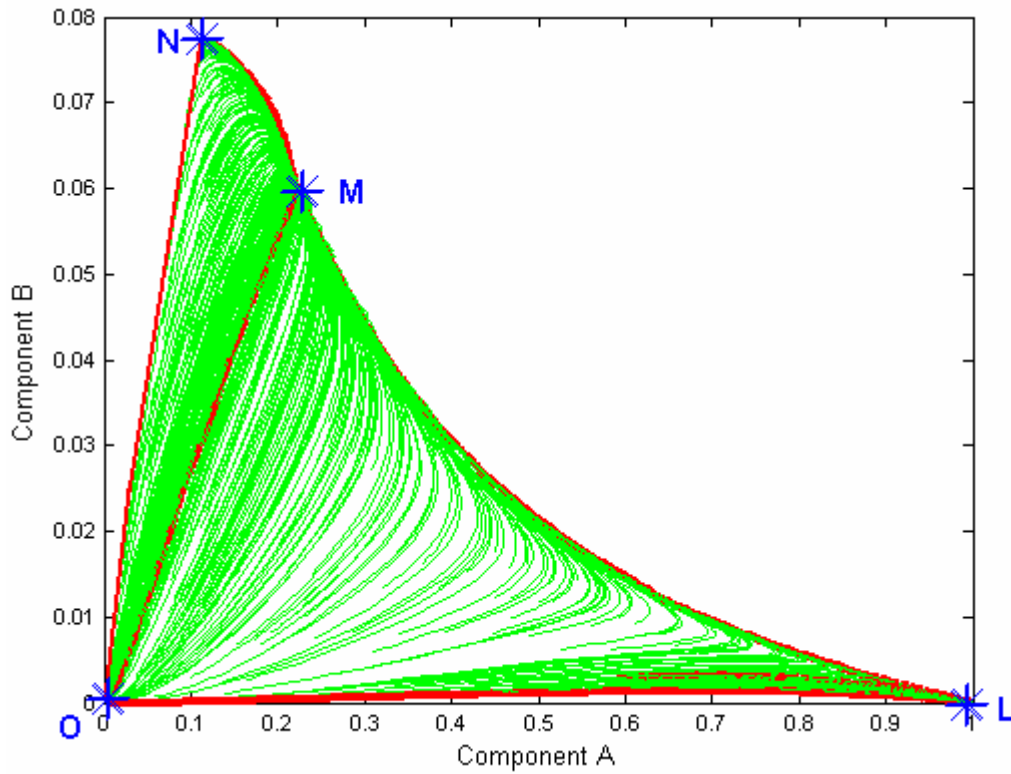
Figure 3.17: A 2D Map Showing the Topology of the Optimal DSR Family.

Figure 3.17 shows a 2D projection map of the family of optimal DSRs along with the critical CFSTRs. The critical CFSTRs play a vital role on the topology of the optimal DSR map. The critical CFSTR point **O** acts as an unstable (generating) node as all the optimal DSRs emanate from it. The CFSTR **M** is a stable (terminating) node. This behaviour can be seen in all projections of the A-B-D-E AR[C].

To fortify this observation the rules of topology are used. The optimal DSRs in the family are described by equation 2.6a in section 2.5.4.

$$\frac{dC_i}{d\tau} = r\big(C_i(\tau)\big) + \alpha(\tau)\big(C_i^* - C_i(\tau)\big) \hspace{3cm} \text{(2.6 a)}$$

From the qualitative theory of ordinary differential equations, singular points or nodes are characterised as the points where the vector space

disappears. This occurrence is observed when the right hand side of equation (2.6a) takes a zero value for all components such that equation (3.5) below is satisfied. (Eells, 1967)

$$r\big(C_i(\tau)\big)+\alpha(\tau)\big(C_i^{*}-C_i(\tau)\big)=0 \qquad (3.5)$$

Point **M**, in Figure 3.17 exhibits this behaviour. The individual terms in equation (3.5), $r(C_i(\tau))$ and $\alpha(\tau)(C_i^{*}-C_i(\tau))$ do not necessarily take zero values but their summation amounts to zero. At point **O**, the reaction term, $r(C_i(\tau))$ is fixed at zero for all components as this is an equilibrium point and the value of the optimal mixing policy, $\alpha(\tau)$ is fixed at zero for all optimal DSRs. This results in the mixing term, $\alpha(\tau)(C_i^{*}-C_i(\tau))$ taking a zero value and equation (3.5) being satisfied. The two points **M** and **O** are therefore clearly singular points.

To further classify the singular points **M** and **O** we take another look at the theory of differential equations. The Jacobian matrix **J**, of the set of four differential equations (3.6)

$$
\begin{aligned}
\frac{dC_A}{d\tau} &= r_A + a(\tau)\big(C_A^{*}-C_A\big)\\[4pt]
\frac{dC_B}{d\tau} &= r_B + \alpha(\tau)\big(C_B^{*}-C_B\big)\\[4pt]
\frac{dC_D}{d\tau} &= r_D + \alpha(\tau)\big(C_D^{*}-C_D\big)\\[4pt]
\frac{dC_E}{d\tau} &= r_E + \alpha(\tau)\big(C_E^{*}-C_E\big)
\end{aligned}
\qquad (3.6)
$$

is given by a 4-by-4 matrix of partial derivatives in equation (3.7) below;

$$J = \begin{bmatrix} \dfrac{\partial}{\partial C_A}\left[\dfrac{dC_A}{d\tau}\right] & \dfrac{\partial}{\partial C_B}\left[\dfrac{dC_A}{d\tau}\right] & \dfrac{\partial}{\partial C_D}\left[\dfrac{dC_A}{d\tau}\right] & \dfrac{\partial}{\partial C_E}\left[\dfrac{dC_A}{d\tau}\right] \\[2ex] \dfrac{\partial}{\partial C_A}\left[\dfrac{dC_B}{d\tau}\right] & \dfrac{\partial}{\partial C_B}\left[\dfrac{dC_B}{d\tau}\right] & \dfrac{\partial}{\partial C_D}\left[\dfrac{dC_B}{d\tau}\right] & \dfrac{\partial}{\partial C_E}\left[\dfrac{dC_B}{d\tau}\right] \\[2ex] \dfrac{\partial}{\partial C_A}\left[\dfrac{dC_D}{d\tau}\right] & \dfrac{\partial}{\partial C_B}\left[\dfrac{dC_D}{d\tau}\right] & \dfrac{\partial}{\partial C_D}\left[\dfrac{dC_D}{d\tau}\right] & \dfrac{\partial}{\partial C_E}\left[\dfrac{dC_D}{d\tau}\right] \\[2ex] \dfrac{\partial}{\partial C_A}\left[\dfrac{dC_E}{d\tau}\right] & \dfrac{\partial}{\partial C_B}\left[\dfrac{dC_E}{d\tau}\right] & \dfrac{\partial}{\partial C_D}\left[\dfrac{dC_E}{d\tau}\right] & \dfrac{\partial}{\partial C_E}\left[\dfrac{dC_E}{d\tau}\right] \end{bmatrix}$$

$$(3.7)$$

The eigenvalues of matrix *J* are four values contained in a 4-by-1 matrix λ, such that the determinant relationship in equation (3.8) below is satisfied;

$$\det (J - \lambda I) = 0 \qquad\qquad (3.8)$$

where *I* is a 4-by-4 identity matrix.

Eells (1967) states that

- If the vector field terminates at a singular point (all eigenvalues of the Jacobian matrix are negative), that singular point is a stable node

- A singular point from which a vector field emanates (all eigenvalues of the Jacobian matrix are positive) is termed an unstable node.

- A singular point from which some vectors emanate and others terminate (eigenvalues of the Jacobian matrix have mixed signs) is called a saddle point.

Evaluating all four eigenvalues for a differential equation set

$$\frac{dC_A}{d\tau} = r_A + a(\tau)\left(C_A^* - C_A\right)$$

$$\frac{dC_B}{d\tau} = r_B + \alpha(\tau)\left(C_B^* - C_B\right)$$

$$\frac{dC_D}{d\tau} = r_D + \alpha(\tau)\left(C_D^* - C_D\right) \tag{3.6}$$

$$\frac{dC_E}{d\tau} = r_E + \alpha(\tau)\left(C_E^* - C_E\right)$$

The rate expressions are as shown in Figure 3.11 with corresponding rate constants and mixing policy values are as computed by the RCC algorithm.

The four eigenvalues for point **O** are found to be all positive classifying the singular point as an unstable node. This is supported by the behaviour of the optimal DSR curves originating from point **O**. Point **M** has all four eigenvalues negative and therefore it is a stable node and is made evident by all optimal DSR curves terminating there. Points **L** and **N** are singular points in the same way point **M** is. The singularity of these points is as discussed in section 2.5.5 that the reaction vector is collinear and points in the opposite direction to the mixing vector. The condition is such that

$$-\mathbf{r}(\mathbf{c}) = \frac{1}{\tau}\left(\mathbf{c}^0 - \mathbf{c}\right) \tag{3.8}$$

With the mixing policy taking a value $\alpha = \dfrac{1}{\tau}$, condition 3.5 is satisfied. The eigenvalues evaluated at the two points, **L** and **N** take mixed signs as two in each are positive and two negative. This gives a classification of the two points as saddle points.

The computational aspects of the RCC algorithm for the above four-dimensional example are detailed below. The computation was carried out on a Pentium 4 2.5 GHz Intel computer with 256MB RAM.

- Initialisation and growth stage – 57 seconds
- First Iteration – 50 seconds
- Second to Fourth Iteration – 182 seconds
- Fifth Iteration – 74 seconds
- Final Stage – 31 seconds

Total – 6 minutes 34 seconds

The termination criterion used in this case was the hyper-volume growth rate which dropped below 0.1% after the fourth iteration.

To validate the results, analytical formulations for conditions required for optimality were checked for consistency (Chapter 2, Feinberg 2000 a & b). The φ condition for four dimensions considering only reaction and mixing was computed. The results are shown in Figure 3.18. The φ value was computed for each iteration to illustrate how the RCC algorithm arrives at the solutions. As the results show the φ value effectively remained fixed at zero after the 5th iteration, indicating that the DSR points computed lies on the φ surface as required by conditions of optimality.
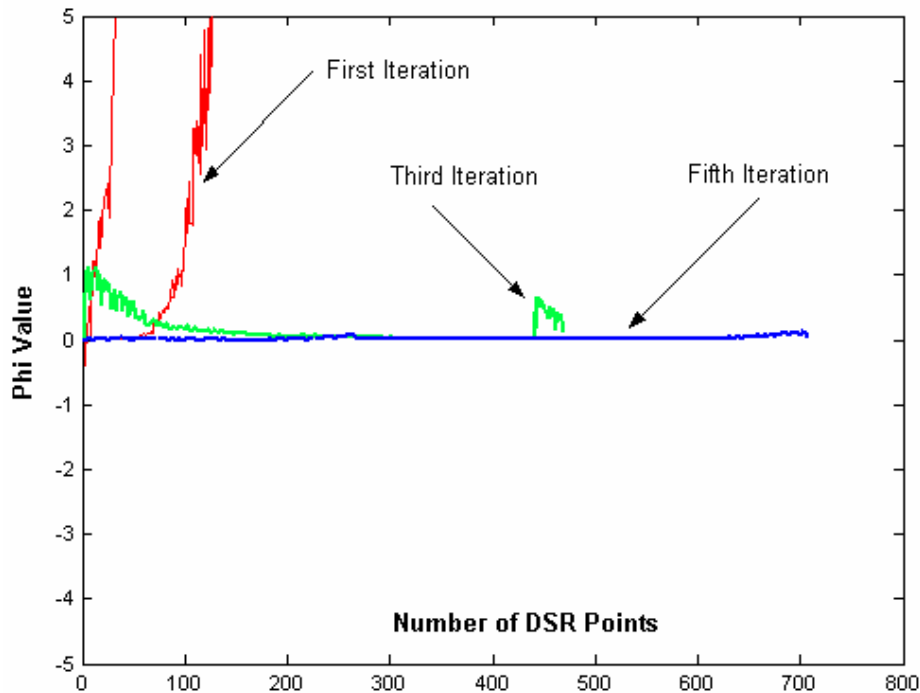
Figure 3.18: The Variation of the Phi Condition with the Number of Iterations

3.6.4 4D Objective Function Optimisation

Once the boundary of the AR has been identified it is often necessary to find a reactor network that optimises a given objective function. Optimisation of an objective function for two-dimensional ARs has been demonstrated to be straightforward (McGregor, 1998). In this work we demonstrate how to find a reactor network structure that optimises a given objective function in four–dimensional space using the RCC algorithm.

Consider a reaction scheme given in Figure 3.11 and the resulting three-dimensional projections of the four-dimensional candidate AR depicted in Figures 3.12 – 3.15. The feed to the system is pure A and the valuable products from the system are considered to be B, D and E. Component C is a valueless by-product that should be minimised. Consider an objective

function of the system that represents some profit generated from products B, D and E and loss of reactant A due to formation of C. The profit function can be given as some theoretical function of concentration as follows;

$$P_{profit} = C_B + C_D{}^{0.5} + C_E{}^{0.5} - C_A C_C{}^{0.5} \qquad (3.9)$$

This profit function is hypothetical and does not necessarily have realistic significance as it is for demonstration purposes.

The profit is expected to be maximised at the point where the profit curve intersects the boundary of the A-B-D-E attainable region. As it is impossible to visualise this in four dimensions, three-dimensional projections will be used with the understanding that the maximum profit point may lie in the interior of the projections (Barvinok, 2002).

The point that gives the highest value of the profit function given by (3.9) is found to be an extreme point on the AR^C at concentrations of

$$[C_A, C_B, C_C, C_D, C_E] = [0.1005, 0.07789, 0.0055, 0.4022, 0.01171]$$

At this point the profit value is 0.8128. The reactor network layout that can be used to attain this maximum profit concentration is that of a CFSTR-DSR-PFR sequence

The sequence of unit operations is obtained by tracing the fundamental processes used to attain the maximum profit state point from the feed state point.

Figure 3.19 illustrates how the profit function intersects the boundary of the AR at the maximum profit point on the A-B-D projection. By coincidence this point lies on the boundary of the three-dimensional A-B-D projection as it can be observed from the two boundaries tangentially intersecting at one point.
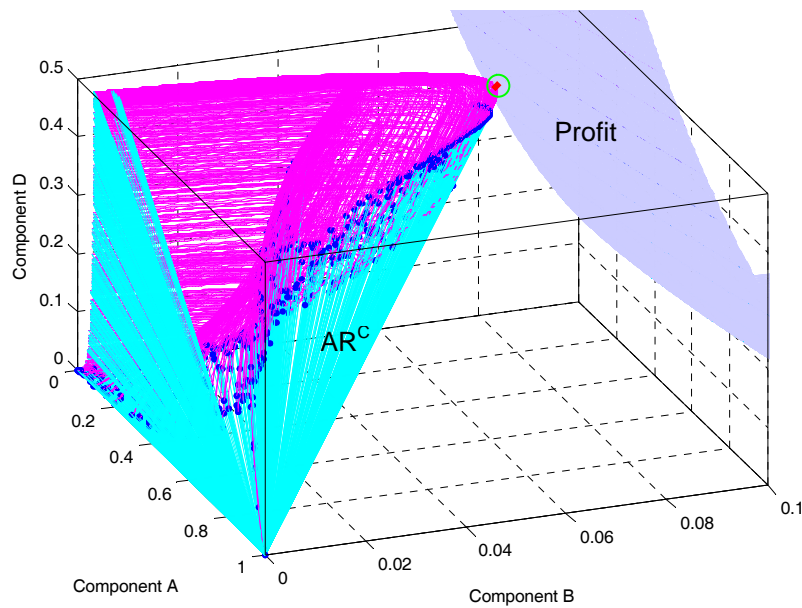
Figure 3.19: A-B-D Projection of the intersection of the AR boundary with the profit function

Figure 3.20 shows the intersection of the profit surface with the AR^C boundary on the A-B-E projection. In case the point of intersection is located in the interior of the AR^C projection. This is observed by the profit surface purportedly cutting through the projection boundary. However it should be noted that the profit function surface does not slice through the AR^C boundary as it intersect the 4D boundary tangentially at one point. The geometric orientation illustrated by the A-B-E projection in Figure 3.20 is due to lower dimensional transformation.

Figure 3.21 also shows that the maximum profit point resides in the interior of the A-D-E projection of the 4D A-B-D-E AR^C. The profit surface in this case also appears to cut through the boundary of the projection.
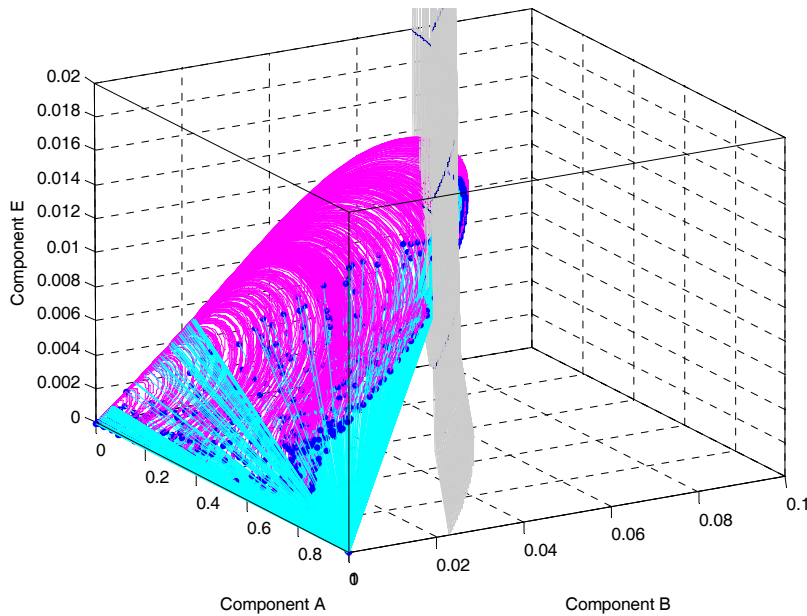
Figure 3.20: A-B-E Projection of the intersection of the AR boundary with the profit function
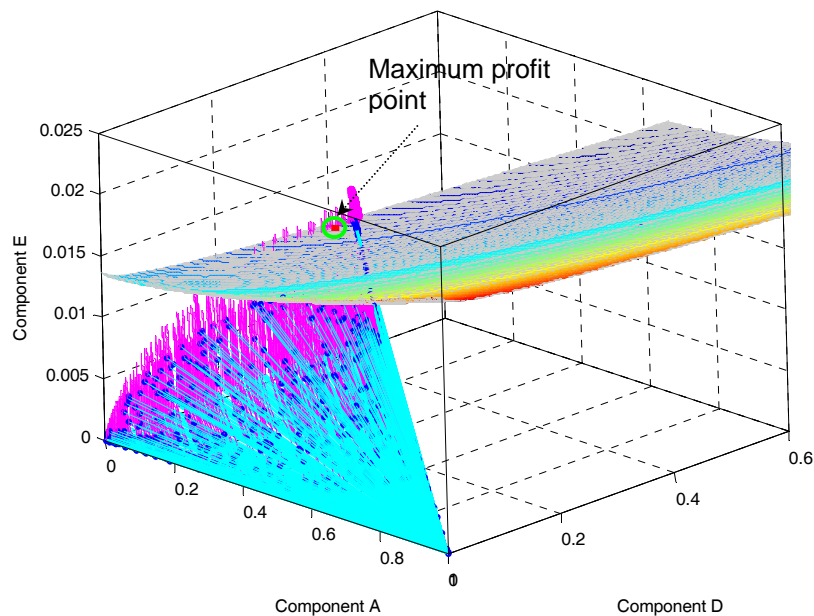
Figure 3.21: A-D-E Projection of the intersection of the AR boundary with the profit function

3.7 Discussion

We have managed to formulate a brute force type algorithm for identifying the attainable regions boundary. The recursive convex control policy algorithm uses simple mathematical ideas, enabling easy and rapid formulation even for problems with intricate reaction schemes, complex kinetic system and high stoichiometric dimensionality. The analytical methods demonstrated in this chapter proved a successful but rather complex procedure to attain AR^{C}s. The 3D illustration carried out resulted in a very complex algebraic process and results, notwithstanding the fact that the kinetics were relatively simple when compared to practical industrial reactions. The same example was solved in a simple and straightforward manner using the RCC algorithm and the results were proven to be consistent.

Higher dimensional problems have not been previously demonstrated due to their algebraically exhaustive nature when approached analytically. Nicol (1998) made some speculations about 4D AR structures. From intuitive grounds, Nicol stated that the entire CFSTR locus is likely to reside on a 4D AR^C for systems with reactions and mixing. The comments turned out to be erroneous after Feinberg (2000b) derived the necessary conditions of optimality that govern the occurrence of the effluent of CFSTR on the boundary of the AR^C. Feinberg (2000b) demonstrated that only special types of CSFTRs, termed critical CSFTRs occur on the AR^C boundary. However, with the intricacy associated with the analytical derivations Feinberg (2000a & b) could not demonstrate the role optimal DSRs and critical CFSTRs played in shaping the AR boundary.

With the use of the RCC algorithm we have managed to illustrate, for the first time, how the critical CFSTR occur on the AR^C boundary and the role

they play on shaping the boundary. Families of optimal DSRs were also shown and all the speculations about the role these DSRs play in shaping the 4D AR^C boundary can be affirmed.

The RCC algorithm only satisfies the conditions of convexity as it uses the convex-hull in the computation to identify AR^{C}s and does not guarantee optimality in its formulation. However, we have demonstrated using a 4D example that the necessary conditions of optimality as derived by Feinberg (2000a& b) can be closely approximated by increasing the number of iterations in the algorithm computation.

Optimisation of a four dimensional objective function using attainable regions analysis has, for the first time, been demonstrated. By use of lower dimensional projections, the intersection of the objective function and the AR^C boundary at the optimum point has also been illustrated and interesting postulates asserted.

The RCC algorithm approximates optimal processes combinations that outline the boundary of the AR^C by growing all possible extensions from the *interior*. Therefore, the AR^{C}s that are generated, within some numerical error, represent the *lower* bounds of the AR. There exists an area of future research where the RCC technique could be coupled with another method that approximates the *outer* or *upper* bounds of the AR^C from the *outside*, such as the Method of Bounding Hyperplanes (Abraham and Feinberg, 2004). A procedure that incorporates these two techniques would approach the AR boundary solution from both the *interior* and *exterior* to guarantee more accurate results and could provide a very powerful technique to identify actual AR boundaries.

3.8 References

Abraham, T.K., Feinberg M., (2004), Kinetic Bounds on Attainability in the Reactor Synthesis Problem, *Ind. Eng. Chem. Res.*, **43**, pp. 449 - 457

Barvinok, A., (2002), *A Course in Convexity*, American Mathematical Society, Rhode Island, USA

Barber, C. B., Dobkin, D. P., Huhdanpaa, H. T., (1996), The Quickhull Algorithm for Convex Hulls, *ACM Transactions on Mathematical Software*, **22**, No. 4, pp. 469-483.

Burri, J. F., Wilson, S. D., Manousiouthakis, V. I., (2000), Infinite DimEnsionAl State-space approach to reactor network synthesis: application to attainable region construction, *Comp. & Chem. Eng.*, **26**, no. 6, pp. 849 – 862

Feinberg, M. & Hildebrandt, D., (1997), Optimal Reactor Design from a Geometric Viewpoint: I Universal Properties of the Attainable Region, *Chem. Eng. Sci.*, **52** (10), pp. 1637-1665.

Feinberg, M., (2000 a), Optimal reactor design from a geometric viewpoint II: Critical sidestream reactors., *Chem. Eng. Sci.*, **55**, pp. 2455 – 3565.

Feinberg, M., (2000 b), Optimal reactor design from a geometric viewpoint III: Critical CFSTRs, *Chem. Eng. Sci.*, **55**, pp. 3553 – 2479.

Kauchali, S.,Rooney, W. C., Biegler, L. T., Glasser, D., Hildebrandt, D., (2002), Linear programming formulations for attainable region analysis, *Chem. Eng. Sci.*, **57** (11), pp. 2015-2228.

Kelley, P. J., and Weiss, M. L., (1979), *Geometry and Convexity*, John Wiley & Sons, Inc., New York, USA.

Lay, S. R., (1982), *Convex Sets and their Applications*, John Wiley & Sons, Inc., New York, USA.

Manning, H. P., (1956), *Geometry in Four Dimensions*, 1st Ed., Dover Publications Inc., New York, USA

McGregor, C. (1998). *Choosing the optimal system structure using the attainable region approach for systems involving reaction and separation*, PhD thesis, University of the Witwatersrand, Republic of South Africa.

Nicol, W. (1998). *Extending the attainable region technique by including heat exchange and addressing four dimensional problems*, PhD thesis, University of the Witwatersrand, Republic of South Africa.

Rooney, W. C., Hausberger, B. P., Biegler, L. T., Glasser, D., (2000), Convex attainable region projections for reactor network synthesis, *Comp. & Chem. Eng.*, **24**, no. 2-7, pp. 225 – 229.

3.9 List of Symbols

Abbreviations

AR   Attainable Regions

AR^C Candidate Attainable Regions

CFSTR   Continuous Flow Stirred Tank Reactors

CSTR   Continuous Stirred Tank Reactors

DSR   Differential Side-stream Reactor

LP   Linear Programming

PFR   Plug Flow Reactor

RCC   Recursive Constant Control Policy algorithm

Symbols

α Control policy for combination of reaction and mixing

c   State variable of the system

c^o State variable of the system at the feeding point

c^* Mixing state variable of the system

c   State vector comprising all variables describing the system

C   Concentration of the reacting components

p   Fundamental processes taking place in the system

r(*c*)   Reaction rate vector defined at *c*

R^N Euclidean space of dimension N

τ Residence time

T   Temperature of reaction

T^* Temperature of mixing

v   Mixing vector, mixing *c* with c^*

x   Reactants and Products state compositions

x^* Reactants and Products mixing compositions

φ (*c*)   The optimum process combination surface (phi surface)

CHAPTER 4

RCC ALGORITHM USER INTERFACE: TEACHING AND APPLICATION TOOL

4.1 Introduction

In this chapter we demonstrate how the RCC algorithm can be completed as a fully automated and easy to use attainable regions analysis tool by use of MATLAB® graphic user interface (GUIDE™). We develop a complete and easy to use software package by under-laying the graphic user interface (GUI) to interface the user with the underlying RCC code. The GUI provides users with an easy to apply graphic interface for input of the required data and output of the results after computation.

This illustration is carried out by developing a customised GUI package for a three-dimensional Van de Vusse type kinetics case study that has been solved in Chapter 3. The elemental problem in this study is fixed, as the underlying reactions and the kinetic models are preset within the software code for the user; however the user has the liberty of changing the rate constant parameters by choosing values from a preset list.

The GUI package shows how the RCC algorithm can be used to solve attainable regions problems by non-specialist users without the need for expertise in the field. This tool can also be used to teach the attainable regions theory to first time users without the complications of using iterative techniques that do not guarantee solutions or solving intricate

algebra arising from analytical derivations. This will also enhance the understanding of different AR structures by use of a number of diverse AR boundaries that result from alternative kinetic parameters. The GUI presents the AR results that are fully colour coded to differentiate and simplify interpretation of the boundary in terms of fundamental processes or combinations thereof that can be further interpreted as a network of unit operations.

The full software package for the RCC that allows the user input of the examples of their choice which also contains a variety of problems including industrial problems studied in Chapters 5, 6, 7 and 8 has been developed during the course of this research. This complete package will not be illustrated in this thesis due to the confidentiality concerns surrounding its commercial viability and will therefore remain in safekeeping of the Centre of Material and Process Synthesis research group at the University of the Witwatersrand.

4.2 The Preset Example

The case study pre-programmed for the illustration of the graphic user interface package is the Van de Vusse kinetic type studied in Chapter 3 using analytical tools derived by Feinberg (2000a & b). The reaction scheme involved comprises mass action kinetics shown in Figure 4.1 below;

$$A \underset{k_r = k_2}{\overset{k_f = k_1}{\longleftrightarrow}} B \overset{k_3}{\to} C$$

$$2A \overset{k_4}{\to} D$$

$$r_A = -k_1 C_A - 2k_4 C_A^2 + k_2 C_B$$
$$r_B = k_1 C_A - k_2 C_B - k_3 C_B$$
$$r_D = k_4 C_A^2$$
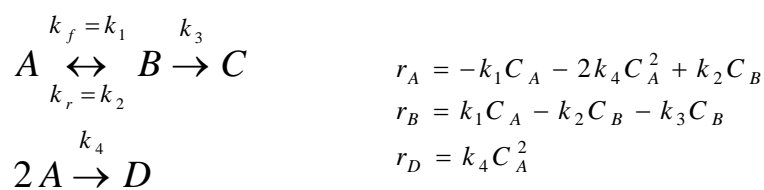
Figure 4.1: Reaction scheme for Van de Vusse mass action kinetics

The rate constants k_1, k_2, k_3, and k_4 are allowed to have any of the values 0; 0.1; 0.5; 1; 10 and 100 which can be chosen from the preset list. The software code uses the values as selected by the user to solve three-dimensional candidate attainable regions in the A-B-D concentration space. The permitted fundamental processes are that of reaction and mixing. The reaction is isothermal and occurs in the liquid phase at constant density. The feed is a liquid of 1 molar concentration of reactant A and contains no B, C or D.

4.3 Components of the GUI

The graphic user interface software is not a stand-alone computer application as it is programmed using MATLAB® and can be used with versions 6.1 or later on a Microsoft® Windows® operating system. A compact disk (CD) containing the source code files for the software package illustrated herein is attached to the back cover of this thesis.

To run the RCC GUI application, the source code files should be loaded into the working directory of MATLAB®. The application can be activated by typing 'vdvgui' in the MATLAB® command prompt (>>). The GUI window shown in Figure 4.2 will be launched as the active window. The components of the GUI window are labelled in Figure 4.3. To discuss these components we will carry out a demonstration on how to solve a candidate AR in the A-B-D stoichiometric space using the rate constant values: $k_1 = 0.1$, $k_2 = 0.5$, $k_3 = 1$, and $k_4 = 100$.
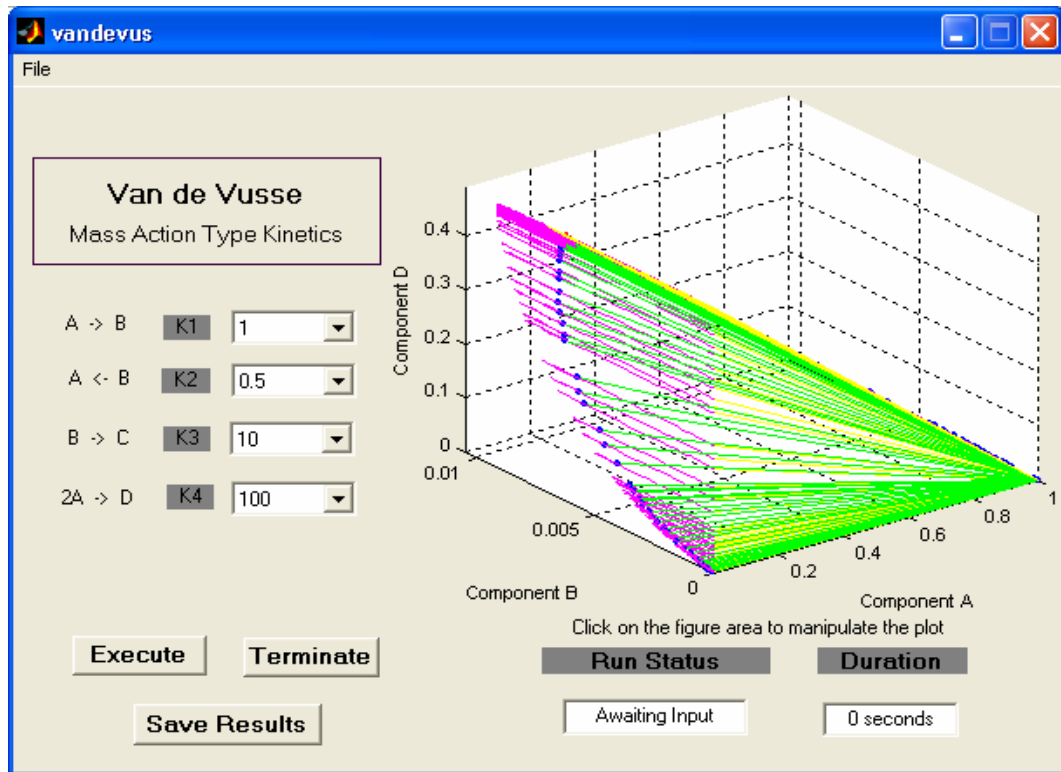
Figure 4.2: The RCC GUI interface window for the Van de Vusse Example
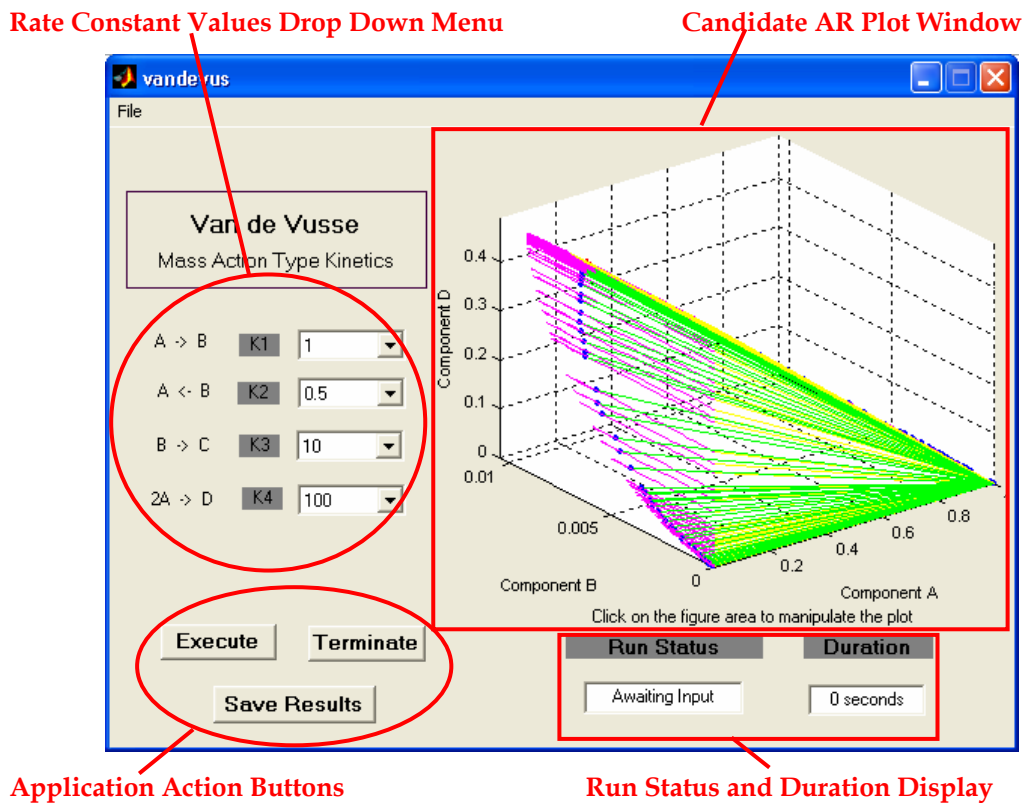
Figure 4.3: Component of the RCC interface window

4.3.1 The Rate Constant Input Drop-down Menu

This component of the GUI allows the user access to key in values of the rate constants of the Van de Vusse reaction by selecting values from the list provided within the drop-down menu. As shown in Figure 4.4, each reaction is catalogued alongside its corresponding rate constant and the drop-down menu for the selection of the respective rate constant value.

(a)   *(b)*

(c)   *(d)*
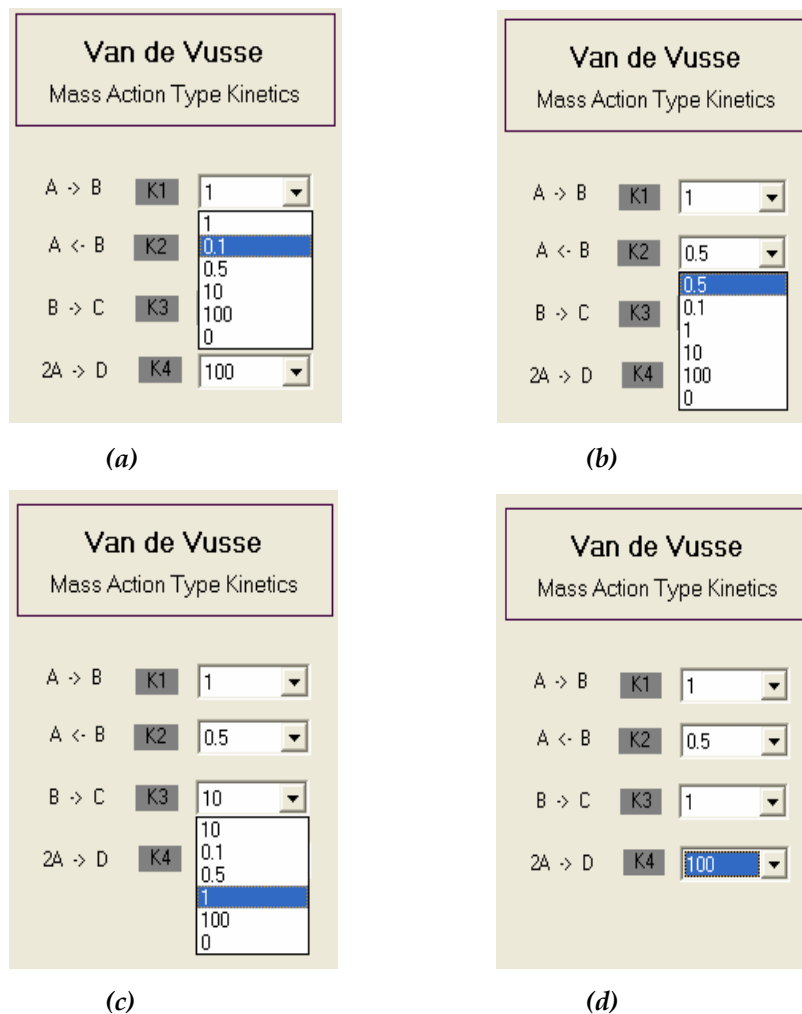
Figure 4.4: Rate constant input drop-down menu

Figures 4.4 (a), (b) and (c) show how the values of constants k_1; k_2 and k_3 can be selected to the desired values. Figure 4.4 (d) displays how a completed selection of all rate constants.

4.3.2 Action Button Console

Figure 4.5 below shows a panel of action buttons that can be applied by the user to execute the desired actions. The actions available to the user in the illustration are;

- Execute: This button allows the user to run the RCC algorithm application to solve candidate ARs after the desired input is keyed in.

- Terminate: This action button can be used to terminate the execution of the RCC application at any time. This action is useful in the case where the user realises the need to change input after executing the application.

- Save Results : In the case where the user needs to save the computational numeric results for later use with other applications, this action button can be used to save the results into a MATLAB® data file 'results.mat' and into a text file 'results.txt' ASCII format delimited with a *tab* character.
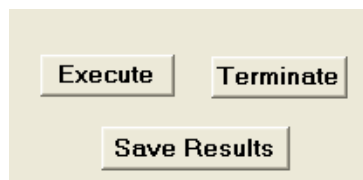
Figure 4.5: Action button console

4.3.3 Run Status Display Panel

The run status window informs the user about the progress of the execution of the application as shown in Figure 4.6. The default status displayed indicates that the application is awaiting input from the user shown in Figure 4.6 (a). After the desired rate constants input is keyed in and the execute button pressed to run the application, the run status window displays 'Initializing' showing that the code is performing the initialisation stage (Figure 4.6 (b)). As the application progresses to solve the AR^C, going through the RCC algorithm stages, the run status window reports the completed stage. The accumulated duration from the start of the execution to the completion of that particular stage is reported in the duration window. This progressive reporting is depicted in Figure 4.6 (c) – (f).

Run Status	Duration		Run Status	Duration
Awaiting Input	0 seconds		Initializing	0 seconds
(a)			*(b)*	
Initialization	8 seconds		Growth	24 seconds
(c)			*(d)*	
Plotting Results	29 seconds		Run Completed	31 seconds
(e)			*(f)*	
Results Saved	results.mat		Terminated	14 seconds
(g)			*(h)*	
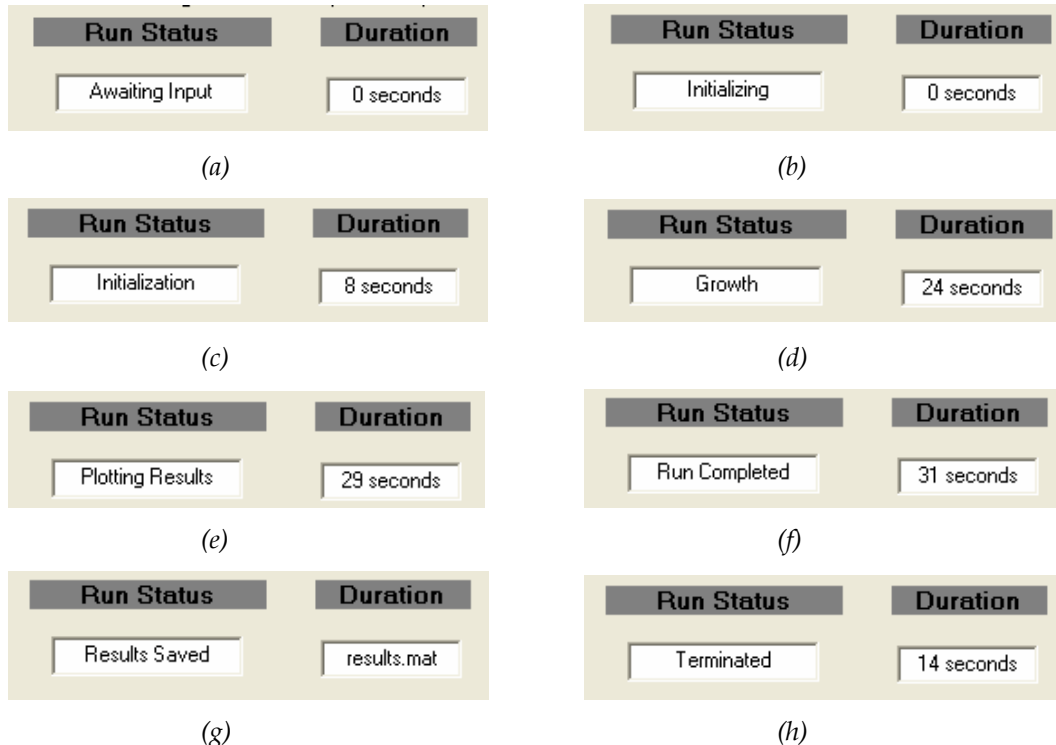
Figure 4.6: Run status and duration display panel

At the end of the computation, the solution which is the AR^C figure is displayed in the plot window and the run status display reports that the application run is completed and the duration display indicates the time taken to complete the entire calculation from start to plotting of the results. If the user chooses to save the numeric results to a file by clicking on the 'Save Results' button on the action button console, the application saves the results into files as stated in section 4.3.2. The run status display in this case will indicate that the results have been saved and the duration window will report the name of the file into which the numeric results have been saved. This property is shown in Figure 4.6 (g). The user can choose to terminate the application execution at any time during the run and the status display window will report the progress of the application as terminated as shown in Figure 4.6 (h). In this case the AR^C plot window will be blank as there will be no results to display.

4.3.4 The Plot Window

The plot window shown in Figure 4.7 displays the solution of the AR as returned by the RCC algorithm. When the GUI is loaded, the plot window shows a default candidate AR structure as shown by the application GUI window in Figure 4.2. This candidate AR figure is the result of the previous solution computed by the RCC algorithm which is automatically saved in a file named 'defaultplot.fig'. The plot window displays text that informs the user that, by clicking anywhere on the plot window area the figure can be pulled off as a standalone MATLAB® figure window. After the AR^C figure window is pulled out, it can then be manipulated by the user with MATLAB® built-in tools such as rotation, editing, formatting, etc.

Click on the figure area to manipulate the plot
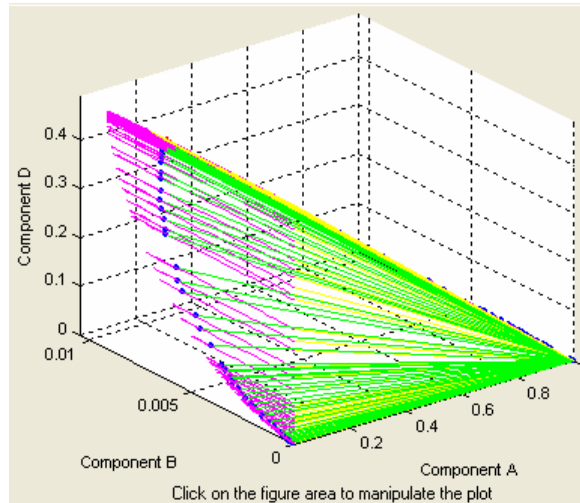
Figure 4.7: Candidate AR plot window

4.4 Results and Interpretations

At the completion of the application execution, the results are shown in the AR^C plot window and the run status display will report the application run as completed and the duration will also be displayed. For the example used in this illustration, the GUI window shows the results at the end of the execution to be as depicted in Figure 4.8.

By using the mouse cursor to click on the plot window area, the AR^C figure can be pulled out to be a standalone MATLAB® figure window as shown in Figure 4.9. The AR^C figure can then be manipulated by a rotation tool to enable view from different projections. Figure 4.9 (a) shows one of the many 3D projections while Figure 4.9 (b) shows a 2D projection in the A-B concentration space.

Rotation of the AR^C figure allows the user to identify fundamental processes and/or combinations thereof that occur on the boundary. This property is made possible by the differentiating colour coding performed by the algorithm.
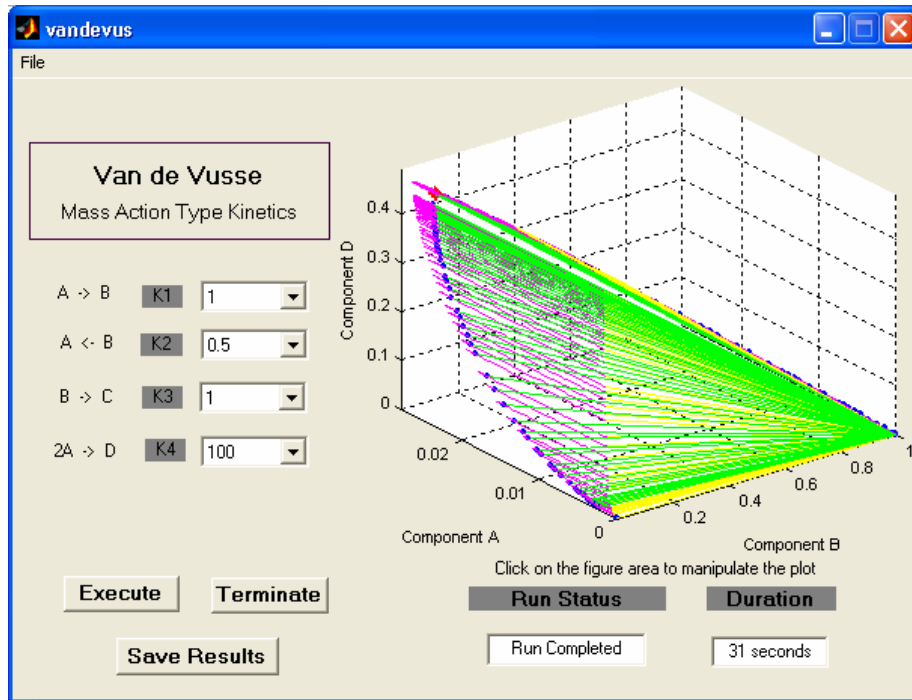
Figure 4.8: Application GUI window showing the completed results

| *(a)* | *(b)* |
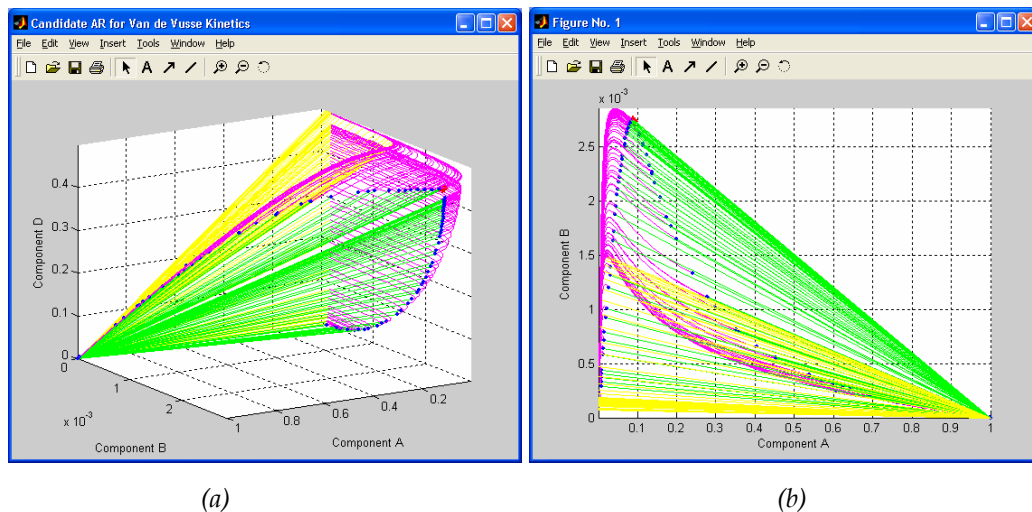
Figure 4.9: AR^C solution in a standalone MATLAB® figure window

The fundamental processes and combinations of fundamental processes that occur on the boundary are distinguished by colours as shown on the AR^C solution depicted in Figure 4.10. These colours make it easy to study how different fundamental processes and combinations thereof form the shape of the boundary of the attainable regions.
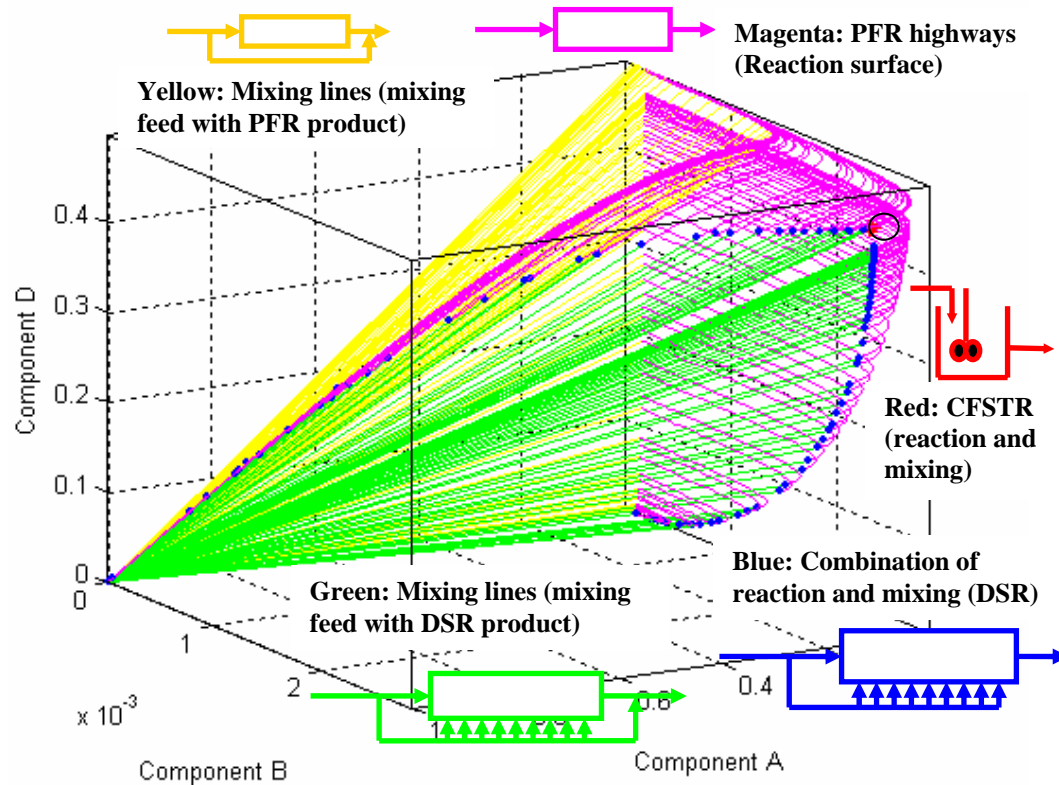
Figure 4.10: AR^C solution illustrating colours used for differentiation

The colour coded figure makes it simple and straightforward to interpret different regions of the AR^C boundary in terms of fundamental processes. This property, however, does not alleviate complications relating to the interpretation of the product states on the AR^C boundary in terms of a sequence of unit operations and key design parameters, which can be construed into a flowsheet with unit operations specifications. The RCC GUI software package offers an application that simplifies the task of interpreting any product state on the AR^C boundary into a network of unit operations applied to attain it.

After the results have been obtained from the execution of the RCC GUI application and the AR^C figure pulled out into a standalone MATLAB® figure window, the user can then execute a command termed 'infer'. By keying in 'infer' at the command prompt, the application activates a built-

in MATLAB® function that can read off data from the figures. The mouse cursor will then be equipped with a cross-pointer that the user can apply to read off any output state point state on the AR^C boundary. Once the data from the output state point has been read and interpreted by the application, a new figure window is activated, graphically showing a sequence of unit operations that can be used to attain it, along with specification such as residence times for each unit.

To demonstrate this function, we will use the AR^C as solved above. By pointing on the AR^C using the cross pointer as shown in Figure 4.11, the application returns the window showing the information about the product state at the point of interest and the network of reactor structures used to attain it, as portrayed in Figure 4.12.
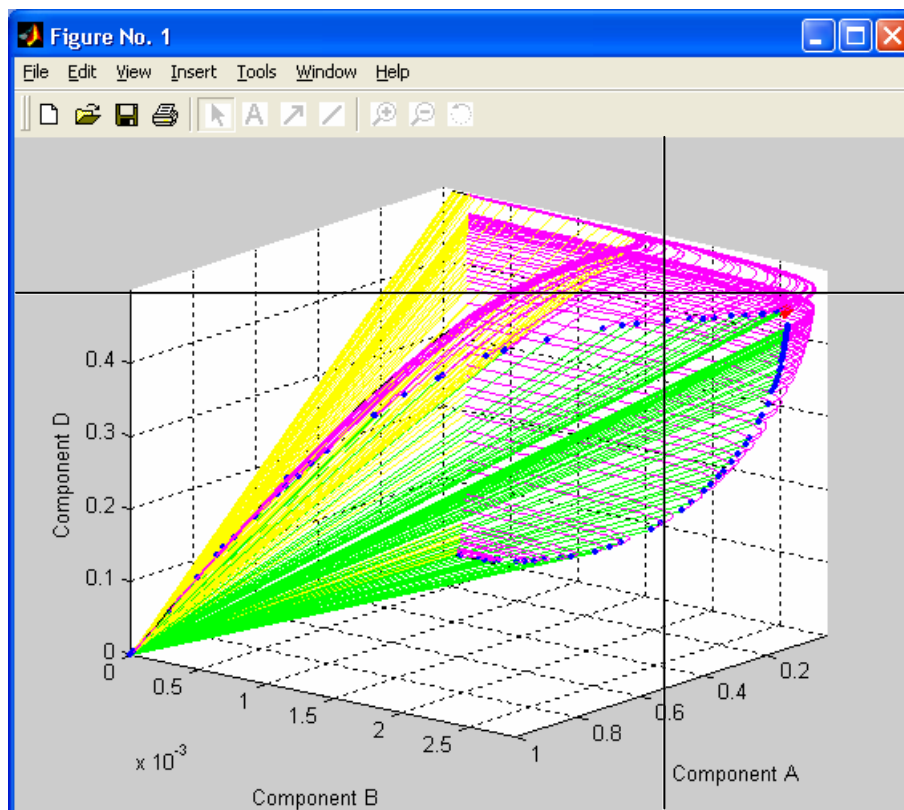
Figure 4.11: Illustration of a cross-pointer used to read off a point

Also shown along with the network of reactor structures, are the residence times of each of the reactors.
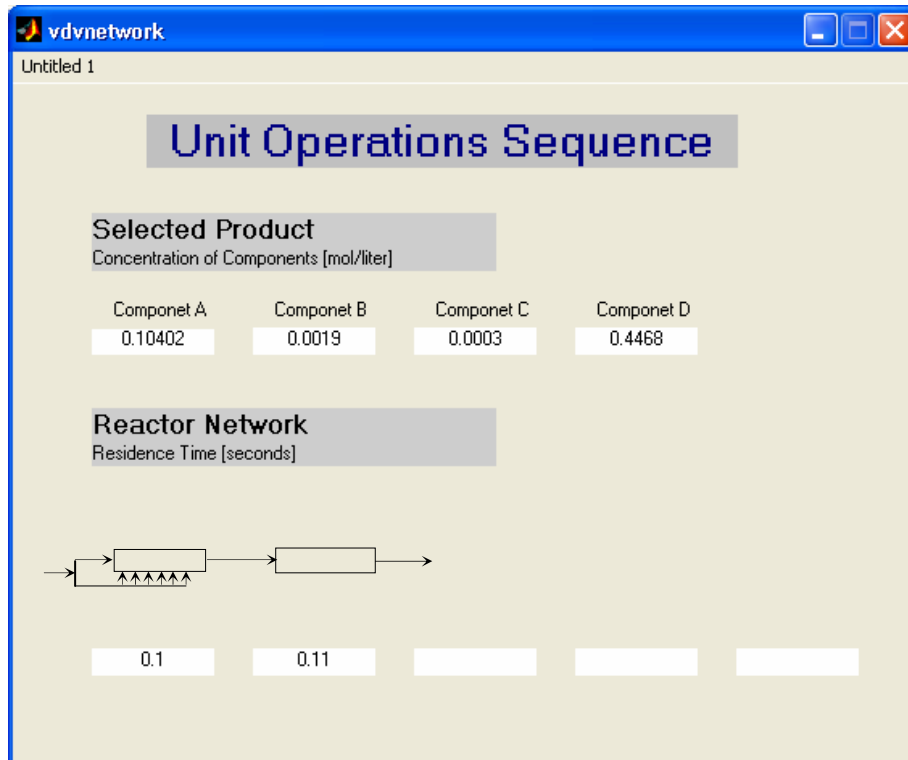
Figure 4.12: Interpretation of product as reactor structures network
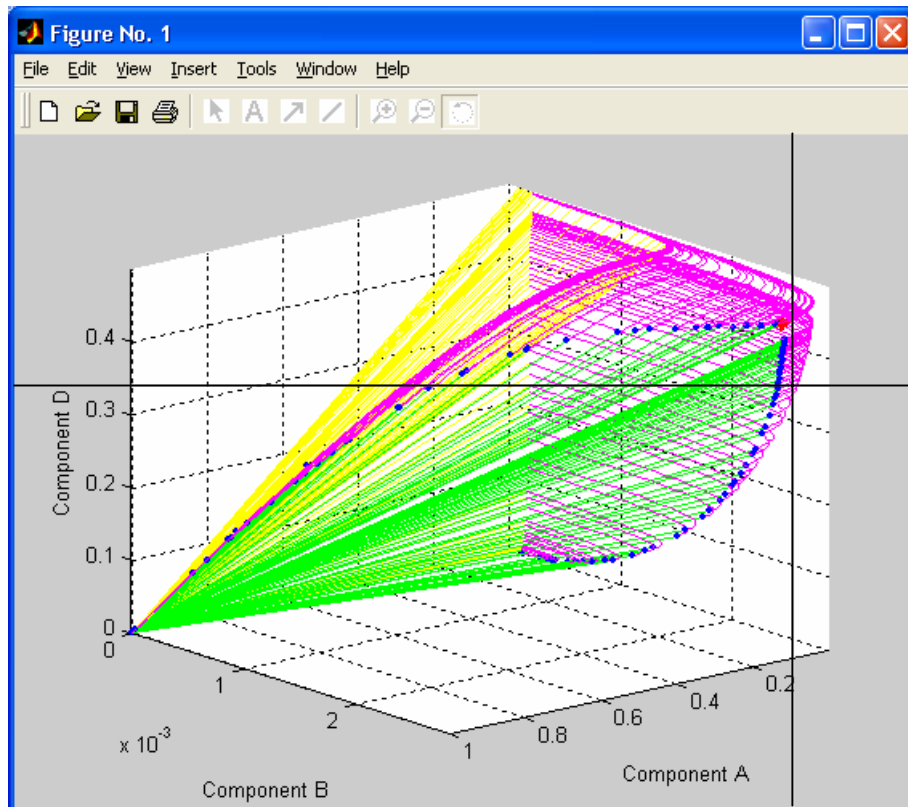
Figure 4.13: 2ⁿᵈ Illustration of a cross-pointer used to read off a point of interest

Figure 4.13 shows another illustration of how a product state can be interpreted into a network of unit operations used to achieve it. The network used in this case is shown in Figure 4.14.
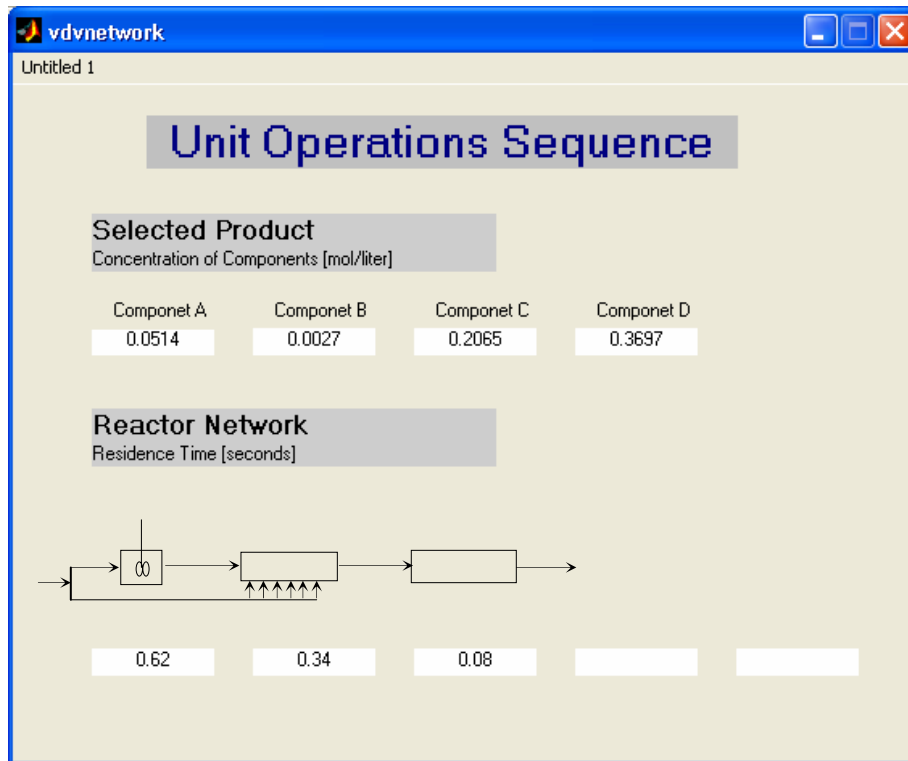
Figure 4.14: Interpretation of the 2nd point as reactor structures network

4.5 Discussion

The graphic user interface (GUI) of the RCC algorithm has been successfully illustrated. A step by step demonstration has been used to introduce the components and functions of the customised GUI application by solving an example. The usefulness of this software package relies mainly on the rapid solutions of AR^C computed by the under-lying RCC algorithm as well as its data tracking capabilities that enabled interpretation of the results as networks of reactor structures.

The application presumes no prior knowledge of attainable regions analysis for the end users. By providing the required kinetic information, a full AR^C is provided and any point on the boundary as chosen by the end user, can be interpreted at the speed of a mouse click.

The RCC algorithm is continually proving to be a powerful process synthesis technique using attainable regions analysis. With the use of simple theoretical examples, we have so far, demonstrated a fully automated reactor network synthesis procedure starting with the given feed and reaction kinetics to yield a complete solution of unit operations sequence with design parameter.

At this point, it is evident that with the use of automated algorithms, AR analysis can be included in computer simulation packages that are extensively used by chemical engineers to synthesise new processes as well as to optimise existing ones. In the next chapters we will start to tackle practical industrial case studies using the RCC algorithm to solve optimal process specifications.

4.6 References

Feinberg, M., (2000a), Optimal reactor design from a geometric viewpoint II: Critical sidestream reactors., *Chem. Eng. Sci.*, **55**, pp. 2455 – 3565.

Feinberg, M., (2000b), Optimal reactor design from a geometric viewpoint III: Critical CFSTRs, *Chem. Eng. Sci*, **55**, pp. 3553 – 2479.

4.7 List of Symbols

Abbreviations

AR   Attainable Regions

AR^C Candidate Attainable Regions

CFSTR   Continuous Flow Stirred Tank Reactors

DSR   Differential Side-stream Reactor

GUI   Graphical User Interface

PFR   Plug Flow Reactor

RCC   Recursive Constant Control Policy algorithm

Symbols

C Concentration of the reacting components

k Reaction Rate constant

$r(c)$ Reaction rate vector defined at c

CHAPTER 5

RCC ALGORITHM: APPLICATION TO INDUSTRIAL CASE STUDIES

5.1 Introduction

Up to now we have developed the RCC algorithm and demonstrated its applications with theoretical case studies. The examples considered isothermal systems with fundamental processes of reaction and mixing only. More importantly, we illustrated the straightforward advancement of the algorithm to handle higher dimensional problems.

In this chapter we apply the RCC algorithm to study more practical examples with chemical reactions of industrial nature. The systems to be considered will consist of reaction kinetics, fundamental processes of reaction, mixing, heating and cooling and some specified constraints. The first case to be studied will be a generic first order exothermic reversible system with a single reaction occurring. The second example will investigate a more practical and specific exothermic reversible reaction, which is the industrially important ammonia synthesis system. In Chapter 6 we will perform a detailed study of a more complex industrial system with a network of reactions and will derive the optimal reactor networks for methanol synthesis. The RCC formulations will be used to generate candidate attainable regions for all these examples from which the optimal reactor network structures will be arrived at.

5.2 Exothermic Reversible Reaction

5.2.1 Background

A wide range of industrial exothermic reactions such as oxidation, polymerisation, isomerisation and esterification reactions have been shown to exhibit characteristics that can be described by first order reversible kinetics (Omoleye, *et al.*, 1989). Systems with exothermic reversible reactions have always presented challenging reactor network synthesis due to the fact that the optimum reactor requires both high temperatures to favour high initial reaction rates and low temperatures to achieve high equilibrium conversions.

Traditional methods of optimising exothermic reversible reactions place emphasis on developing techniques for identifying the required falling temperature progressions. Denbigh (1944) demonstrated for a wide range of exothermic reaction schemes, how to determine the theoretical optimum temperature profiles from which more practical temperature progression could be determined. This method falls apart when the costs of cooling start to play a role and reactor residence times and cooling utilities trade-offs have to be considered as the best temperature profiles are not so obvious.

To achieve the decreasing temperature progression two cooling methods are commonly employed in practise. The direct cooling method uses cold feed addition to cool the reaction mixture while indirect cooling utilizes heat exchange to cool the reaction mixture. Research to optimise cold feed addition in cold shot reactors with direct cooling methods has been carried out by many researchers (Hellinckx and Rompay, 1968; Burghardt and Patzek, 1978). Glasser *et al.* (1992) used AR analysis to identify optimal

cold shot reactor profiles. Ravella and de Lasa (1987); and Beckett and Evans (1989) studied the methods of indirect cooling, and the practical applications of these methods can be seen in methanol and ammonia synthesis reactors. The reactor network in these cases involves adiabatic reactor stages with inter stage coolers.

Further work involving AR analysis to identify optimal cooling profiles for exothermic reactions was carried out by Godorr (1998). Godorr's study permitted only direct cooling as it considered an adiabatic reaction scheme allowing only reaction and mixing processes. Hausberger (2003) applied an automated AR analysis technique, called the iso-state algorithm to identify an optimal reactor structure for ammonia synthesis. Although this study allowed for both direct and indirect methods of cooling, the costs to be incurred for heat transfer were not taken into consideration. Hausberger also investigated the effects of internal heat exchange as a means of indirect cooling. This study revealed that the optimal cold shot reactor and optimal cooled reactor (internal heat exchange) form the optimal reactor network for ammonia synthesis. Research carried out by Kauchali *et al.* (2004) focused on finding AR[C]'s for the water gas shift reaction. This study allowed for both methods of cooling to be investigated. The heat transfer costs were not considered for indirect cooling and the cooling profiles for this reaction scheme appeared straightforward.

Nicol *et al.* (1997, 2001) studied AR[C]'s for exothermic reversible reactions with both internal and external cooling. The authors also investigated cases where cost incurred for heat transfer were incorporated. Nicol *et al.* (1997) considered cases where the cost of external heat exchange is zero, less, equal and greater than the cost of reaction. The AR[C]'s for this study revealed interesting reactor networks comprising isothermal cold fed

reactors, optimum cold fed reactors, and optimum cooled reactors (internal and external heat exchange).

In this study we apply the automated RCC algorithm to case studies similar to those investigated by Nicol *et al.* (1997, 2001). In our study we will use the same reaction scheme and kinetics as in Nicol *et al.* (1997, 2001).

5.2.2 The system

A generic first order exothermic reversible reaction considered herein has the following reaction where reactant **A** is converted to product **B** as

$$A \leftrightarrow B \tag{5.1}$$

The reversible rate of formation of **B** takes the Arrhenius type kinetics defined by

$$r_x(x,T) = A_1 \exp\left(\frac{-E_1}{T}\right) \cdot (1-x) - A_2 \exp\left(\frac{-E_2}{T}\right) \cdot x \tag{5.2}$$

where x is defined as conversion (fraction of **A** that has reacted) and T is the reaction temperature. The rate constants A_1 and A_2 have values of 5×10^5 and 5×10^8 respectively. The Arrhenius constants related to the activation energies of both the forward and reverse reactions, E_1 and E_2 are taken to have values of 4000 and 8000 with corresponding units respectively. The assumptions made in this example are that the pressure, density and heat capacity of the reaction system remain constant as the reaction mixture and temperature change. It is also assumed that mixing occurs ideally such that the heat of mixing is insignificant in comparison

with the reaction enthalpy (ΔH_{rxn}). Subsequently, the energy balance of the system can be derived such that the adiabatic reactor effluent temperature is a linear function of conversion;

$$T = T_o + T_{ad} \cdot x \tag{5.3}$$

where T_{ad} is the adiabatic temperature gradient equal to $\Delta H_{rxn}/Cp$. The value for T_{ad} will be taken to be 200 for all cases studied in this section. T_o is the basis temperature from where the adiabatic reaction is started ($x = 0$), and would correspond to the feed temperature of the reactor. If pre-heating is undertaken prior to reaction, T_o will correspond to the pre-heating temperature. The feed temperature to the system in this example is taken to be 300K.

External cooling can be done with a constant temperature utility where the temperature of the utility is T_c. For a process stream of temperature T being cooled with a cooling utility of temperature T_c, the rate of cooling per unit heat exchange area can be defined as:

$$w(T, T_c) = h_o(T_c - T) \tag{5.4}$$

Equation (5.4) does not consider the cost of cooling. The heat transfer coefficient h_o, is assumed to be constant for simplification.

5.2.3 System State Variables and Process Vectors

The fundamental processes allowed in this example are reaction, mixing and cooling. The variables involved with these processes are conversion, temperature and residence time. Residence time is generally used as a cost indicator for a reactor as it gives an indication of the reactor size for a

given flow capacity. For heat transfer, the heat transfer area is normally used as a cost indicator. Nicol *et al.* (1997) combined the two different costs by assuming a linear cost relationship between heat transfer area and reactor residence time such that the resulting cost variable obeys linear mixing.

To consider the cooling duty, heat transfer cost can be linearly related to the cost of reaction using reaction residence time τ_r, and some constant factor k_c such that the combined cost for reaction and cooling is given by:

$$\tau = \tau_r + k_c \omega \tag{5.5}$$

where ω the heat exchange area per unit flow of heat exchange (Nicol *et al.*, 1997). The rate of change of temperature can now be revised with the relative cost integrated in, when allowing only cooling as the fundamental process and is given by:

$$\frac{dT}{d\tau} = \frac{h_o k_c}{C_P}\left(T_c - T\right) \tag{5.6}$$

Equation (5.6) can be rewritten as:

$$\frac{dT}{d\tau} = K_c\left(T_c - T\right) \quad \text{with} \quad K_c = \frac{h_o k_c}{C_P} \tag{5.6}$$

K_c gives some measure of cooling costs in relation to the cost of reaction (Nicol *et al.* (1997)). The relation of K_c to the heat transfer costs is such that, very small values of K_c signify high costs or expensive heat transfer, while very large values ($K_c = \infty$) correspond to cheap or very low cost of cooling.

The state variables that can be used to describe our system at this point are; a variable associated with the process of reaction x, secondly, a variable relating to changes in temperature of the system T, and thirdly, the cost variable τ. The characteristic vector of the system can now be defined as $c = [x, \text{T}, \tau]$.

The fundamental processes can be defined as vectors in the c space. The process of reaction $r(c)$ is described by a vector;

$$r(c) = \begin{bmatrix} r_x(x,T) \\ T_{ad} \cdot r_x(x,T) \\ 1 \end{bmatrix} \tag{5.7 a}$$

The mixing process can be performed using a mixing state $c_0 = [x_0, T_0, \tau_0]$ such that mixing is characterised by;

$$v(c,c_0) = \begin{bmatrix} x_0 - x \\ T_0 - T \\ \tau_0 - \tau \end{bmatrix} \tag{5.7 b}$$

Cooling is carried out using a constant temperature cooling utility at T_c. This fundamental process can be described by a vector given by;

$$k(c) = \begin{bmatrix} 0 \\ K_c(T_c - T) \\ 1 \end{bmatrix} \tag{5.7 c}$$

Kc is as defined in equation (5.6) to be some measure relating the cost of cooling to the cost of reaction. At this stage the system variables have been fully defined and the fundamental processes occurring are characterised as vectors in the state variable space.

The overall processes combination vector for this system can be written as:

$$P(c) = r(c) + \alpha v(c, c_0) + \beta k(T, T_c) \qquad\qquad \alpha, \beta \geq 0 \qquad\qquad (5.8a)$$

In Chapter 2, we asserted from the postulates derived by McGregor (1998) that the smooth intersector that are optimal combinations of fundamental processes for this case are formed by the combinations of reaction and mixing and combinations of reaction and cooling. The intersectors of mixing and cooling form non-smooth ridges that are not trajectories and do not have generalised mathematical descriptions. This problem can therefore be formulated with two process combination vectors for the combination of reaction and mixing;

$$P_1(c) = r(c) + \alpha v(c, c_0) \qquad\qquad \alpha \geq 0 \qquad\qquad (5.8b)$$

And the combination of reaction and cooling as;

$$P_2(c) = r(c) + \beta k(T, T_c) \qquad\qquad \beta \geq 0 \qquad\qquad (5.8c)$$

The above formulation solves for the optimal process combinations that are known to be smooth trajectory intersectors. These intersectors give pathways to manifolds of distinct process trajectories that give rise to the final shape of the AR boundary (Chapter 2 & 3, Feinberg 2000 a & b). The optimal combination of reaction and mixing is a DSR trajectory and that of reaction and cooling is a differentially cooled reactor (DCR) trajectory.

The non-smooth intersectors that are not trajectories but intersections of terminating process manifold such as the mixing and cooling intersectors will be automatically established on the boundary of the AR if there are such points that exist.

5.2.4 System Constraints and Limits

Before the construction of the AR^C we need to state the constraints and the limits placed on the system. We will restrict the maximum preheating temperature to 450K. This constraint could in reality be limited by the temperature of the preheating media. Furthermore, the minimum cooling utility temperature in this case is limited to a minimum of 300K. For interest we will further state that the catalyst activity requires temperatures above 450K, placing a minimum reaction temperature bound of 450K on the system.

5.2.5 RCC Formulation

5.2.5.1 The Boundary Objective

The problem is then formulated using the objective as maximisation of reaction conversion for a given system residence time. Alternatively, the objective can be written out as minimising the residence time for a given conversion. At this stage it becomes evident that the problem can be solved in two-dimensions as the objective function involves identifying the convex boundary in reaction conversion and residence time (cost) space. The problem can be solved by identifying a two-dimensional convex structure of fundamental processes and/or combinations thereof that will give the highest conversion of product x, at a given overall system residence time τ or the lowest system residence time to reach a given conversion.

5.2.5.2   The Termination Criterion

The boundary objective states that the problem will be completely solved by finding a two-dimensional convex boundary of combinations of processes in the conversion-residence time space. The area percentage growth of the two-dimensional region can be used as a termination criterion in this case if accuracy is not crucial. The solution in this case serves satisfactorily in situations where the aim is to quickly identify reactor structures that occur on the AR^C boundary. Percentage deviational error methods can be coupled with a number of iterations to terminate the algorithm in cases where high accuracy of parameters such as residence times and optimal process combination policies are required. The deviational error gives an indication of how the boundary is improving or not improving towards the solution after every iteration. In the light of the fact that the approximate boundary solution as returned by the algorithm at the end of each iteration is a set of points that continually change with the number of iterations, linear interpolation is used for comparison.

Consider a boundary contained in data set C_j returned by iteration j. For a two-dimensional τ-x region, C_j will contain N_j number of state points defined as;

$$C_j = [c_{j,1}; c_{j,2}; ...; c_{j,N_j}] \qquad \text{such that } c_{j,i} = [\tau_{j,i}, x_{j,i}(\tau_{j,i})] \text{ for } i=1,2,...N_j$$

$$(5.9)$$

The preceding iteration would have the outcome C_{j-1}, with C_{j-1} taking a definition analogous to equation (5.9) with corresponding subscripts. It should be noted that $N_j \neq N_{j-1}$, in fact it is more likely that $N_j > N_{j-1}$ as the

boundary set gets populated with more data as the number of iterations progresses (Chapter 3, section 3.4.3).

Linear interpolation can be carried out to evaluate $x_{j,i}(\tau_{j-1,i})$ as shown in Figure 5.1.
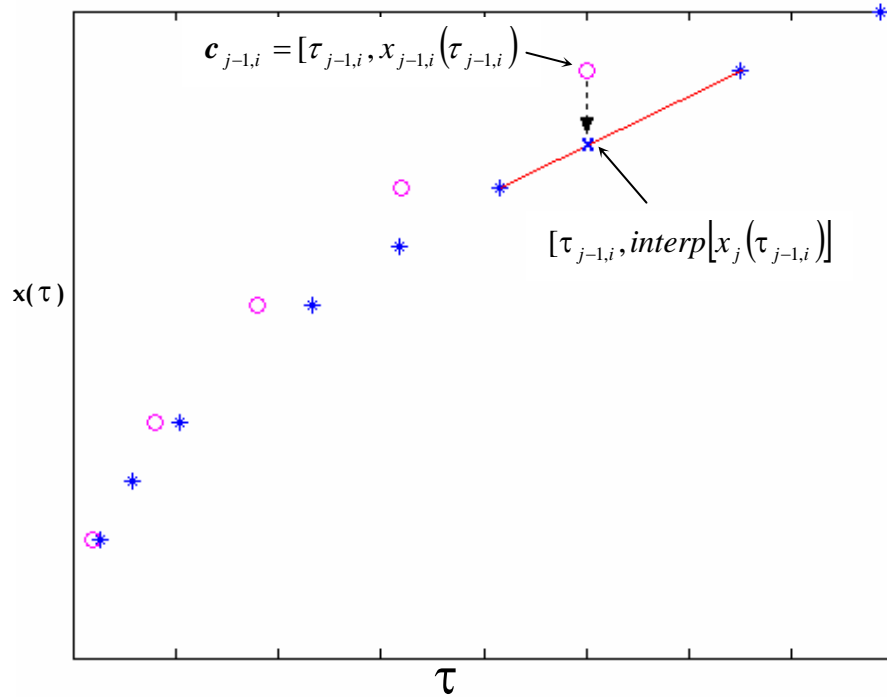
Figure 5.1: Illustration of linear interpolation of boundary results

It should be noted that linear interpolation is performed as C_{j-1} into C_j due to the fact that C_j is populated with more data points, and therefore will yield more accurate interpolation results as compared to interpolation of C_j into C_{j-1}. Percentage deviational error methods can be then applied to the interpolated results to compare the solutions of two sequential iterations as shown by equation (5.10) below;

$$E_{\%} = \sum_{i=1}^{i=N_{j-1}} \frac{\left|(x_{j-1,i}) - interp[x_j(\tau_{j-1,i})]\right|}{interp[x_j(\tau_{j-1,i})]} \times \frac{100}{N_{j-1}} \tag{5.10}$$

The termination criterion used in the two cases of this example is such that the algorithm terminates when $E_\%$ < 1 or the number of iterations exceeds 20.

5.2.5.3   The Algorithm

Using the system specifications, constraints and the termination criterion, the RCC algorithm for the exothermic reversible reaction can be formulated as detailed in Chapter 3 (section 3.4.2).

Stage 1

The algorithm is formulated the AR in three-dimensional conversion-residence time-temperature space. Pre-heating is applied to the maximum pre-heating temperature and minimum catalyst activity temperature of 450K. PFR trajectories and CFSTR locus are generated from the preheated feed. The points that optimise the objective function in this case are taken as extreme points.

Stage 2

The cooling utility is fixed at 300K for this example (Section 5.2.4). The mixing points are selected as points satisfying conditions detailed in Section 3.4.3. The process combination trajectories given by (5.8 b) and (5.8 c) are generated from the generating extreme mixing and cooling at respective mixing and cooling points.

Stage 3

The iteration stages are performed to refine the control policies for combinations given by (5.8 b) and (5.8 c) and grow the region until the termination criterion is satisfied (Section 5.2.5.2).

Stage 4

Once the termination criterion is met, the boundary can be completed using single process combination trajectories. From the optimal combinations of reaction and mixing, reaction trajectories and mixing lines are generated to complete the boundary of the AR^C. Similarly, from reaction and cooling intersectors, the AR^C boundary is completed with single process operation surfaces that are either unions of reaction trajectories or cooling lines.

5.2.5.4   Traditional Methods Review

The traditional methods used by Nicol *et al.*, (1997, 2001) to solve this problem involved the algebraically exhaustive procedure of deriving the optimal control policy equations for combinations (5.8 b) and (5.8 c). Another difficulty in these methods lies in identifying points on the boundary where these optimal combinations initiate, switch and/or terminate. These two steps require intervention by a specialist in the field of AR analysis.

5.2.6 Results

5.2.6.1   Case 1

In this case the cost of cooling was not taken into consideration, thus allowing free cooling. The RCC algorithm was formulated and implemented in MATLAB®. The termination criterion was satisfied and the boundary completed after five (5) iterations. Figure 5.2 depicts a two-dimensional temperature-conversion projection of a 3D temperature-extent-residence time AR^C for this case.
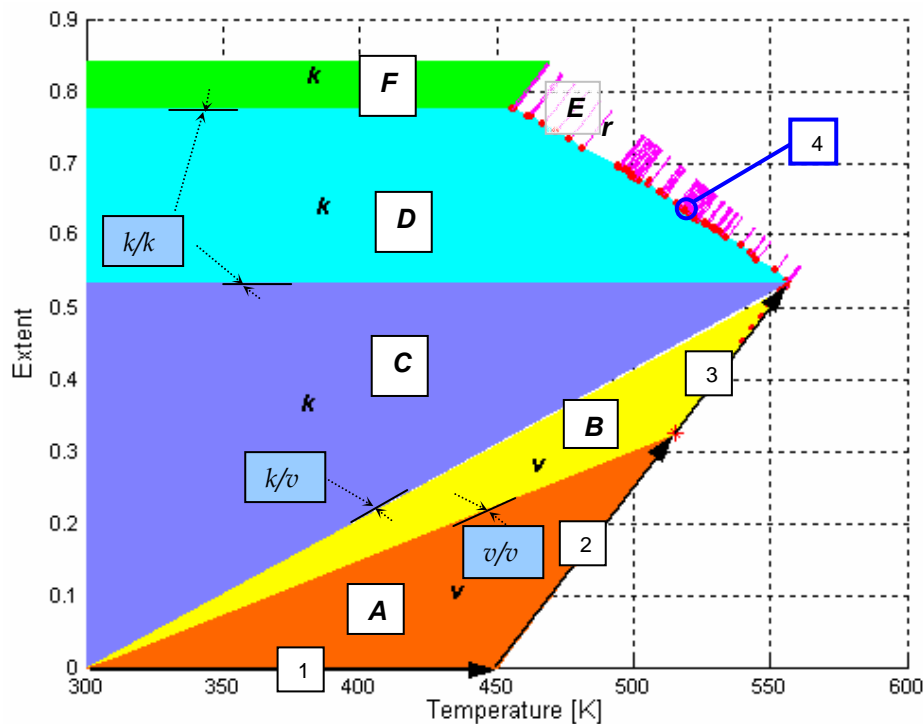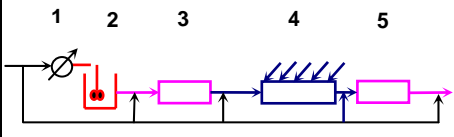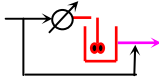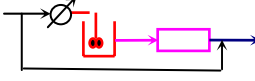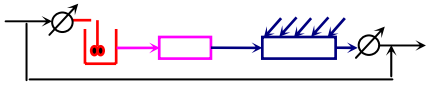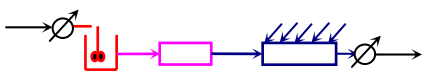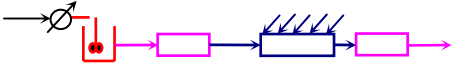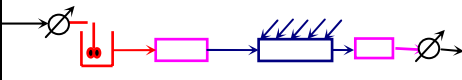
Figure 5.2:A 2D temperature-conversion projection of case 1 AR^C

The different process surfaces with their corresponding vectors are shown. Fundamental process layouts for this case are tabulated in Table 5.1 showing the main process pathways and regions as indicated on the AR^C in Figure 5.2. The main process pathways are outlined with numbering from **[1]** to **[6]**.

Table 5.1: Process Layout for Exothermic Reversible Reaction Case 1

Process Curve	Process Pathway	Process Layout
1 - 5	The general process layout for the AR^C	
Surface	**Occurring Processes**	**Process Layout**
A	Pre-heater - CFSTR with by-pass	
B	Pre-heater – CFSTR – PFR with by-pass	
C	Pre-heater – CFSTR – PFR – DCR-Cooler with by-pass	
D	Pre-heater – CFSTR – PFR – DCR - Cooler	
E	Pre-heater – CFSTR – PFR – DCR - PFR	
F	Pre-heater – CFSTR – PFR – DCR – PFR - Cooler	

The general process layout utilises the permitted free pre-heating,**[1]**, to the maximum allowable temperature of 450K. The preheated feed is then followed by an optimum adiabatic reactor sequence. This sequence comprises a CFSTR **[2]** followed by a PFR **[3]**. Initially the CFSTR locus yields higher conversion per residence time compared to the PFR. However there is a switching point from which the PFR begins to yield higher conversions per residence time. This switch point is indicated by ×️ on Figure 5.2. Regions of mixing and heat transfer are also shaded and

indicated using v for mixing and k for heat transfer. There also exists an optimal process combination path for reaction and cooling **[4]** or a DCR smooth trajectory intersector on the boundary of this AR^C. There are no DSR intersectors found on the boundary of this structure. In this case the costs of cooling are not considered and the reactor is maintained at optimum cooling rates for high reaction rates.

The non-smooth intersectors that are not trajectories are also identified on the boundary of the AR^C. The first non-smooth ridge indicated in Figure 5.2 is the *v/v* intersector for the intersection of two mixing surfaces due to the switch in the main reaction pathway from a CFSTR **[2]** to a PFR **[3]**. The second ridge on the boundary is the *k/v* intersector where cooling surface intersects the mixing surface due to the reaction and cooling intersector **[4]** that initiates on the boundary. The third ridge on the boundary is the *k/k* non-smooth intersector indicating the intersection of two cooling boundaries due to the termination of the reaction and cooling intersector **[4]** at the minimum catalyst reaction temperature limit**.** The occurrence of these non-smooth intersectors on the boundary serves as evidence of the postulate in Section 5.2.4 that their occurrence is not governed by mathematical expressions but as a result of the intersection of two distinct surfaces.

5.2.6.2   Case 2

In this case the cost of cooling was considered to enable the comparison with the cost of reaction. The value of K_c was taken to be 150. This value was chosen randomly without any basis and therefore, there are no presumptions on whether the cooling costs are very high or low relative to the reaction costs. The RCC algorithm was formulated and implemented

in MATLAB®. The termination criterion was satisfied and the boundary completed after thirteen (13) iterations. Figure 5.3 shows a 2D temperature-extent projection of the AR^C as returned by the RCC algorithm. In this case, both combinations of reaction and mixing and reaction and cooling are observed on the boundary of the AR^C.

In section 5.2.5 we stated that the objective when solving the AR^C of this exothermic reversible reaction will be to find combinations of processes that form a convex boundary of the highest conversion at a given residence time. To further illustrate this, we show, in Figure 5.4, a two-dimensional τ-x projection of the structure of combinations of fundamental processes that forms the main outline of the AR^C boundary from which single process regions such as reaction, mixing and cooling emanate.
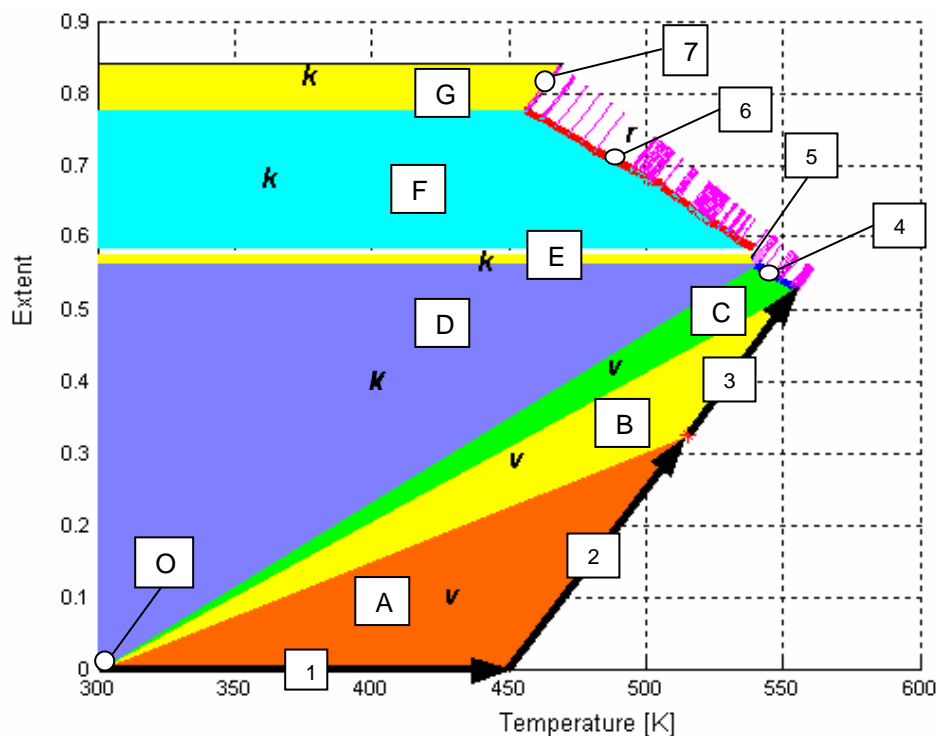
Figure 5.3: A 2D temperature-conversion projection of case 2 AR^C
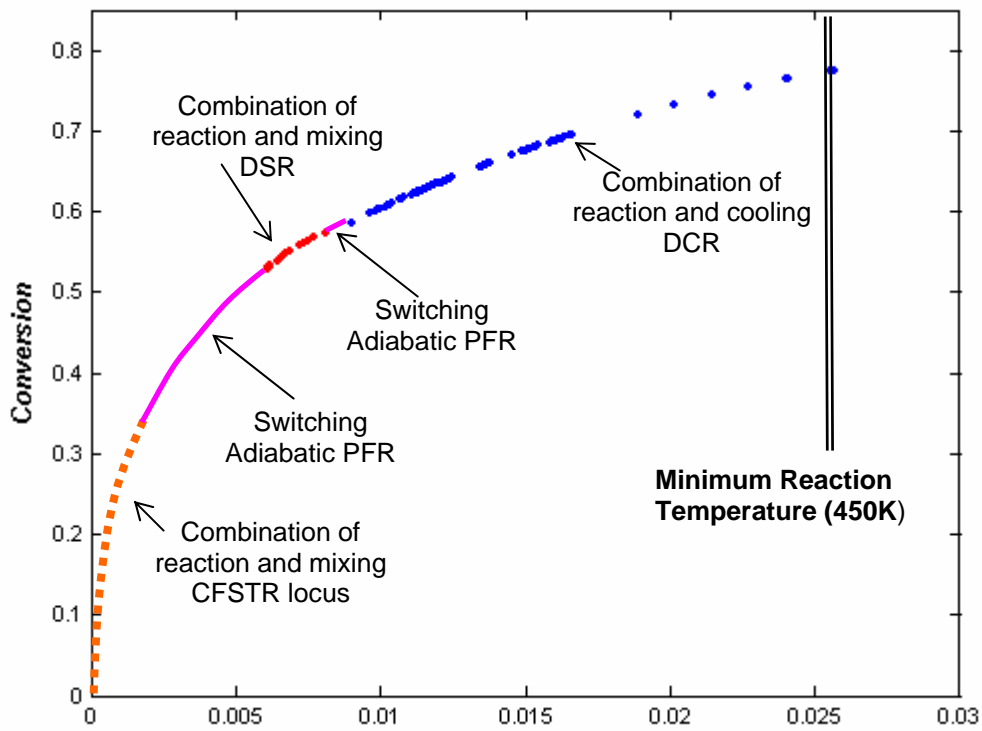
Figure 5.4: The Convex boundary showing combinations of fundamental processes that outlines the AR^C.

The combinations of fundamental processes are linked into a continuous boundary by switching processes; in this case reaction is a switching process as shown by the PFR curves in Figure 5.4.

The 3D temperature-conversion-residence time AR^C is shown in Figure 5.5. The occurrence of non-smooth intersectors on the AR^C boundary is still acknowledged in this case. Figure 5.3 shows different mixing and cooling surfaces as indicated by colour coding. The intersection of these surfaces at the ridges is clearly demarcated by the change in colour.
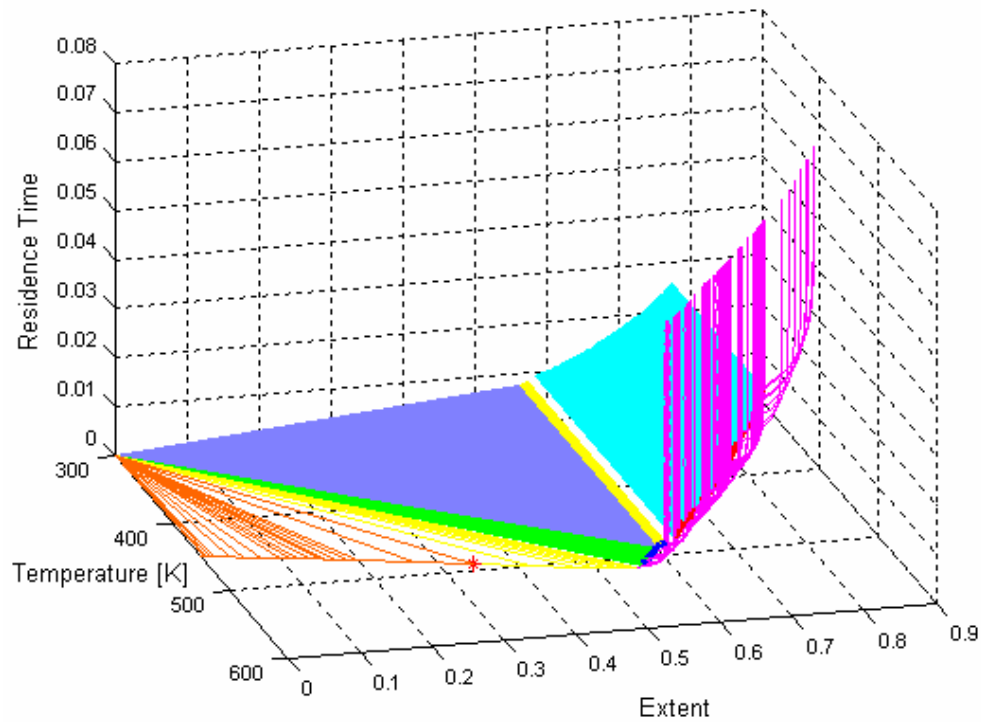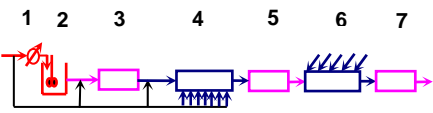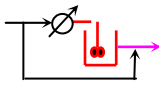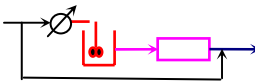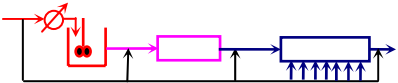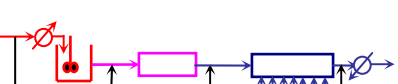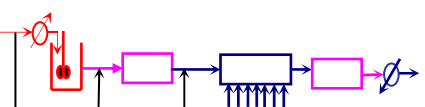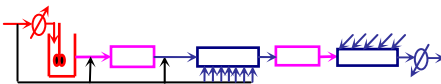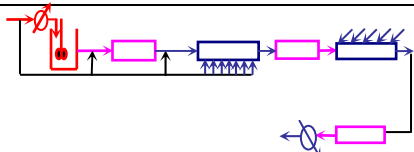
Figure 5.5: A 3D temperature-conversion-residence time AR^C for case 2

Table 5.2 details the interpretation of the AR^C in terms of process layouts. The general process layout is given in numbers **[1]** to **[7]**. The sequence starts with free pre-heating of feed to 450K, **[1]**. Second in series is the adiabatic CFSTR, **[2]** followed by the adiabatic PFR, **[3]**. Process **[4]** is the DSR structure where the combination of reaction and mixing occurs optimally. From DSR **[4],** the reaction is used to switch from a reaction and mixing combination to a reaction and cooling combination curve DCR as can be seen in Figure 5.3 by the PFR **[5]** connecting to the DCR **[6]** where the combination of reaction and cooling occurs optimally. The DCR **[6]** continues until the minimum reaction temperature is reached at 450K. From the DCR at minimum reaction temperature, the process is switched to reaction **[7]** until chemical equilibrium is reached.

Shown also in Figure 5.3 are the mixing and cooling surfaces **A** to **G**. surfaces A, B and C are mixing surfaces as denoted by *v*. Cooling surfaces D, E, F and G are labelled *k*. Mixing is performed using the feed indicated

as point O in Figure 5.3 and is carried to a temperature of 300K as stated earlier to be limited by the feed temperature.

Table 5.2: Process Layout for Exothermic Reversible Reaction Case 2

Process Curve	Process Pathway	Process Layout
1 - 7	The general process layout for the AR^C	
Surface	**Occurring Processes**	**Process Layout**
A	Pre-heater - CFSTR with by-pass	
B	Pre-heater – CFSTR – PFR with by-pass	
C	Pre-heater – CFSTR – PFR – DSR with by-pass	
D	Pre-heater – CFSTR – PFR – DSR - Cooler	
E	Pre-heater – CFSTR – PFR – DSR – PFR-cooler	
F	Pre-heater – CFSTR – PFR – DSR – PFR – DCR-Cooler	
G	Pre-heater – CFSTR – PFR – DSR – PFR – DCR-PFR-Cooler	

5.2.7 Computational Aspects for Example 1

Another impressive aspect of identifying AR^C boundaries using the RCC algorithm is the reduced computational runtimes. Although this example has not being solved using systematic attainable regions methods before, the computational run-times proves the feasibility of including the RCC algorithm in standard simulation packages.

For case 1 of this example the stage-wise algorithm run-times on a Pentium 4, 2.5GHz Intel computer with 256MB RAM are as follows;

- Initialisation Stage:- 12 seconds

- First Iteration:- 31 seconds

- Second Iteration:- 13 seconds

- Third – Fifth Iteration:- 127 seconds

- Polish Stage:- 69 seconds

Total Time: 4 min 12 seconds

For case 2 of this example the stage-wise algorithm run-times are as follows;

- Initialisation Stage:- 13 seconds

- First Iteration:- 37 seconds

- Second Iteration:- 26 seconds

- Third – Fifth Iteration:- 183 seconds

- Polish Stage:- 94 seconds

Total Time: 5 min 53 seconds

5.2.8 Discussion: Example 1

The RCC Algorithm has been successfully implemented to identify the candidate AR structures for this exothermic reversible reaction example and handled the system constraints without any difficulties. The two cases investigated showed how the optimum process structures changed when the relative cost parameters were changed.

In the first case (case 1), the costs of cooling were not considered and the boundary comprised mainly of reaction and cooling as the optimum combination of processes. The AR^C structure comprises of the optimal cooling profile as the optimum combination of processes. This solution could have been arrived at using traditional methods of finding the theoretical optimum cooling profile (Denbigh 1944).

As the costs of cooling were introduced in case 2, other optimal combinations started to appear on the boundary. The optimum combination of reaction and mixing (DSR trajectory intersector) was observed along with that of reaction and cooling (DCR trajectory intersector). This indicates that as the cooling costs are considered, the trade-offs between combinations of reaction and mixing and combinations of reaction and cooling start to play a role and the optimal reactor structures can no longer be determined from theoretical profiles.

The computational run-times were also detailed to show the robustness and expediency of the RCC algorithm as a process synthesis tool. The optimal reactor structures were identified in minutes, and more importantly without preceding complex algebraic computations as in other techniques (Nicol *et al.*, 1997 & 2001, Hausberger 2003, Kauchali,

2004). The procedure was simple plug and play without the need for a specialist in the field.

5.3 Ammonia Synthesis

In this section we study ammonia synthesis as a more specific example of exothermic reversible reactions. Ammonia synthesis exhibits similar characteristics to the generic example studied in section 5.2 as there is only one reaction occurring. However, a number of modifications have to be considered because ammonia synthesis involves a number of reacting components and there is an overall change in the number of moles in the balanced chemical reaction resulting in the reduction in the total flow.   If the total pressure of the system is assumed constant, the ammonia system can be fully modelled as in example 1 in section 5.2.

5.3.1 System kinetics

The reaction governing ammonia synthesis is given out as

$$N_2 + 3H_2 \leftrightarrow 2NH_3 \qquad (5.11)$$

Temkin and Pyzhev, 1940 give the rate of this reaction as

$$r = k\left\{ K_{eq} P_{N_2}\left(\frac{P_{H_2}^{\ 3}}{P_{NH_3}^{\ 2}}\right)^{a} - \left(\frac{P_{NH_3}^{\ 2}}{P_{H_2}^{\ 3}}\right)^{1-a}\right\} \qquad (5.12)$$

P_i is the partial pressure of component i in the reacting gas mixture. The rate constant of the reaction is given by the Arrhenius type equation as:

$$k = k_{(0)} \exp\left\{-\left(\frac{\Delta E_k}{R}\right)\left(\frac{1}{T} - \frac{1}{T_0}\right)\right\}$$

(5.13)

The equilibrium constant K_{eq} can be related to the change in the Gibb's free energy of the reaction ΔG_{rxn}, as

$$K_{eq} = \exp\left\{\frac{-\Delta G_{rxn}}{RT}\right\}$$

(5.14)

The change in the Gibb's free energy of the reaction is given as a function of temperature below (Temkin and Pyzhev, 1940);

$$\Delta G_{rxn}(T) = -9130 + 7.46\ln T - 3.69 \times 10^{-3} T^2 + 2.35 \times 10^{-7} T^3 - 12.07RT$$

(5.15)

T is temperature in K and R is the universal gas constant in units corresponding to that of ΔG_{rxn} and T.

5.3.2 System State Variables and Process Vectors

As we have already remarked that, the ammonia synthesis problem has the same description as the generic problem in section 5.2. Variables were chosen to fully describe the system. The selected variables were temperature, partial pressure of reacting components, and residence time. If the reaction is assumed to occur at constant pressure, partial pressures

of reaction components can be expressed in terms of the conversion of the limiting reagent for a fixed feed, in which case the state variable vector becomes

$$\boldsymbol{c} = [x, T, \tau] \tag{5.16}$$

The fundamental processes considered in the system are that of reaction, mixing and cooling. These processes can be expressed as mathematical vectors as derived in section 5.2. For a reaction the process vector is described as;

$$\boldsymbol{r}(\boldsymbol{c}) = \begin{bmatrix} r_x(x,T) \\ T_{ad} \cdot r_x(x,T) \\ 1 \end{bmatrix} \tag{5.17 a}$$

The mixing process is characterised by;

$$\boldsymbol{v}(\boldsymbol{c},\boldsymbol{c}_0) = \begin{bmatrix} x_0 - x \\ T_0 - T \\ \tau_0 - \tau \end{bmatrix} \tag{5.17 b}$$

The fundamental process of cooling can be described by a vector given by;

$$\boldsymbol{k}(\boldsymbol{c}) = \begin{bmatrix} 0 \\ K_c(T_c - T) \\ 1 \end{bmatrix} \tag{5.17 c}$$

All the symbols carry the same definitions as in section 5.2.

5.3.3 System Specifications, Constraints and Assumptions

A stoichiometric gaseous mixture with a mole ratio of 3:1 hydrogen and nitrogen is provided at 300K as the system feed. The operating pressure is 200atm and assumed to remain constant as the reaction occurs. Pre-heating is free to a maximum temperature of 550K, as this is limited by the heating utility. The cooling utility is available to a minimum temperature of 300K. The catalyst used is taken to be active in the temperature range 500-800K, placing temperature constraints on the system.

5.3.4 RCC Formulation

The RCC formulations were derived and implemented in MATLAB® to obtain the AR^C for ammonia synthesis. The boundary objective was formulated as that of the generic exothermic reversible reaction detailed in Section 5.2.5. The percentage deviational error used in Section 5.2.4.2 was adopted as a termination criterion for this example and the tolerance was set to $E_\% < 1$.

The ammonia synthesis problem is similar to the example in Section 5.2 as they are both exothermic reversible with a single reaction. The ammonia synthesis problem was therefore also formulated with two process combination vectors for the combination of reaction and mixing;

$$P_1(c) = r(c) + \alpha v(c, c_0) \qquad\qquad \alpha \geq 0 \qquad\qquad (5.8b)$$

And the combination of reaction and cooling as;

$$P_2(c) = r(c) + \beta k(T, T_c) \qquad\qquad \beta \geq 0 \qquad\qquad (5.8c)$$

Stage 1

One modification in this part was that the minimum catalyst activity temperature is 500K and the maximum pre-heating temperature is set at 550K. Thus, the pre-heating range to be exploited is from 500-550K, not a fixed point as it was for the previous example. The pre-heating range was divided into 5 points from which PFR trajectories and CFSTR loci were generated. An allowance was made to refine this temperature grid wherever a need arises. However, this was later deemed unnecessary as only the points from the pre-heating temperature of 550K remained on the boundary when the objective function of optimising product conversion was applied.

Stage 2

The cooling utility temperature was fixed at 300K for the combinations of reaction and cooling (5.8c). For the combinations of reaction and mixing, mixing with feed within the range of 300K to 550K was considered.

Iteration Stages

After stage 2, only mixing with feed at 300K resulted with extreme points on the boundary. Therefore, the other feed temperatures (>300K) were discarded as mixing points. Once the termination criterion is met, the AR^C boundary was completed with manifolds of reaction trajectories, mixing lines and cooling lines. The results at the end of the computations are detailed in the next section.

5.3.5 Results

5.3.5.1   Introductory Discussions

Using the rate expression given by equation (5.12), the constant rate contours can be mapped out on a temperature-conversion (*T-x*) diagram as shown in Figure 5.6 below.
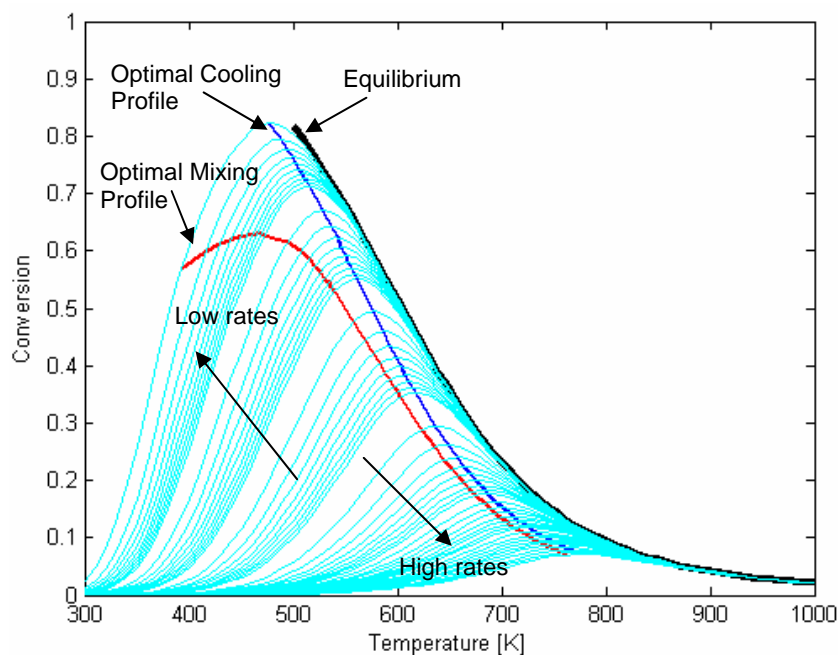
Figure 5.6: Isorate map for ammonia synthesis

These rate contours are called isorates. The *T-x* diagram with isorates has extensively been used by process engineers as a tool to identify the theoretical optimal cooling and mixing profiles. The optimal cooling profile can, on a *T-x* diagram, be identified as a locus of points of highest conversion per isorate curve as shown by the blue curve in Figure 5.6. In section 5.2, we observed this optimal cooling profile being the outlining structure of the AR^C for exothermic reversible reactions permitting processes of reaction, mixing and cooling; when the cost of heat transfer is

not considered (free cooling). This occurrence is also observed when mixing is not allowed as a fundamental process.

The optimal mixing profile can also be outlined on a *T-x* diagram as locus of points where the mixing vector is tangential to the rate of reaction. This profile is shown as the red curve in Figure 5.6. The optimal mixing profile forms a part of the outlining structure of the AR^C boundary when the cost of cooling is considered. For cases where the cost of cooling is very high when compared to that of reaction (e.g. when refrigeration is used), the outlining occurrence of the optimal cooling profile on the AR^C boundary diminishes and the optimal mixing profile outlines the boundary. This incidence is also observed when cooling is not allowed as a fundamental process.

5.3.5.2   Case 1: Free Heat Transfer with no External Cooling

The first case considered is that of a system which permits no external cooling and heat transfer costs are assumed insignificant when compared to reaction cost. Without external cooling or heating, heat exchange is allowed only between the process streams and the overall system is adiabatic. Given a feed at 300K, the final product has to lie on the adiabatic energy balance curve **AB** on Figure 5.7. The two-dimensional temperature-conversion projection of a candidate AR obtained using the RCC algorithm is shown on Figure 5.7.
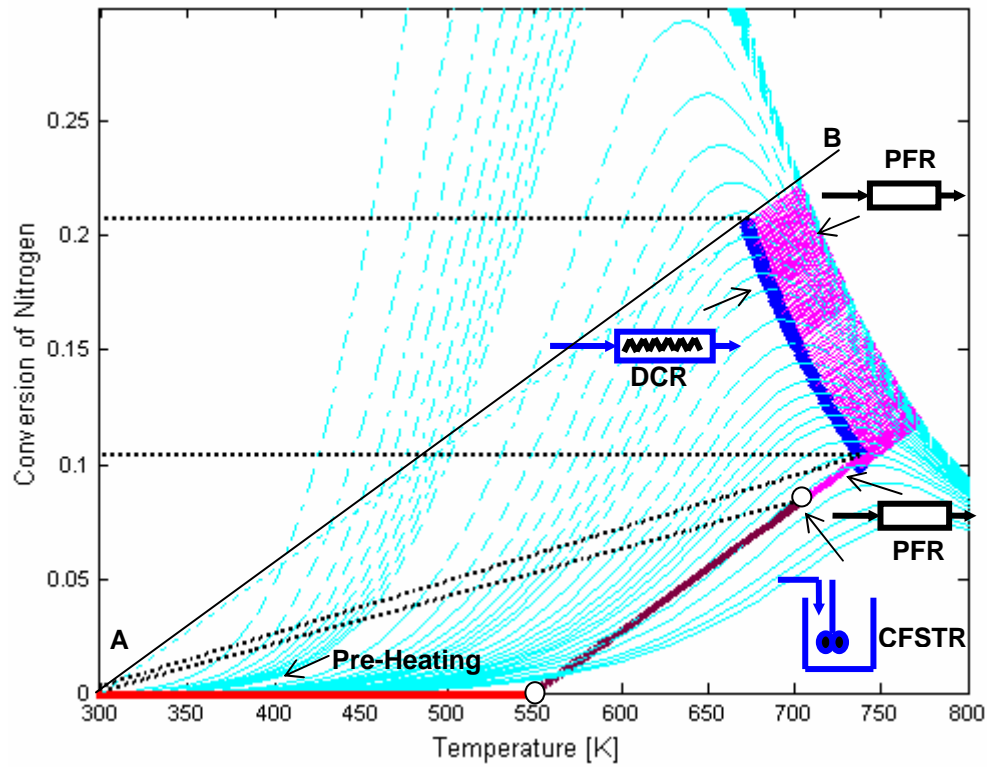
Figure 5.7: A 2D projection of AR^C for case 1 of ammonia synthesis

An optimal reactor network for this case is shown in Figure 5.8 below. The DCR is cooled using cold feed at 300K which in turn gets pre-heated to 550K.
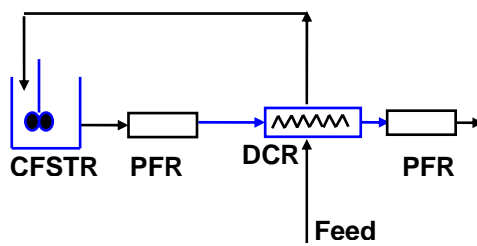
Figure 5.8: The optimal reactor structure for case 1 of ammonia synthesis

5.3.5.3   Case 2: Free Heat Transfer with External Cooling

The second case allows external heat exchange with free heat transfer. Reaction is bounded by a lower temperature limit of 500K. A two dimensional projection of case 2 is shown in Figure 5.9.
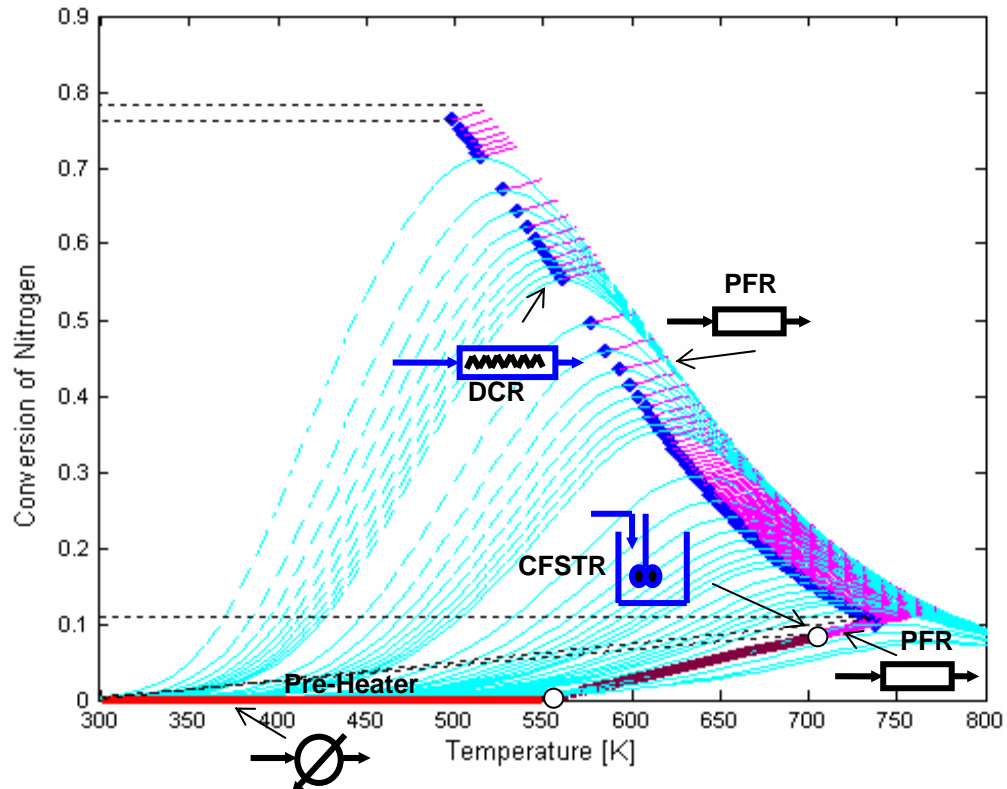
Figure 5.9: A 2D projection of AR^C for case 2 of ammonia synthesis

An optimal reactor network for the second case is shown below.
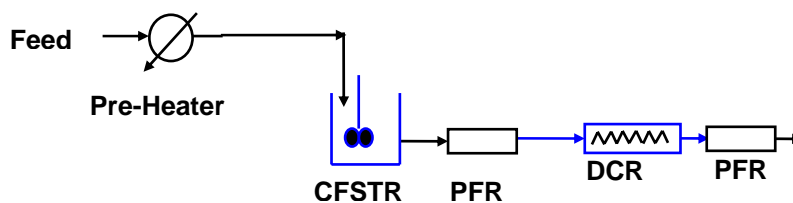
Figure 5.10: The optimal reactor structure for case 2 of ammonia synthesis

5.3.5.4   Case 3: Considering the Cost of Heat Transfer

In the third case, external heat exchange is still allowed and heat transfer costs are taken into consideration. Figure 5.11 shows a two-dimensional projection of the AR^C.
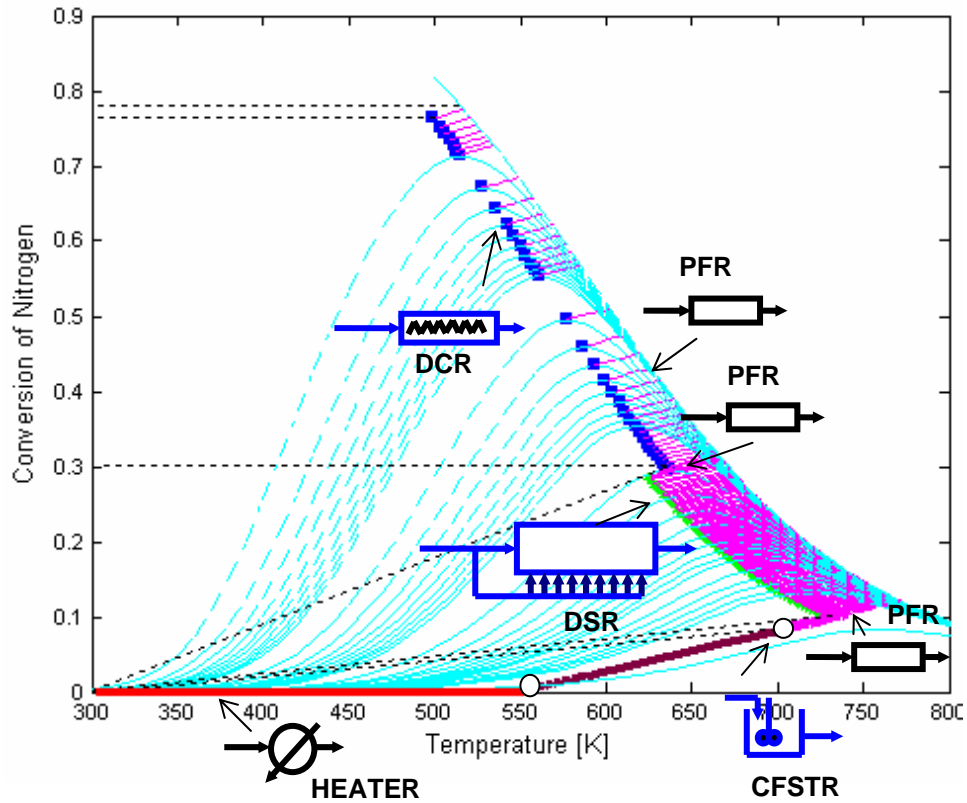
Figure 5.11: A 2D projection of AR^C for case 3 of ammonia synthesis

An optimal reactor network for this case is shown below. In this case, both DSR and DCR are observed to appear on the boundary of the AR^C connected by PFRs.
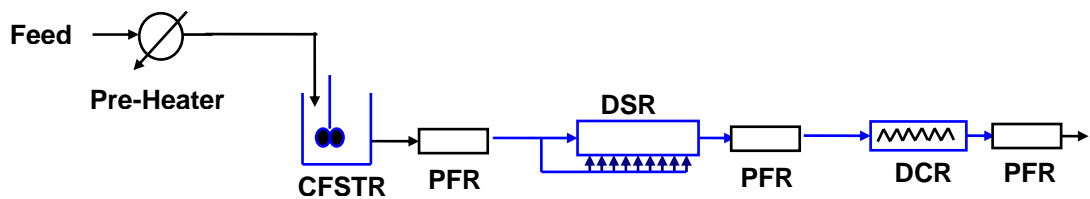
Figure 5.12: The optimal reactor structure for case 3

5.3.5.5   Computational Aspects

The summary of the computational run-times on a Pentium 4, 2.5GHz Intel computer with 256MB RAM for the three cases investigated for ammonia synthesis are shown below

Case 1

- Number of iterations:- 9
- Total computational time:- 7 minutes 36 seconds

Case 2

- Number of iterations:- 6
- Total computational time:- 5 minutes 14 seconds

Case 3

- Number of iterations:- 14
- Total computational time:- 9 minutes 47 seconds

The speed of the RCC algorithm shows significant improvement when compared to other systematic techniques solving the same problem. The Iso-state algorithm run-times were well above five (5) hours when applied to identify candidate attainable regions for the ammonia synthesis problem (Hausberger 2003).

5.3.5.6   Discussion: Ammonia Synthesis Example

We have identified optimal reactor networks for ammonia synthesis via attainable regions. These networks are as might be expected from the solution of the generic exothermic reversible reaction example. In this case we have included the use of isorates on a *T-x* diagram as a traditional tool used to solve optimal cooling and mixing profiles for exothermic reversible reactions. The RCC algorithm successfully solved optimal reactor structures as expected from the use of a *T-x* diagram for simple cases where the costs of heat transfer were not considered for cooling. We further solved a complex case where the costs of cooling were incorporated and once again found the optimal reactor structures successfully.

The most important aspect in solving the ammonia synthesis problem is the computational speed. By comparison, the RCC algorithm proves to be the fasted systematic AR analysis tool to date.

5.4 Discussion

In this chapter we have started using the RCC algorithm to solve candidate attainable regions for practical examples of industrial nature with real kinetic models. These problems were not restricted to be isothermal as the kinetics were temperature dependent and heat transfer was included as a fundamental process along with reaction and mixing.

The problems addressed in this chapter were all of exothermic reversible nature with a single reaction occurring. We have indicated how traditional methods have been used to solve these problems where simple cases are considered and how these methods fall apart as the problems become more of a practical nature, when the costs of cooling were considered. The RCC algorithm formulations were implemented to solve the AR^C boundaries for these problems which were further interpreted as sequences of fundamental processes and combinations of fundamental processes. The sequences of fundamental processes and combinations thereof were further interpreted as reactor networks. These interpretations were clear cut due to colour coding differentiating sections of the AR^C as made possible by the data tracking capabilities of the RCC algorithm.

The RCC algorithm has also shown fast computational run-times when compared to other systematic attainable regions tools. Another aspect that can be highlighted for the RCC algorithm is the ease of changing parameters and investigating different scenarios of the same problem as was done for the two examples studied in this chapter. The results obtained in all cases are discernible and interpretable, showing the robustness of this tool.

5.5 References

Beckett, P. C., Evans, T. I, Ryan, W. E., Akgerman, A., (1989), Designing a multistage adiabatic reactor for minimum catalyst volume, *Chem. Eng. Comm.*, **76**, pp. 107-124

Burghardt, A., Patzek, T., (1978), Constrained Optimisation of Cold Shot Converters, *Chem. Eng. Jour.*, **16**, pp. 153-164

Denbigh, K. G., (1944), Velocity and Yield in Continuous Reaction Systems, *Faraday Society Transcripts*, **40**, pp. 352-373.

Glasser, B., Hildebrandt D., Glasser, D., (1992), Optimal mixing for Exothermic Reversible Reactions. *I&EC Research*, 1992, **31**, 1541-1549.

Godorr, S. A. (1998). *Optimising chemical reactor structures and other systems by means of the attainable region*, PhD thesis, Republic of South Africa: University of the Witwatersrand.

Hausberger, B.P., *Process Synthesis – Developing a toolbox for the process synthesis engineer*, (2003), PhD Thesis, Republic of South Africa: University of the Witwatersrand, Johannesburg.

Hellinckx, L. G., van Rompay, P.V., (1968), Optimum Adiabatic Bed Reactor with Cold Shot Cooling, *Ind. Eng. Chem. Process Des. Dev.* **7**, pp. 595-596

Kauchali, S., Hausberger, B., Hildebrandt, D., Glasser, D., Biegler, L. T., (2004), Automating reactor network synthesis: finding a candidate attainable region for the water-gas shift (WGS) reaction, *Comp. Chem. Eng.*,**28**, pp. 149-160.

Nicol, W., Hildebrandt, D., Glasser, D., (1997), Process Synthesis for Reaction Systems with Cooling via finding the Attainable Regions, *Comp. & Chem. Eng.*, **21**, pp. 35 – 40.

Nicol, W., Hernier, M., Hildebrandt, D., Glasser, D., (2001), The attainable region and process synthesis: reaction systems with external cooling and heating: The effect of relative cost of reactor volume to heat exchange area on the optimal process layout , *Chem. Eng. Sci.*, **56, (1)**, pp. 173 – 191.

Omoleye, J. A., Adesina, A. A., Udegbunam, E. O., (1989), Optimum Design of Nonisothermal Reactors: Derivation of Equations for the Rate-Temperature-Conversion and the Optimum Temperature Progression for a General Class of Reversible Reactions, *Chem. Eng. Commun.*, **79**, pp. 95-107.

Ravella, A.& de Lasa, H., (1987), Cooling Exothermic Catalytic Fixed Bed Reactors: Co-Current Versus Countercurrent Operation in a Methanol Conversion Reactor, *Can. Jour. Chem. Eng.*, **65**, pp. 1021-1025.

Temkin, M. I. & Pyzhev, V., (1940), *Acta Physicochim*, **12,** pp.327

5.6 List of Symbols

Abbreviations

AR	Attainable Regions
AR^C	Candidate Attainable Regions
CFSTR	Continuous Flow Stirred Tank Reactors
DCR	Differentially Cooled Reactor
PFR	Plug Flow Reactor
DSR	Differential Side-stream Reactor
RCC	Recursive Constant Control Policy

Symbols

α	Combination control policy for fundamental processes (mixing)
A_1, A_2	Arrhenius constants
β	Combination control policy for heat transfer
c	State variable of the system
c_o	State variable of the system at the feeding point
c^*	Mixing state variable of the system
$\boldsymbol{c}$	State vector comprising all variables describing the system
Cp	Isobaric specific heat capacity of the material
E_1, E_2	Arrhenius constants
h_o	Heat Transfer coefficient
k_c	Heat Transfer constant
K_c	A measure of cooling costs relative to reaction costs
P	Partial pressure of the reacting components
$\boldsymbol{r}(c)$	Reaction rate vector defined at c
$\boldsymbol{r}(P,T)$	Reaction vector defined at P and T
R	Universal Gas constant
T	Temperature of reaction
T_{ad}	Adiabatic temperature gradient

T_c	Cooling utility temperature
T_o	Feed temperature
T^*	Temperature of mixing
τ	Residence time
τ_r	Reaction residence time
υ	Mixing vector, mixing c with c^*
w	Heat Exchange vector
x	Conversion of limiting reactant
ω	Residence time for the cooling process
ΔG_{rxn}	Gibbs free energy of the reaction
ΔH_{rxn}	Enthalpy of the reaction

CHAPTER 6

ATTAINABLE REGION ANALYSIS FOR METHANOL SYNTHESIS

6.1 Introduction

In this section we will identify optimal reactor networks for low-pressure methanol synthesis. Unlike in the previous industrial examples which comprised a single exothermic reversible reaction, methanol synthesis is a more complex system with three reactions occurring. Low pressure methanol synthesis is done by the reaction of carbon monoxide and hydrogen. This has been studied by many researchers such as Natta, (1955); Bakemeier *et al.*, (1970); Leonov *et al.*, (1973); and Monnier *et al.*, (1984) among others. The reaction for methanol synthesis from CO is given by,

$$CO + 2H_2 \leftrightarrow CH_3OH \qquad \Delta H^{\circ}_{298} = -90.64 \text{ kJ mol}^{-1} \quad (I)$$

For this proposed reaction route the role of CO_2 in methanol synthesis was considered to be and restricted to competitive adsorption on the active sites of the catalysts. Contrary to this some researchers (Chinchen *et al.*, (1984); Dybkjaer, (1985)) claimed that methanol is formed from CO_2 only due to its strong adsorption power, subduing and inhibiting the co-adsorption of CO. It was only in the past two decades that researchers started to assimilate the role of CO_2 together with that of CO in methanol synthesis reaction models. Denise and Sneeden (1982) and Klier *et al.*, (1982) proposed a kinetic model incorporating both CO and CO_2 reactions

from conclusions based on kinetic experiments. Liu *et al.*, (1985) came to the same conclusion based on experiments with labelled oxygen in CO_2. Graaf *et al.*, (1988) proposed a kinetic model which considered the two reactions over a Cu-Zn-Al catalyst. This catalyst is also known to promote the water-gas-shift (WGS) reaction as the third reaction as considered by Graaf *et al.*, (1988) in their model. Struis and Stucki (1996 and 2001) reviewed the kinetic models proposed by Graaf *et al.*, (1988) with modifications for their study of a membrane reactor concept for methanol synthesis.

In this work we apply attainable regions analysis to the modified Graaf *et al.*, (1988) kinetic models to identify optimal reactor networks for methanol synthesis. We start by first studying the kinetics in detail to investigate if there are any evident optimal structures to be expected and then apply automated techniques to identify optimal reactor structures which can further be compared to prior expectations.

6.2 Methanol Synthesis: The Kinetics

The kinetic model used in this study is that of Graaf *et al.*, (1988) as modified by Struis and Stucki (2001). Methanol synthesis comprises three equilibrium limited reactions as shown below

$$CO + 2H_2 \leftrightarrow CH_3OH \qquad \Delta H^\circ_{298} = -90.64 \text{ kJ mol}^{-1} \quad \text{(I)}$$

$$CO_2 + H_2 \leftrightarrow CO + H_2O \qquad \Delta H^\circ_{298} = 41.17 \text{ kJ mol}^{-1} \quad \text{(II)}$$

$$CO_2 + 3H_2 \leftrightarrow CH_3OH + H_2O \qquad \Delta H^\circ_{298} = -49.47 \text{ kJ mol}^{-1} \quad \text{(III)}$$

The two reactions for methanol formation (I) and (III), are exothermic as written, and are influenced towards the product side by high pressures.

The WGS reaction, (II) is endothermic and its equilibrium is not a function of pressure as the number of moles does not change as the reaction occurs. For reactions (I) and (III), high temperatures are required for high rates of reaction whilst high equilibrium conversion is favoured by low temperatures, a general trend observed with exothermic reversible reactions. However, the WGS reaction is endothermic as written and therefore favours high temperatures for both reaction rates and high equilibrium conversion.

Graaf *et al.*, (1988) derived the kinetic rate expressions for each of the three reactions, by defining chemical reaction as the rate controlling step and advocated the adsorption mechanism to be a dual-site Langmuir-Hinshelwood mechanism, where CO, CO2, H_2 and H_2O can all adsorb competitively. The rates of formation of species in the reaction system are given by Graaf *et al.*, (1988) as;

$$r'_{CH_3OH,1} = \frac{k'_{ps,1} K_{CO} \left[f_{CO} f_{H_2}^{3/2} - f_{CH_3OH} / \left(f_{H_2}^{1/2} K_{p1}^o \right) \right]}{\left(1 + K_{CO} f_{CO} + K_{CO_2} f_{CO_2} \right) \cdot \left[f_{H_2}^{1/2} + \left(K_{H_2O} / k_{H_2}^{1/2} \right) f_{H_2O} \right]} \quad (6.1)$$

$$r'_{H_2O,2} = \frac{k'_{ps,2} K_{CO_2} \left(f_{CO_2} f_{H_2} - f_{H_2O} f_{CO} / K_{p2}^o \right)}{\left(1 + K_{CO} f_{CO} + K_{CO_2} f_{CO_2} \right) \cdot \left[f_{H_2}^{1/2} + \left(K_{H_2O} / k_{H_2}^{1/2} \right) f_{H_2O} \right]} \quad (6.2)$$

$$r'_{CH_3OH,3} = \frac{k'_{ps,3} K_{CO_2} \left[f_{CO_2} f_{H_2}^{3/2} - f_{CH_3OH} f_{H_2O} / \left(f_{H_2}^{3/2} K_{p3}^o \right) \right]}{\left(1 + K_{CO} f_{CO} + K_{CO_2} f_{CO_2} \right) \cdot \left[f_{H_2}^{1/2} + \left(K_{H_2O} / k_{H_2}^{1/2} \right) f_{H_2O} \right]} \quad (6.3)$$

The gas composition is given by fugacities (f_i) for each gas species *i* (in pressure units: bar). For the purpose of this study the fugacities will be considered to be adequately approximated by partial pressures and this assumption will be carried henceforth. The adsorption equilibrium

constants are symbolised by K_{CO}, K_{CO2}, K_{H_2} and K_{H_2O} respectively, and chemical equilibrium constants for the three reactions are denoted by $K_{p_1}^0$, $K_{p_2}^0$ and $K_{p_3}^0$, respectively, with subscripts p_j indicating that these constants are based on partial pressure. Each reaction rate, r_j, is characterised by a rate constant, $k'_{ps,j}$, where subscript j refers to the consigned reaction (viz. j = 1, 2, 3 for reaction (I), (II), (III) respectively). The chemical equilibrium constants are reported by Struis and Stucki (2001) as

$$K_{p_1}^o = 10^{(3921/T)-7.971\times10^{10}\log(T)+2.499\times10^{-3}\times T-2.953\times10^{-7}\times T^2+10.20} \tag{6.4}$$

$$K_{p_2}^o = 10^{6.959-(2489/T)-1.565\times10^{10}\log(T)+6.6\times10^{-5}\times T+(2.3\times10^4/T^2)} \tag{6.5}$$

$$K_{p_3}^0 = K_{p_1}^0 \cdot K_{p_2}^0 \tag{6.6}$$

The modified parameters for the Graaf *et al.*, (1988) kinetic model were resolved by Struis and Stucki (2001) as the following;

$$k'_{ps,1} = (1.23 \pm 0.17) \times 10^6 \exp(-104430 \pm 3110/RT) \tag{6.7}$$

$$k'_{ps,2} = (2.21 \pm 0.13) \times 10^{10} \exp(-123500 \pm 1450/RT) \tag{6.8}$$

$$k'_{ps,3} = (3.390 \pm 0.080) \times 10^3 \exp(-65250 \pm 430/RT) \tag{6.9}$$

$$K_{CO} = (9.72 \pm 0.38) \times 10^{-7} \exp(57260 \pm 590/RT) \tag{6.10}$$

$$K_{CO_2} = (1.190 \pm 0.050) \times 10^{-7} \exp(66710 \pm 670/RT) \tag{6.11}$$

$$(K_{H_2O}/K_{H_2}^{1/2}) = (4.14 \pm 0.10) \times 10^{-11} \exp(104500 \pm 525/RT) \tag{6.12}$$

The model parameters were fitted for the experimental conditions within the range of T =200-260°C and P = 30-60 bar. However, the Cu-Zn-Al

catalyst is known to be active for the three methanol synthesis reactions in the temperature range T = 400 – 600K (Twigg, 1996).

For a feed mixture of CO and CO_2 in mole ratio of 1:1 and the stoichiometric amount of H_2, the following chemical equilibrium curves can be established at various outlet pressures as indicated in Figure 6.1. The molar composition of the feed for this case can be evaluated as [CH_3OH CO CO_2 H_2 H_2O] = [0 0.14 0.14 0.72 0].
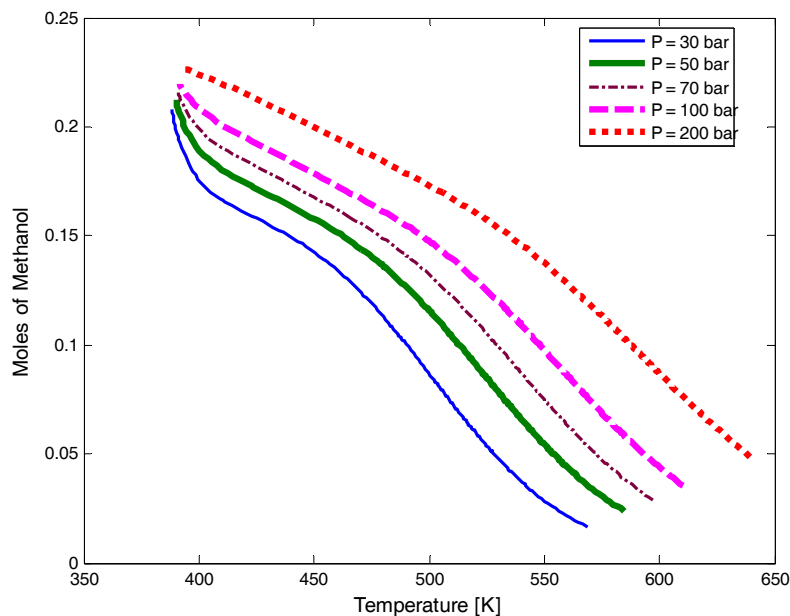
Figure 6.1: Variation of chemical equilibrium with pressure

In agreement with the expectations, the equilibrium conversion of methanol increases with increasing pressure at a specified temperature. This behaviour is as stated earlier, due to the fact that the methanol forming reactions; (I) and (III), both result in decreased total number of moles and therefore high pressure will favour conversion towards the product. Figure 6.2 shows how the equilibrium composition of methanol changes as the mole ratio of CO_2: CO is varied. The observed trend is that the equilibrium amount of methanol decreases as the ratio of CO

decreases. This observation could be attributed to the fact that CO has a higher tendency to react to form methanol than CO_2. To investigate this proposal the average rate contours are used to study the kinetics in more detail. The rate contour study is carried out at a fixed pressure of 50 bar using the feed gas composition as stated above.
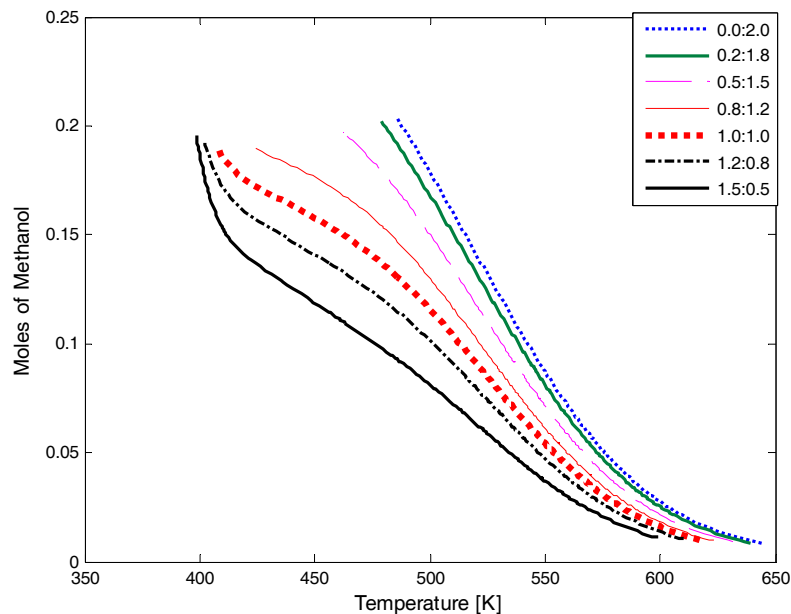
Figure 6.2: Variation of chemical equilibrium with CO2:CO mole ratio

The average rate contours for formation of methanol are shown in Figure 6.3. The rate contours plotted are the summed individual rates of formation of methanol from reaction (I) and (III) as defined by expressions (6.1) and (6.3) respectively. In this case, the WGS reaction (II) is not considered. The rates as quoted are in units of mol s^{-1} kg-catalyst^{-1}. Figure 6.4 depicts contours for the rate of formation of methanol from CO (reaction I). By comparison of magnitude with rate of formation of methanol from both CO and CO_2 (Figure 6.3), it appears that methanol is likely to form mainly from CO through reaction (I). This observation is supported by the low rate values of formation of methanol from CO_2 as shown in Figure 6.5, which are in the range of one-tenth of the combined effect in Figure 6.3.
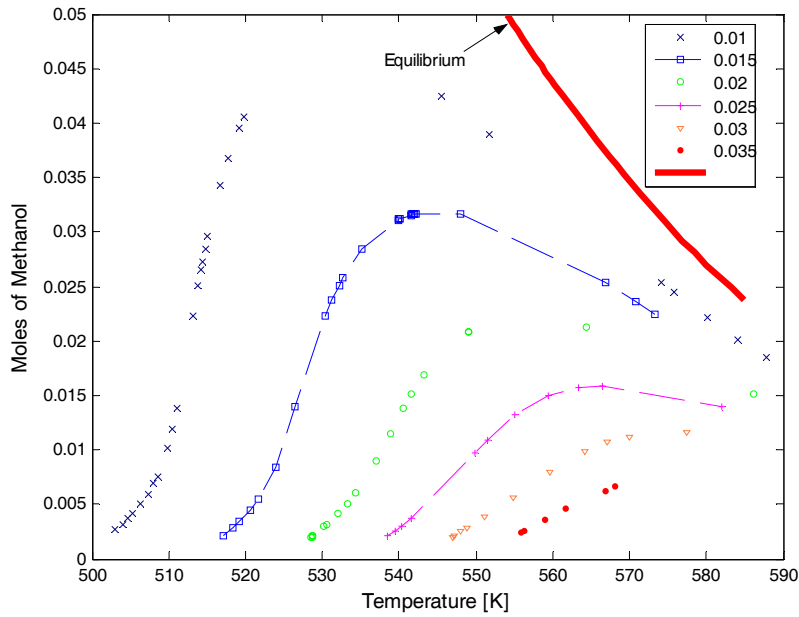
Figure 6.3: Average isorate contours for methanol formation
(r = r_CH3OH,1 + r_CH3OH,3)
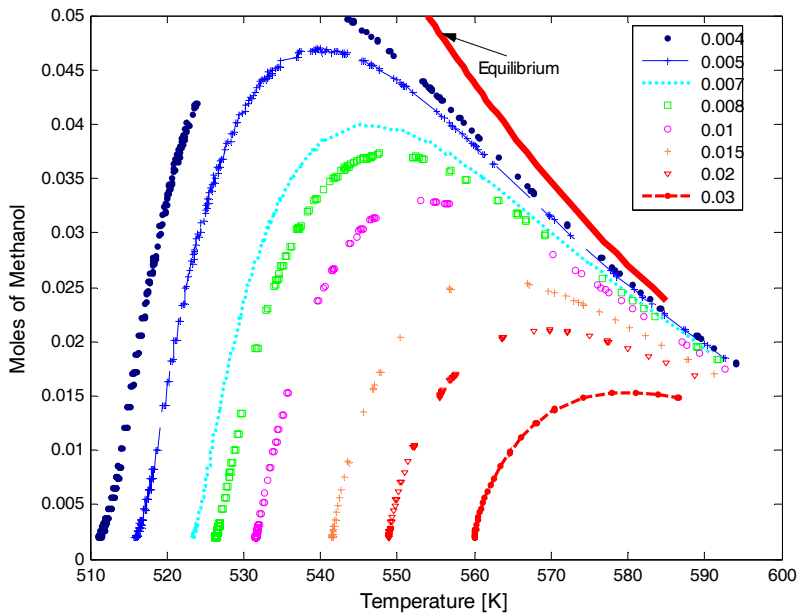
Figure 6.4: Isorate contours for methanol formation from reaction (I)
(r = r_CH3OH,1)

To investigate the effect of the WGS reaction, the contours for the rate of reaction of CO from reactions (I) and (II) are shown in Figure 6.6. The contours show an oval shape as compared to the S-shape of Figure 6.4. It

can be seen from the slightly reduced rate of consumption of CO when compared to the trend in Figure 6.4 that the WGS reaction effects the formation CO. In the case where the WGS reaction is redundant, the contours in Figure 6.6 would resemble that in Figure 6.4.
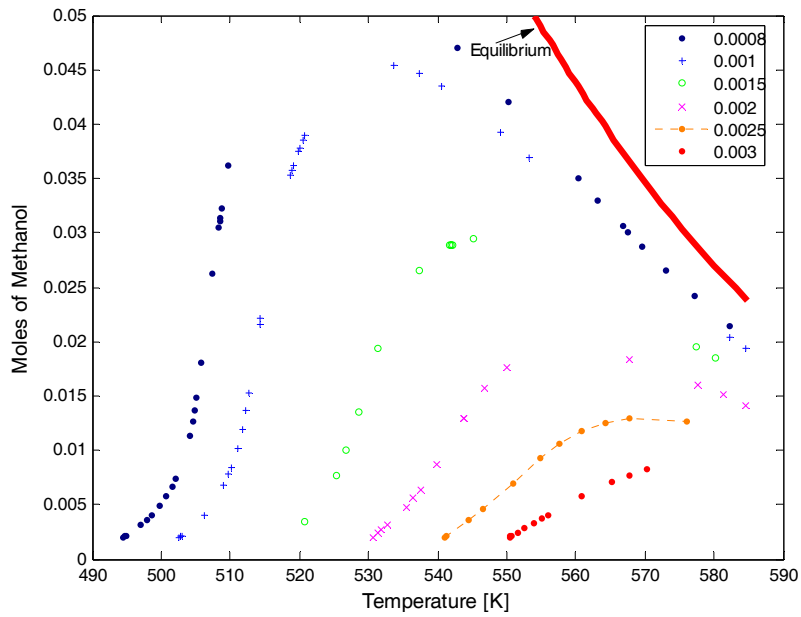
Figure 6.5: Isorate contours for methanol formation from reaction (III)
(r = rCH3OH,3)
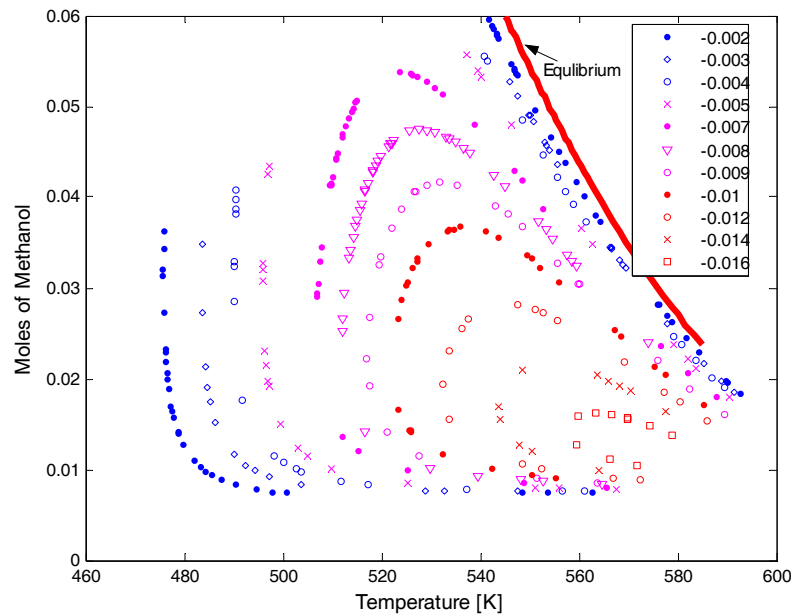
Figure 6.6: Average isorate contours for CO reaction from reactions (I)
and (II)   (r = rCO,2 - rCO,1)

It is evident from the observation of the plots of rate contours that the determination of optimal reactor structures for methanol synthesis will not be clear-cut from a theoretical aspect as the optimum profiles of all three reactions have to be considered. In theory, the rate contours in Figure 6.3 for the average formation of methanol from reaction (I) and (III) could be used if the effect of the water gas shift reaction is considered insignificant. However, it can be noted in Figure 6.6 that the WGS reaction affects the reaction scheme in a considerable manner.

Depicted in Figure 6.7(a) are the adiabatic plug flow reactor profiles at varying feed temperature. These profiles show how the temperature changes with the mole fraction of methanol formed as the reaction system progresses. At low temperatures the reaction is exothermic as shown by the increase in temperature with increasing methanol conversion, giving an indication that the methanol forming reactions (I) and (III) are clearly dominating. As the reaction occurs the system gets more exothermic as indicated by the flattening of the PFR curves. At low methanol conversions and high temperatures (high feed temperature) the methanol reaction system becomes endothermic as indicated by the shaded area where the slope of the adiabatic PFR is negative indicating a decrease in temperature with increasing methanol conversion. In this region the endothermic WGS reaction (II) dominates. This behaviour is the expected trend with endothermic reactions as high temperatures favour both high rates of reaction and high equilibrium conversions. Figure 6.7(b) shows the expansion of this endothermic region.

This mixed exothermic-endothermic behaviour of the methanol synthesis system asserts that, the theoretical methods of determining optimum reaction-cooling and reaction-mixing profiles cannot be used to solve optimal reactor networks.
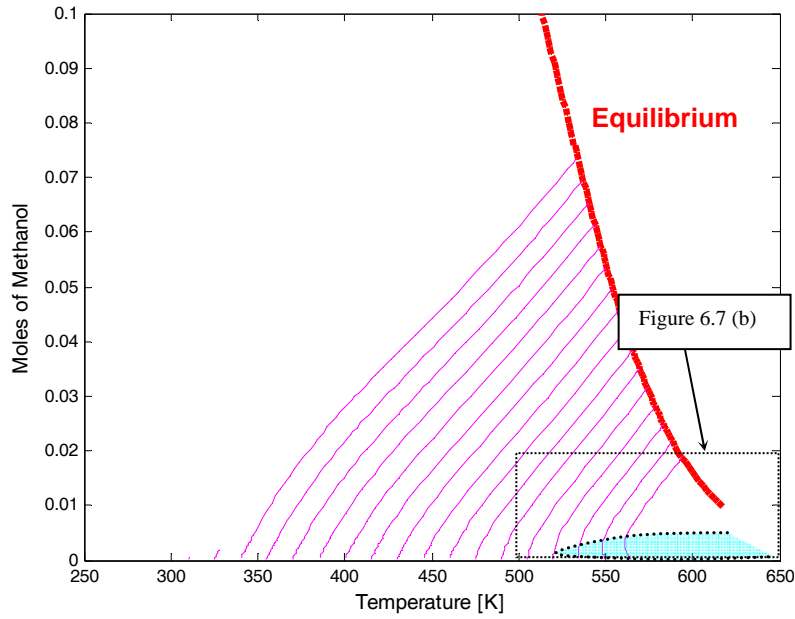
Figure 6.7(a): Methanol synthesis adiabatic plug flow reactor profiles
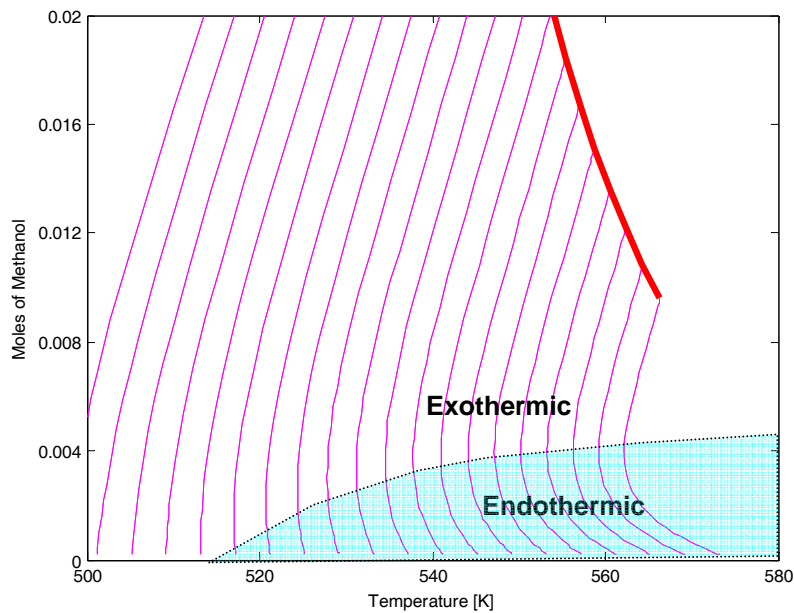
Figure 6.7(b): Methanol synthesis adiabatic plug flow reactor profiles
(Endothermic region expansion)

In the next section we will formulate the RCC algorithm to solve the candidate AR for methanol synthesis using Graaf kinetics, from which the optimal profiles will be identified.

6.3 Methanol Synthesis: Problem Formulation

6.3.1 Process Vectors

The permitted fundamental processes in this formulation of methanol synthesis are reaction, cooling, heating and mixing. The feed is provided at a temperature of 300K and is considered to be that of a 1:1 mixture of $CO:CO_2$ with the stoichiometric amount of hydrogen.

For the fundamental process of reaction all components that partake in the reaction are considered. A vector describing the rates of reaction of each component is given in (6.13). A vector associated with the rate of reaction of components is given by equation (6.13a)

$$\boldsymbol{r_m}(\boldsymbol{m},T,\tau) = \begin{cases} r_1 = r_{CH_3OH} = r_I + r_{III} \\ r_2 = r_{CO} = -r_I + r_{II} \\ r_3 = r_{CO_2} = -r_{II} - r_{III} \\ r_4 = r_{H_2} = -2r_I - r_{II} - 3r_{III} \\ r_5 = r_{H_2O} = r_{II} \end{cases} \tag{6.13a}$$

The rates r_I, r_{II} and r_{III} are that of reactions (I), (II) and (III) as described in section 3.1 with expressions given by equations (6.1), (6.2) and (6.3) respectively. To describe the composition state, mass fraction of components, $\boldsymbol{m}$ is used as a variable.

The rate of change of temperature as the reactions occur is given by the net effect of all three chemical reactions as shown by equation (6.13b) below;

$$r_T(\boldsymbol{m},T,\tau) = \left\{ r_I \cdot T_{ad_I} + r_{II} \cdot T_{ad_{II}} + r_{III} \cdot T_{ad_{III}} \right\} \tag{6.13b}$$

And the rate associated with the change in residence time, τ is as described in the earlier chapters;

$$r_\tau(\tau) = \{1\} \tag{6.13c}$$

The general reaction vector for the system becomes

$$r(c) = \begin{bmatrix} r_m(m,T,\tau) \\ r_T(m,T,\tau) \\ r_\tau(\tau) \end{bmatrix} \tag{6.14}$$

The characteristic vector of the system containing all variables that fully describe the system can now be defined as;

$$c = \begin{bmatrix} m \\ T \\ \tau \end{bmatrix} \tag{6.15}$$

Mixing, cooling and heating vectors as previously shown are characterised by equations (6.16), (6.17) and (6.18) respectively (Chapter 5).

$$v(c,c_0) = \begin{bmatrix} m_0 - m \\ T_0 - T \\ \tau_0 - \tau \end{bmatrix} \tag{6.16}$$

$$k(c) = \begin{bmatrix} 0 \\ K_c(T_c - T) \\ 0 \end{bmatrix} \tag{6.17}$$

$$h(c) = \begin{bmatrix} 0 \\ K_h(T_h - T) \\ 0 \end{bmatrix} \tag{6.18}$$

Where mixing is performed with the mixing state $c_0 = [m_0, T_0, \tau_0]$ and cooling is assumed to be carried out using a constant temperature cooling utility at T_c. The heating utility temperature is symbolised as T_h. K_c is as

defined in equation (5.6) of Chapter 5 to be a measure of the relative cost of cooling in comparison to cost of reaction. K_h takes the analogous definition for heating.

The process combination vectors considered in this study are limited to smooth trajectory intersectors that always include reaction as one of the fundamental processes. Thus, the fundamental process of reaction will be included in all combinations. The reasoning for these combinations is based on the conjecture we asserted in Chapter 2 when reviewing the postulates pertaining to the structure of the AR boundary derived by McGregor (1998) and the results obtained in Chapters 3 and 5 to prove this conjecture. The conjecture stated that the occurrence on the AR boundary of non-smooth intersectors is not governed by mathematical expressions but by intersection of two or more distinct process surfaces. The vectors describing the combinations of processes that are smooth trajectory intersectors are discussed in equation set (6.19) as follows.

Reaction and mixing are combined using the combination control policy α, as represented in equation (6.19a) below;

$$\boldsymbol{g}_{r,v} = \boldsymbol{r}(\boldsymbol{c}) + \alpha \cdot \boldsymbol{v}(\boldsymbol{c}, \boldsymbol{c}_0) \tag{6.19a}$$

The process vector in equation (6.19b) shows the combination of fundamental processes of reaction and cooling using the control policy symbolised by β,

$$\boldsymbol{g}_{r,k} = \boldsymbol{r}(\boldsymbol{c}) + \beta \cdot k(T, T_c) \tag{6.19b}$$

The combination control policy θ, combines the processes of reaction and heating as represented by the combination vector given in equation (6.19c) below;

$$\boldsymbol{g}_{r,h} = \boldsymbol{r}(\boldsymbol{c}) + \theta \cdot \boldsymbol{h}(T, T_h) \tag{6.19c}$$

The general process vector for combination of all permitted fundamental processes in the system can then be expressed by as;

$$\boldsymbol{g}_{r,v,k,h} = \boldsymbol{r}(\boldsymbol{c}) + \alpha_G \cdot \boldsymbol{v}(\boldsymbol{c},\boldsymbol{c}_0) + \beta_G \cdot \boldsymbol{k}(T,T_c) + \theta_G \cdot \boldsymbol{h}(T,T_h) \tag{6.20}$$

However, this general net process vector will not be used in the RCC algorithm formulation as stated above.

The subscript '$_G$' in the control policies indicates that the control policies are for the general process vector and not for the paired combinations as in (6.19). This will help differentiate between the general process vector and the paired combinations.

6.3.2   The RCC Algorithm

Given the problem specifications such as variable constraints, feed specifications, heating and cooling relative cost factors, utility limitations, *etc*, the RCC algorithm for the problem can now be formulated and implemented in MATLAB® to solve the optimal profiles of combinations of permitted fundamental processes and complete AR^C for the methanol synthesis problem. The AR^C boundary can further be interpreted as a sequence of application of fundamental processes and/or combinations thereof, which are applied to the feed states to attain the product states that shape the boundary. This interpretation is useful as the sequences of applied fundamental process and/or their combinations can be further interpreted into unit operations with design key parameters that essentially specify the optimal process flowsheet.

The reaction vector for methanol synthesis system as formulated in Section 6.3.1 comprises seven state functions. These functions are; five that represent the rate of change in the states of reaction components, the rate of change of reaction system temperature and the rate associated with the change in residence time of the system as given by equations (6.13) and (6.14). The methanol synthesis problem is therefore formulated as a seven-dimensional system.

The objective of this problem is to maximise the conversion of carbon (C) in the form of CO and CO_2 to methanol (CH_3OH). This objective is attained by exploiting combinations of reaction with mixing, cooling and/or heating in order to attain reaction temperatures that yield maximum rates of reactions and maximum equilibrium conversions of carbon to methanol at the minimum possible residence time. Thus, the attainable regions for this problem can be constructed in three-dimensional space using the variables that describe the system objective. These variables are conversion of carbon to methanol, temperature and residence time.

The RCC algorithm is formulated to solve the methanol synthesis problem using seven system variables. The AR boundary construction, convexification and optimisation of the objective function are carried in three-dimensional space. This transformation simplifies a complex seven-dimensional problem into a geometrically representable three-dimensional problem.

The feed to the system is, as stated earlier, to be a mixture of CO and CO_2 in mole ratio of 1:1 and the stoichiometric amount of H_2 resulting in molar composition of [CH_3OH CO CO_2 H_2 H_2O] = [0 0.14 0.14 0.72 0]. The feed is available at the temperature of 300K. The system pressure is taken

to be 50bar and assumed to remain constant as the reaction occurs for simplification purposes. The catalyst activity range is adopted from Twigg (1996) to be between 400K and 600K. Cooling can be carried out to a minimum temperature of 300K as may be limited by the cooling utility temperature. Heating is similarly limited to a maximum of 600K.

Using these system specifications and constraints the RCC algorithm can be formulated as summarised below.

Stage 1

PFR trajectories and CFSTR loci are generated from feed temperature within the temperature range of 300K to 600K. Pre-heating is used as the initial process to heat the feed mixture from 300K. The resulting structure is convexified and the starting points for smooth trajectory intersectors that are combinations of reaction and mixing, reaction and cooling and reaction and heating are selected along with the corresponding mixing, cooling and heating points.

Stage 2

Trajectories that are combinations of processes are initiated at selected starting points. The resulting structure is convexified to eliminate all states that are not extreme points on the convex boundary. The starting points, mixing, cooling and heating points that did not yield any extreme points on the convex boundary are discarded.

Iteration Stage

Stage 2 is performed iteratively until the termination criterion is satisfied. The termination criterion is formulated as the percentage deviational error given in Section 5.2. For this example the tolerance is set to $E_\%$ < 10%. This

relatively high tolerance value is revised as a result of the complexity and computational intensity of the methanol synthesis problem.

In the next section we present the results for the two case studies investigated. The details of the mathematical programming of the RCC algorithm is not detailed herein as they are analogous to the presentations outlined in Chapter 3.

6.4 Results

The primary objective of the two case studies detailed herein is to investigate the effect of cooling and heating relative cost factors on the shape of the AR^C boundary and the occurrence of combinations of fundamental processes on the boundary.

6.4.1   Case 1

The cooling and heating relative cost factors K_c and K_h, are taken to be equal at a fixed value of 500 with corresponding time units. This value is arbitrarily chosen. The reasoning behind the choice of this value is that the study does not aim at comparing the costs of heating and cooling to that of reaction, but instead investigates how the AR^C boundary changes as the relative (to one another) costs of cooling and heating change.

Using the process specifications the AR^C was solved in the 3D carbon conversion-residence time-temperature space and the results are show in Figure 6.8 on a Temperature-Conversion (T-X) 2D projection.
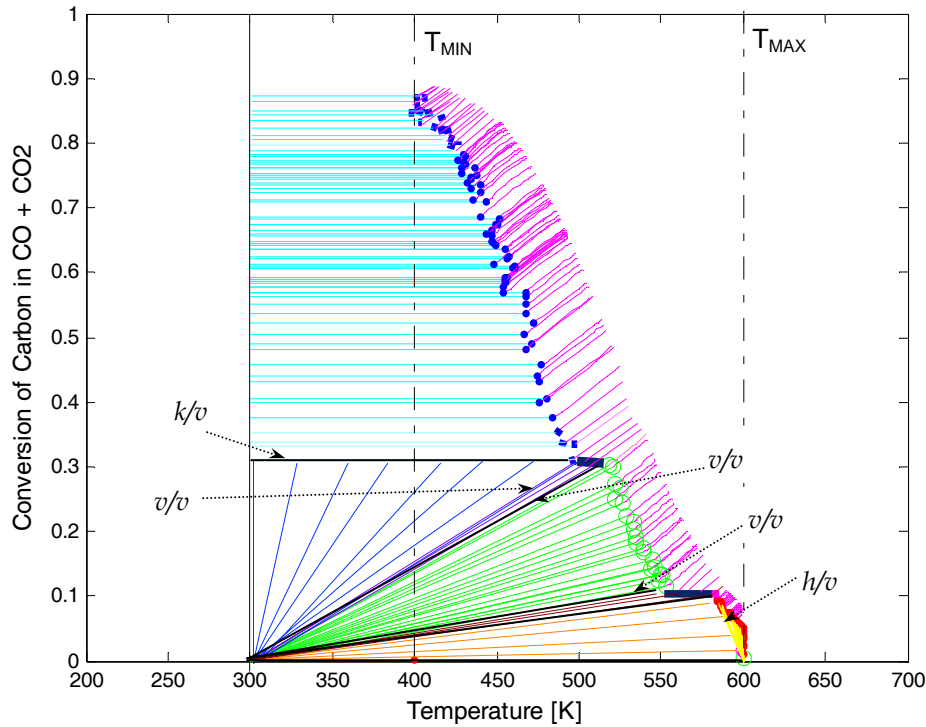
Figure 6.8: A 2D T-X AR^C Projection of Methanol Synthesis Case 1

Carbon conversion is defined as the mole fraction of carbon atoms (from both CO and CO_2) that reacted to form methanol.

The boundary of the candidate attainable region is outlined by trajectory intersectors that are optimal combinations of reaction and mixing, reaction and cooling, and reaction and heating. The characterisation of the optimal intersectors is carried out in Figure 6.9. From these intersectors manifolds that are unions of reaction trajectories, mixing lines, cooling lines, and heating lines emanate. Once again we will emphasise the occurrence of non-smooth ridges that are intersection of different process surfaces. These ridges are indicated in Figure 6.8 by *v/v*, *k/v*, *h/v* for the intersection of mixing and mixing, cooling and mixing, heating and mixing surfaces respectively.

The interpretation of the AR^C boundary as a sequence of unit operations is enabled by a fully labelled boundary depicted in Figure 6.9.
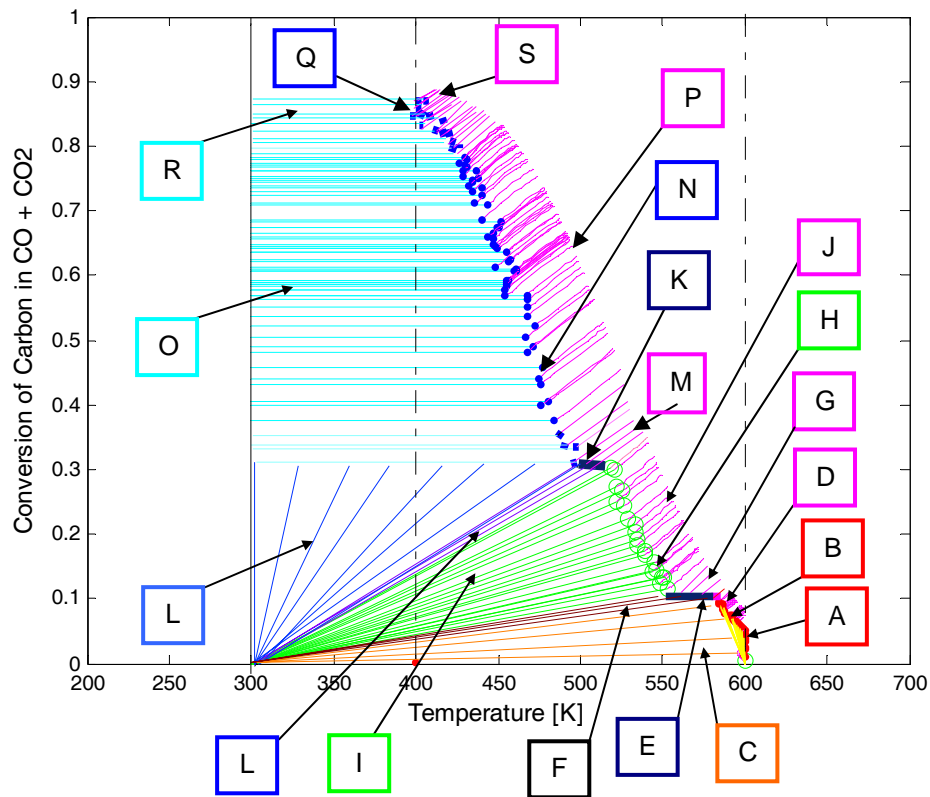
Figure 6.9: A Labelled AR^C Projection of Methanol Synthesis Case 1

The product states in the regions labelled on the AR^C boundary can be attained by using the following unit operations sequence in Table 6.1;

Table 6.1: AR^C Boundary interpretation for Methanol Synthesis (Case 1)

A	Isothermal DHR
B	Isothermal DHR with by-pass feed mixing
C	Isothermal DHR followed by a DHR (non-isothermal)
D	Isothermal DHR - DHR –PFR

Table 6.1: AR^C Boundary interpretation for Methanol Synthesis (Cont..)

E   Isothermal DHR - DHR –Cooler

F   Isothermal DHR - DHR –Cooler - By-pass feed mixing

G   Isothermal DHR - DHR –Cooler - PFR

H   Isothermal DHR - DHR –Cooler - DSR

I   Isothermal DHR - DHR –Cooler – DSR – By-pass feed mixing

J   Isothermal DHR - DHR –Cooler – DSR – PFR

K   Isothermal DHR - DHR –Cooler – DSR – Cooler

L   Iso DHR - DHR –Cooler – DSR – Cooler - By-pass feed mixing

M   Isothermal DHR - DHR –Cooler – DSR – Cooler - PFR
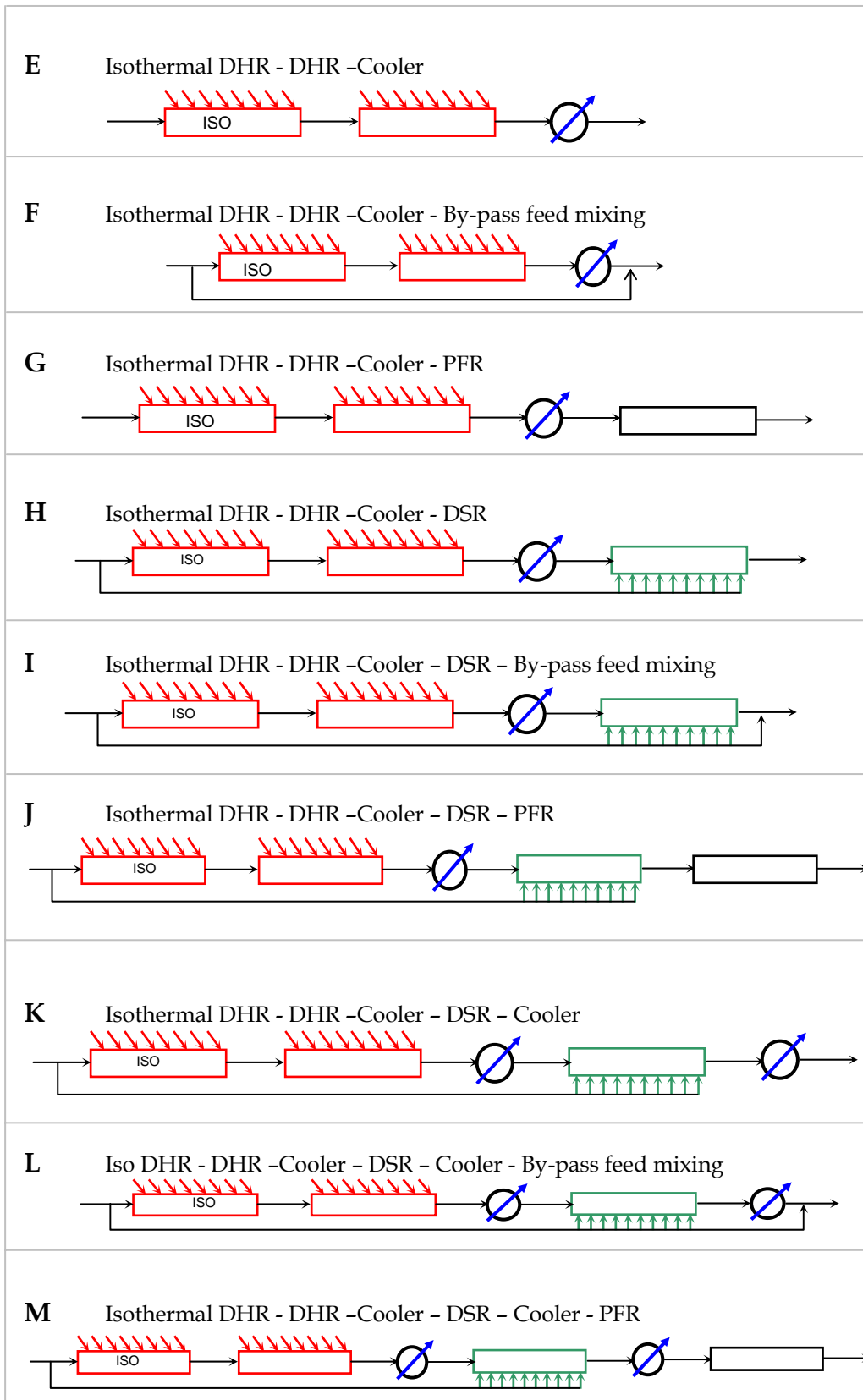
Table 6.1: AR^C Boundary interpretation for Methanol Synthesis (Cont..)

N   Isothermal DHR - DHR –Cooler – DSR – Cooler - DCR

O   Isothermal DHR - DHR –Cooler – DSR – Cooler – DCR –By-pass feed mixing

P   Isothermal DHR - DHR –Cooler – DSR – Cooler – DCR –PFR

Q   Isothermal DHR - DHR –Cooler – DSR – Cooler – DCR – Isothermal DCR

R   Isothermal DHR - DHR –Cooler – DSR – Cooler – DCR – Isothermal DCR – By-pass feed mixing

S   Isothermal DHR - DHR –Cooler – DSR – Cooler – DCR – Isothermal DCR – PFR

At low conversions (corresponding to the feed), high temperatures are required to influence the dominating water gas shift reaction which is endothermic. This is achieved by an isothermal differentially heated reactor (DHR) operating at a temperature of 600K. An isothermal DHR is essentially a DHR operating with a very large control policy θ, such that the heating process is dominating the reaction process in the combination

vector given by equation (6.19c). There exists a point where there is a switch from isothermal to a non-isothermal DHR. This switching point is characterised by a sudden decline in the control policy θ, from very large values to moderately low values. This behaviour in the DHR control policy is shown in Figure 6.10.
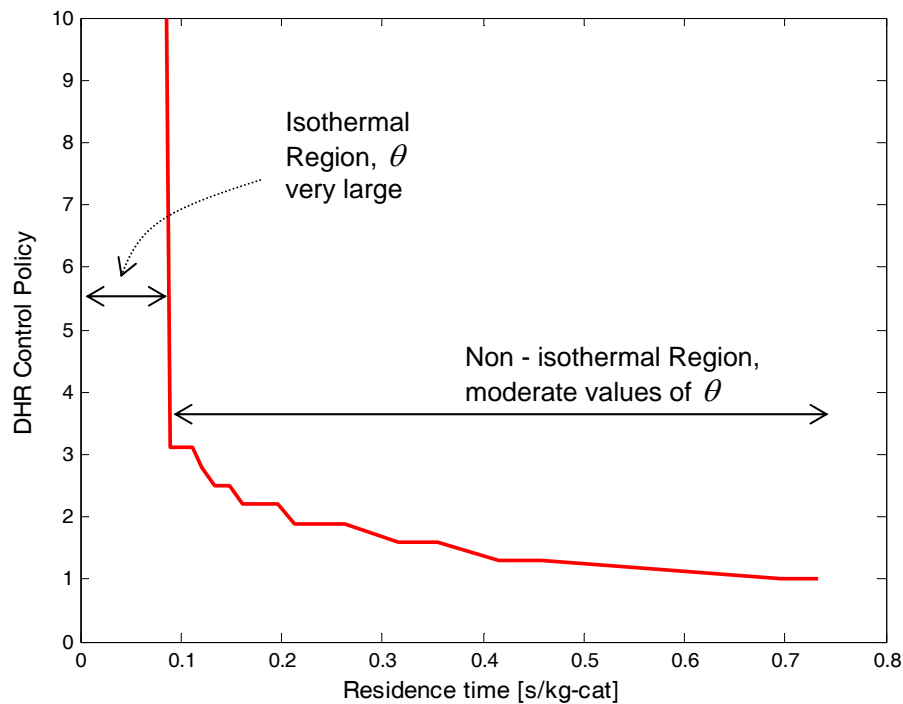
Figure 6.10: Variation of the DHR Control Policy with Residence Time

The control policy of this DHR *bang-singular* in nature as the control policy is kept at the largest value (isothermal region) and suddenly drops to a continuous variation of moderate values (non-isothermal). In the continuous region, the control seems to follows a singular arc. The control policy plot is non-smooth with fluctuations, a factor which can be attributed to the inaccuracies of the RCC algorithm computation. These inaccuracies are common when solving *ill-conditioned* singular control problems (Brenan *et al.*, 1989). Such problems generally require some regularisation when solved with classical optimisation techniques. Such regularization techniques would require reformulation in the RCC algorithm and are therefore focus for future research.

The cooling processes are used to switch from a DHR to a differential side stream reactor (DSR). At this stage the dominating reactions are reactions I and III of methanol formation and the overall reaction system is exothermic. The reaction mixture is optimally cooled by mixing with cold feed to maintain optimum balance between fast rates of reaction and high equilibrium conversion. The DSR control policy α, varies with residence time as depicted in Figure 6.11.
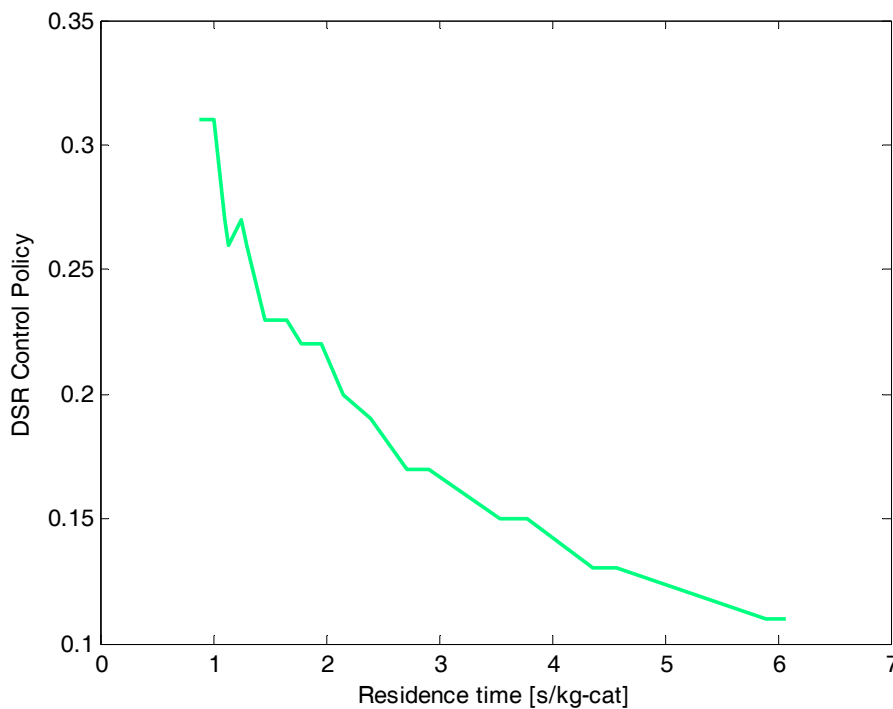
Figure 6.11: Variation of the DSR Control Policy with Residence Time

The DSR control policy seems to follow a continuous residence time varying profile. The perturbations in the profile are due to inaccuracies from the RCC algorithm, and as stated above are associated with the *ill-conditioned* nature of the problem.

The cooling process is applied to switch from a DSR to a differentially cooled reactor (DCR). The DCR follows the optimum cooling profile by combining reaction and cooling such that at any given conversion,

reaction occurs at the highest possible rate. The DCR control policy β, is shown in Figure 6.12. The non-isothermal DCR control policy follows a smooth continuous arc throughout its entire operation until the minimum catalyst activity temperature is reached. At this point, the control policy takes a sharp discontinuous bend into another continuous arc. This second arc is the isothermal DCR control policy for reaction occurring at a fixed temperature of $T_{min} = 400K$
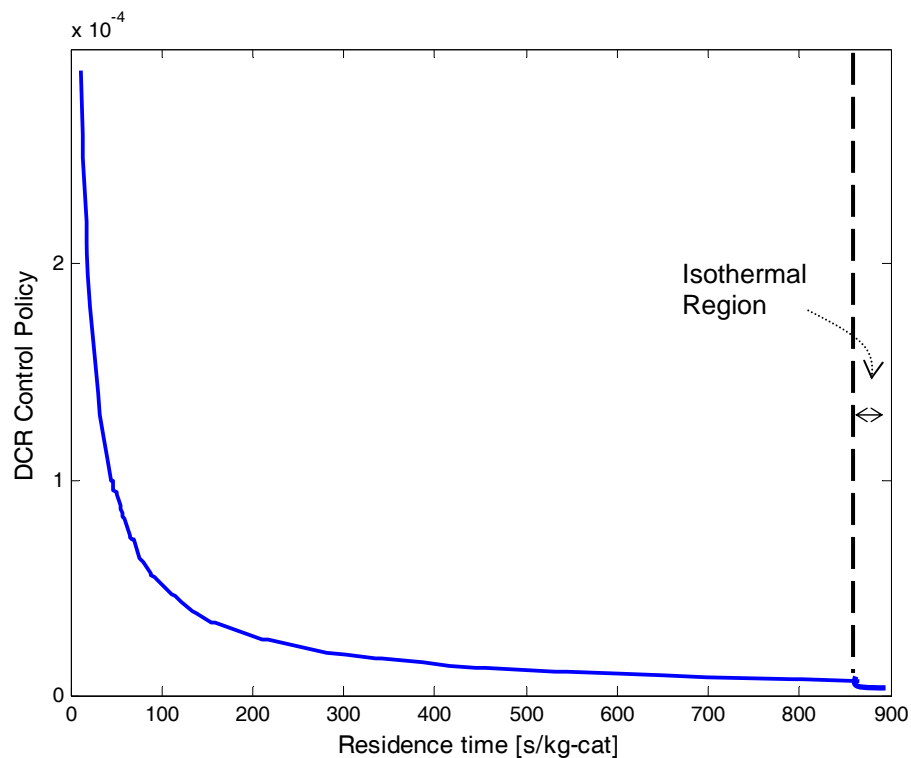
Figure 6.12: Variation of the DCR Control Policy with Residence Time

The variation of carbon conversion with residence time as the optimal process combinations are applied is depicted in Figure 6.13. The structure shown in Figure 6.13 forms the spine of the AR^C boundary as it gives process combinations for the set of highest carbon conversions at the lowest residence times. All other process operations and/combinations will fall below the convex curve in Figure 6.13. However, this behaviour is characteristic of the shown projection and is not necessarily true for other projections. . The convex process combination curve is formed by the arcs

of combinations of reaction and heating (DHR), reaction and mixing (DSR) and reaction and cooling (DSR).
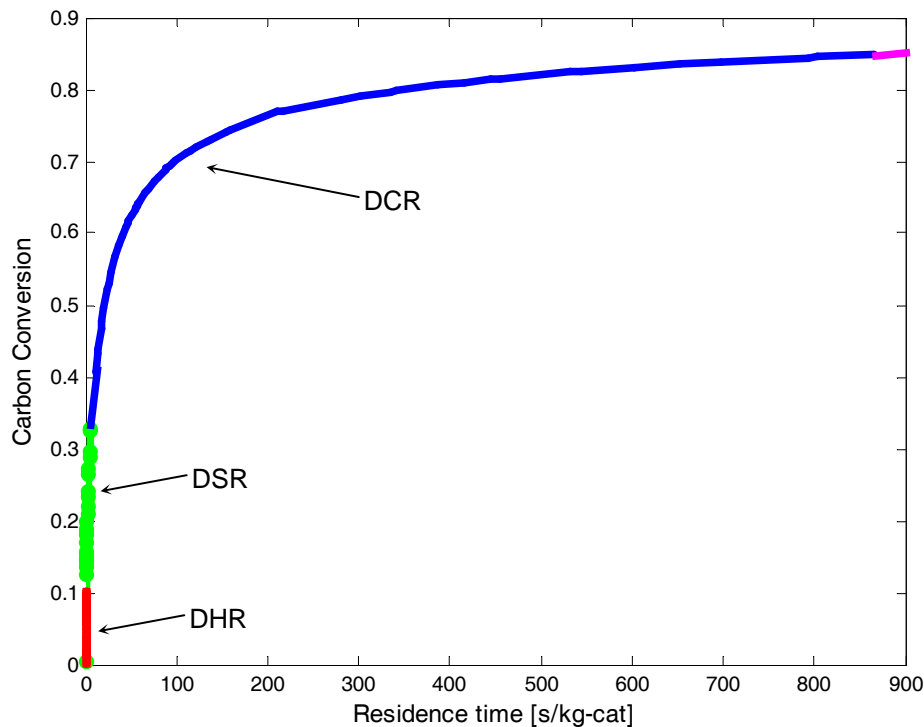
Figure 6.13: Carbon Conversion along the Optimal Process Combinations

6.4.2   Case 2

In the second case we formulate the problem with a varied value of factors, K_c and K_h. The factors are still kept equal in magnitude and their value is varied to 10000. This value indicates that the cooling and heating costs are much cheaper than that of case 1 (Nicol *et al.*, 1997, 1999). The two dimensional temperature–carbon conversion projection of the AR^C for this case is depicted in Figure 6.14. The AR^C shows that a DCR operates in the regions that were previously DSR regions. As the cooling cost decreases, a DCR is preferred to a DSR as it provides lower residence time pathways. There are no visible changes in the DHR profile.

Another visible difference between the two cases is that the switch from a DSR to a DCR in the second case is no longer a cooling process but reaction.
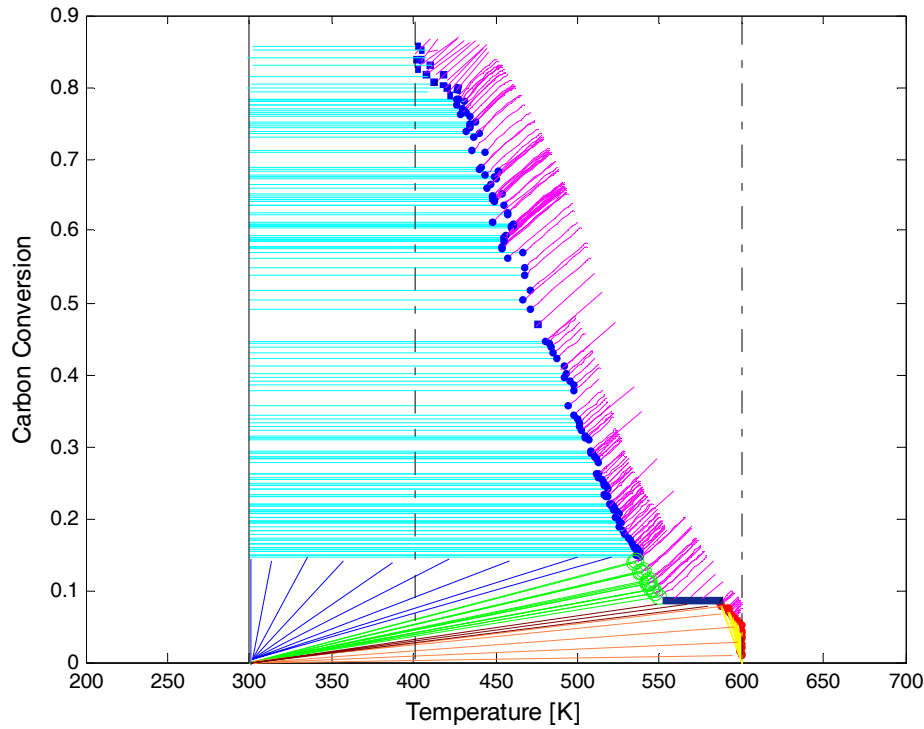
Figure 6.14: A 2D T-X AR^C Projection of Methanol Synthesis Case 2

6.4.3   Computational Aspects

The of the computational run-times on a Pentium 4, 2.5GHz Intel computer with 256MB RAM for the two cases investigated for methanol synthesis are summarised below

Case 1

- Number of iterations: 17
- Total computational time: 23 minutes 17 seconds

Case 2

- Number of iterations: 11
- Total computational time: 16 minutes 21 seconds

Due to the numerical complexity of the methanol synthesis example arising from the number of reactions occurring, the number of components handled in the calculations and the kinetic intricacy, the RCC algorithm required longer run-times to identify the candidate attainable regions. However, it should be emphasised that it would be impractical to solve the methanol synthesis example using analytical methods. The previously known systematic techniques would on comparison require days of computational run-time to solve this example (Hausberger, 2003; Kauchali, 2004).

6.5 Discussion

We have used the RCC algorithm to solve the AR^C for methanol synthesis. The product states that shape the AR^C boundary were then interpreted in terms of processes and combinations of processes that are applied to the feed to attain such product states. The control policies for combinations of processes were also obtained by the computation. The methanol synthesis problem has very complex kinetic models and it will not be viable to attain the control policies and solve the AR^C via analytical methods used to study simple problems by Feinberg (2000a &b) and Nicol *et al.*, (1997, 1999), among others.

For a feed of 1:1 $CO:CO_2$ mole ratio, conversion is generally limited by the low rates of conversion of CO_2 to methanol. In section 6.2 we demonstrated with the aid of constant rate curves that the reaction rates of CO_2 to methanol are in the order of one-tenth of the rates of CO to methanol. The optimal reactor structure obtained via AR analysis takes advantage of the high water-gas-shift activity of the Cu-Zn-Al catalyst. CO_2 is shifted to a more active CO by a high temperature DHR. The CO is then converted to methanol by a sequence of DSR and DCRs.

By changing the relative costs of cooling and heating, we showed that the optimal reactor sequence shifts to the favoured application of the lower rate DCR as opposed to DSR. Thus, we have conversely inferred that, as the cooling costs increases, the DSR becomes a more economical (lower residence time) pathway of reaction and cooling as compared to the DCR. As the heating costs are varied, the application of a DHR remains unaffected as it is the only optimal process pathway for combination of

reaction and heating to perform the high temperature water-gas-shift of CO_2 to CO.

The obtained reactor sequence achieves a 92% conversion of carbon to methanol without the use of excess hydrogen. An advantage that will eliminate the costs associated with excess hydrogen in methanol synthesis processes such as separation and recycling. This also reduces the volume of the reactor as there will be no volume occupied by the excess hydrogen.

The computational run-times of the RCC algorithm for the numerically complex methanol synthesis system are still faster when compared to that of the other systematic AR techniques applied to solving simpler examples such as the ammonia synthesis example (Hausberger, 2003).

6.6 References

Bakemeier, H., Laurer, P. R., Schroder, W., (1970), Development and application of a mathematical model of the methanol synthesis, *Chem. Eng Prog. Symp. Ser.*, **66**(98), pp1-10

Brenan, K. E., Campbell, S. L., Petzold, L. R., (1989), *Numerical Solution Of Initial-value Problems In Differential-Algebraic Equations*, North-Holland, New York, USA

Chinchen, G. C., Denny, P. J., Parker, D. G., Short, G. D., Spencer, M. S., Waugh, K. C., Whan, D. A., (1984), The activity of copper-zincoxide-aluminiumoxide methanol synthesis catalyst, *Prep. Pap. Am. Chem. Soc. Div. Fuel Chem.*, **29**(5), pp178-188

Denise, B., Sneeden, R. P. A., (1982), Hydrocondensation of carbon dioxide IV., *J. Molec. Catal.*, **17**, pp359-366

Dybkjaer, I., (1985), Design of ammonia and methanol synthesis reactors, Paper presented at the NATO conference on chemical reactor design and technology, Canada

Graff, G. H., Stamhuis, E. J., Beenackers, A. A. C. M., (1988), Kinetics of low-pressure methanol synthesis, Chem. Eng. Sci. 43, No. 12, pp. 3185-3195

Kauchali, S., Glasser, D., Hildebrandt, D., (2002), Linear programming formulations for attainable region analysis, *Chem. Eng. Sci.*, **57** (11), pp. 2015-2228.

Klier, K., Chatikavanij, V., Herman, R. G., Simmons, G. W., (1982), Catalytic synthesis of methanol from CO/H_2. *J. Catal.*, **74**, pp. 343-360

Leonov, V. E., Karavaev, M. M., Tsybina, E. N., Petrishcheva, G. S., (1973), Kinetics of metanol synthesis on a low- temperature catalyst, *Kinet. Katal.* **14**, pp. 970-975.

Liu, G., Willcox, D., Garland, M., Kung, H. H., (1985), The role of CO_2 in methanol synthesis on Cu-Znoxide: an isotope labeling study, *J. Catal.* **96**, pp. 251-260.

Monnier, J. R., Apai, G., Hanrakan, H. J., (1984), Effect of CO_2 on the conversion of H_2/CO to methanol over copper-chromia catalysts, *J. Catal.* **88**, pp. 523-525.

Natta, G., (1955), Synthesis of methanol, in *Catalysis*: *Hydrogenation and Dehydrogenation* (Edited by P. H. Emmett), pp. 349-411, Rheinhold, New York.

Shivakumar Kameswaran, 2005, *PhD Thesis*, Carnegie Mellon University, To be submitted

Struis, R. P. W. J., Stucki, S., Wiedom, M., (1996), A membrane reactor for methanol synthesis, *J. Membr. Sci.* **113**, pp. 93-100

Struis, R. P. W. J., Stucki, S., (2001), Verification of the membrane reactor concept for the methanol synthesis, *Applied Catalysis A*: *General*, **216**, pp. 117-129

Twigg, V., (1996), *Catalyst Handbook*, 2nd Ed., Manson Ltd., pp. 293-338,

6.7 List of Symbols

Abbreviations

AR	Attainable Regions
AR^C	Candidate Attainable Regions
CFSTR	Continuous Flow Stirred Tank Reactors
DCR	Differentially Cooled Reactor
DHR	Differentially Heated Reactor
DSR	Differential Side-stream Reactor
PFR	Plug Flow Reactor
RCC	Recursive Constant Control Policy

Symbols

α	Combination control policy for fundamental processes (mixing)
β	Combination control policy for cooling
θ	Combination control policy for heating
c	State variable of the system
c_o	State variable of the system at the feeding point
c^*	Mixing state variable of the system
f_i	Fugacity of gas species i
$g(c)$	General process vector defined at c
$h(c)$	Heating process vector defined at c
$k(c)$	Cooling process vector defined at c
K_c	A measure of cooling costs relative to reaction costs
K_i	Adsorption equilibrium constant of species i
$K^0_{p,j}$	Chemical equilibrium constant of reaction j based on partial pressure
$k_{ps,j}$	Rate constant of reaction j
m	Mass fraction of reaction componets

$\boldsymbol{P}$	Partial pressure of the reacting components
$\boldsymbol{r(c)}$	Reaction rate vector defined at c
$r'_{i,j}$	Rate of reaction of species i from reaction j [mol.s^{-1}.kg-cat^{-1}]
R	Universal Gas constant
T	Temperature of reaction [K]
T$_{ad}$	Adiabatic temperature gradient
T$_c$	Cooling utility temperature [K]
T$_h$	Heating utility temperature [K]
T$_o$	Feed temperature [K]
τ	Residence time
$\boldsymbol{v}$	Mixing vector, mixing c with c^*
ΔH_{rxn}	Enthalpy of the reaction

CHAPTER 7

SINGULAR OPTIMAL CONTROL TECHNIQUES FOR ATTAINABLE REGION ANALYSIS

7.1 Introduction

In this work, singular optimal control methods are applied to identify candidate attainable regions boundaries. This procedure involves using optimal control techniques to identify optimum profiles of combinations of fundamental processes that outline the boundary of the AR^C. As demonstrated in the previous chapters, once the optimum profiles of combinations of fundamental processes have been identified, the boundary of the AR^C can be completed by the extreme surfaces and planes that are of single process operations. These extreme surfaces and planes originate from optimum profiles of combinations of fundamental processes. This work considers the class of problems that address linear time optimal control. The theory of such problems is discussed in section 7.3 following the background literature review in section 7.2.

This work was completed in collaboration with Shivakumar Kameswaran under the supervision of Prof. Biegler at Carnegie Mellon University. The formulations for solving differential algebraic equations (DAE) using Radau quadrature discussed in section 7.4 were derived as part of Shivakumar's research. We will apply the formulations to solve problem formulated as attainable region. This is demonstrated through the use of the industrially important water-gas-shift (WGS) reaction as a case study.

The results are then compared to that of Kauchali *et al.*, (2004a & b) obtained using the iso-state and RCC algorithms for attainable regions.

7.2 Background Literature

Singular optimal control problems form a large part of optimisation challenges in chemical process engineering. In the past six decades most researchers focused their work on developing numerical algorithms to solve singular optimal control problems. Sienbenthal and Aris (1964a & b) used Pontryagin's maximum principle to solve for the optimal control profiles of stirred tank, batch and tubular reactors. Hermes (1964) applied the maximum principle to solve singular control problems. Hermes (1964) defined a vector as "totally singular" when the maximum principle yields no information in the time optimal problem for any of the components of the optimal control set.

In a series of publications, researchers formulated algorithms using the maximum principle to solve the singular optimal control problems that are encountered in chemical engineering systems. Among the researchers responsible for this work were; Jackson (1968); Jackson and Senior (1968), Jackson *et al.* (1971); Ko and Stevens (1971 a & b); King *et al.* (1972); King and Glasser (1973), to mention only a few.

More recently, Modak *et al.*, (1989) developed a unidirectional method to solve optimal singular control problems. The authors proposed an algorithm that uses the maximum principle and a unidirectional scheme to reduce the iterations required to solve a two-point boundary value problem. Cuthrell and Biegler, (1989) presented a method for solving optimal control problems using discretisation of the state functions. The

method was successfully demonstrated for a fed batch reactor system.

7.3 Theory

The theory of the class of singular optimal control problems that this study focuses on is detailed below as adopted from Bryson and Ho (1969) and Hermes (1969). The control problems considered in this work are those of linear time optimal control systems, described by a generic vector differential equation

$$\dot{x}(t) = \frac{d}{dt} x(t) = f(x(t)) + u g(x(t)) \tag{7.1}$$

with given initial conditions,

$$x(t = t_0) = x_0$$

The state vector x, will be n-dimensional and is given by

$$x = \begin{pmatrix} x_1 \\ \vdots \\ x_n \end{pmatrix}$$

The control u is a time measurable scalar that can be constrained by bounds

$$a \leq u \leq b$$

The functions f and g are n-dimensional vector functions given by

$$f = \begin{pmatrix} f_1 \\ \vdots \\ f_n \end{pmatrix} \quad \text{and} \quad g = \begin{pmatrix} g_1 \\ \vdots \\ g_n \end{pmatrix}$$

We will be focusing on a class of problems where the objective is to minimise the performance index of this form;

$$\min_{u} \int_{t_0}^{t_f} \left[f_0(x) + ug_0(x) \right] dt + \phi\left[x(t_f) \right] \tag{7.2}$$

The approach used by the Pontryagin's Maximum Principle to solve optimisation problems requires that the constraints of the control be adjoined to the performance index (Pontryagin, 1962). Thus, determining the constrained Hamiltonian, H defined as;

$$\mathrm{H}(x, \lambda, u, \mu_1, \mu_2, t) = \left[f_0(x) + ug_0(x) \right] + \lambda^T \left[f(x) + ug(x) \right] + \mu_1(a - u) + \mu_2(u - b) \tag{7.3}$$

Where λ^T is known as the co-state vector, which is the transpose vector of the adjoint variables vector λ (Lagrange multipliers for the system state equations), μ_1 and μ_2 are the Lagrange multipliers for the control path constraints. As can be noted in equation (7.3), the Hamiltonian is linear in control variable u.

The necessary conditions required for optimality are derived as follows. For a dynamic system with the state function as given by equation (7.1)

$$\frac{d}{dt} x(t) = f(x(t)) + ug(x(t)) \qquad x(t = t_0) = x_0 \tag{7.1}$$

Pontryagin's maximum principle states that for u and x to be optimal it is necessary that the co-state vector, λ^T which is a non-zero and continuous function should satisfy the following equations;

$$\frac{d\lambda}{dt} = -\frac{\partial H(x, \lambda, u, \mu_1, \mu_2, t)}{\partial x} \tag{7.4a}$$

and

$$\lambda\left(t_f\right) = -\left.\frac{\partial \varphi}{\partial x}\right|_{t_f} \tag{7.4b}$$

The necessary conditions of optimality are such that (Pontryagin 1962),

$$\boldsymbol{H}_u\left(x, \lambda, \mu_1, \mu_2, t\right) = \frac{\partial \boldsymbol{H}\left(x, \lambda, \mu_1, \mu_2, t\right)}{\partial u} = \boldsymbol{g}_0\left(x\right) + \lambda^T\left[\boldsymbol{g}\left(x\right)\right] - \mu_1 + \mu_2 = 0$$

$$\tag{7.5}$$

over a non-zero time interval [t_0, t_f]. All the time derivatives of $\partial H/\partial u$ are also required to remain fixed at zero.

Kelly *et al.*, (1967) states that to determine a singular optimal control in terms of variables x, λ^T and t, successive even derivatives of $\partial H/\partial u$ with respect to t should be fixed at zero as given by condition (7.6) below;

$$\frac{d^{2m}}{dt^{2m}}\left(\frac{\partial \boldsymbol{H}\left(x, \lambda, \mu_1, \mu_2, t\right)}{\partial u}\right) = 0 \qquad m = 0, 1, 2, \ldots \tag{7.6}$$

Condition (7.6) is a useful quantity necessitated by the fact that the Hamiltonian is linear in the control variable u, therefore the necessary condition (7.5) is not an explicit function of the control variable. Thus the maximum principle yields no sufficient information on determining an optimal control of the system. These type of problems are termed high-index problems (Brenan *et al.*, 1989). In order to determine the expression for the singular optimal control, the necessary condition (7.5) should be differentiated successively with respect to t until the control variable u appears explicitly in one of the even derivatives given by (7.6) (Kelly *et al.*, 1967).

Another necessary condition that should be satisfied along an optimal

singular control arc is the generalised Legendre-Clebcsh condition given by equation (7.7) below (Aly, 1978);

$$(-1)^m \frac{\partial}{\partial u}\left[\frac{d^{2m}}{dt^{2m}}\left(\frac{\partial \boldsymbol{H}(\boldsymbol{x}, \boldsymbol{\lambda}, \mu_1, \mu_2, t)}{\partial u}\right)\right] \le 0 \quad m = 0, 1, 2, \ldots \quad (7.7)$$

The maximum principle requires that condition (7.8) below holds, otherwise the method fails to identify the optimal control solution.

$$\boldsymbol{g}_0(\boldsymbol{x}) + \boldsymbol{\lambda}^T\left[\boldsymbol{g}(\boldsymbol{x})\right] \ne 0 \quad (7.8)$$

For condition (7.5) to be established without violating condition (7.8), at least one of the Lagrangian multipliers; μ_1 or μ_2 of the control should remain nonzero (Aly, 1978).

However it is not always possible to guarantee the satisfaction of conditions (7.6) and (7.7) as the state function and the Hamiltonian are not explicit functions of t. Their differentiation with respect to time will therefore yield no useful information about the problem.

The problem commonly encountered with solving singular optimal control problems using the maximum principle is that the solution is often oscillatory and unstable. These perturbations in the solutions are consequential to the condition called matrix ill-conditioning which occurs when the standard maximum principle methods are applied to solve high index problems (Brenan *et al.*, 1989).

7.4 Case Study: The Water-Gas Shift Reaction

7.4.1 Reaction Kinetics

The kinetics for the water-gas-shift reaction was presented by Podolski and Kim (1974). They adopted the Langmuir-Hinshelwood models to describe the kinetic behaviour of the WGS reaction over an iron-based catalyst. The reaction rate models were derived for experiments carried out at atmospheric pressure. The exothermic reversible WGS reaction for the production of hydrogen is characterised by an equation given below;

$$CO \ + \ H_2O \ \leftrightarrow \ CO_2 \ + H_2 \qquad \Delta H^{\circ}_{298} \ = \ - \ 41.17 \text{ kJ mol}^{-1} \quad (7.9)$$

The Langmuir-Hinshelwood model for the rate of reaction allowing adsorption of all reaction species is given by;

$$r_{CO} = \frac{kK_{CO}K_{H_2O}\left[P_{CO}P_{H_2O} - P_{CO_2}P_{H_2}/K_p\right]}{\left[1 + K_{CO}P_{CO} + K_{H_2O}P_{H_2O} + K_{CO_2}P_{CO_2} + K_{H_2}P_{H_2}\right]^2} \qquad (7.10)$$

The reaction rate and adsorption constants used in the rate expression are modelled to vary with temperature as shown in equation (7.11) below;

$$K_i = \exp\left(-\frac{\Delta H_i}{RT} + \frac{\Delta S_i}{R}\right) \qquad (7.11)$$

The corresponding parameters for the rate expression constants are given by Podolski and Kim(1974) as shown in Table 7.1.

Table 7.1: Parameters for the Kinetics (Podolski and Kim, (1974))

Constant	ΔH	ΔS
k	29 364	40.32
K_{CO}	-3 064	-6.74
K_{H_2O}	6 216	12.77
K_{CO_2}	-12 542	-18.45

7.4.2 The Process State Function

The fundamental processes considered in this example are limited to that of reaction and mixing. The state variables used in this system to describe the system are the conversion of CO, temperature and residence time with corresponding symbols X, T and τ, respectively. These variables are given in a state vector $\boldsymbol{c}$ as;

$$\boldsymbol{c} = \begin{bmatrix} X \\ T \\ \tau \end{bmatrix} \tag{7.12}$$

The reaction state function vector is described by;

$$\boldsymbol{r}(\boldsymbol{c}) = \begin{bmatrix} r_{CO} \\ T_{ad} \cdot r_{CO} \\ 1 \end{bmatrix} \quad \text{given} \quad \boldsymbol{c}(\tau = \tau_0) = \boldsymbol{c}_0 = \begin{bmatrix} X_0 \\ T_0 \\ \tau_0 \end{bmatrix} \tag{7.13}$$

For mixing, the state function vector is given by;

$$\boldsymbol{v}(\boldsymbol{c}, \boldsymbol{c}_m) = \begin{bmatrix} X - X_m \\ T - T_m \\ \tau - \tau_m \end{bmatrix} \tag{7.14}$$

Where $\boldsymbol{c}_m$ is the mixing state, which in this case is the cold feed at a temperature of 300K.

The general process state function is given by the controlled combination of reaction and mixing using control policy α, as shown below;

$$y_{r,v}(c) = \frac{dc}{d\tau} = r(c) + \alpha \cdot v(c, c_m) \qquad (7.15)$$

Equation (7.15) above has the same form as the generic singular control problem state function given by equation (7.1). Another description is that equation (7.15) represents the combination of reaction and mixing and therefore is essentially a differential sidestream reactor expression (Glasser *et al.*, (1992); Chapter 3 & 5). Thus, the DSR equation is by its nature, an optimal singular control problem. In general, the DSR, DCR, DHR and any combinations of these reactor models are representative of singular control problems.

7.4.3 **Process Specifications and Constraints**

The initial conditions for this problem are given as a feed of stoichiometric mixture of pure CO and H_2O at a temperature of 300K. As stated earlier cold feed will be used as a mixing state, therefore c_m becomes;

$$c_m = \begin{bmatrix} 0 \\ 300 \\ 0 \end{bmatrix} \qquad (7.16a)$$

Free preheating of feed is allowed to a temperature of 823K. Thus, the initial conditions of a DSR will be given by;

$$c_0 = \begin{bmatrix} 0 \\ 823 \\ 0 \end{bmatrix} \qquad (7.16b)$$

The catalyst activity is constrained to operate within the temperature range of 500K – 823K (Kauchali *et al.*, 2004 a). Conversion is known to take values between 0 and 1, representing the feed and complete reaction conversion of CO, respectively. Thus, the state variables are constrained within minimum and maximum bounds as follows;

$$X_{max} \geq X \geq X_{min} \qquad\qquad 1 \geq X \geq 0$$

$$\Rightarrow \qquad\qquad\qquad\qquad (7.17a)$$

$$T_{max} \geq T \geq T_{min} \qquad\qquad 823K \geq T \geq 500K$$

The control policy α, is bounded within the limits 0 and 20,000 as shown below. The upper bound of 20, 000 in the control policy is not fixed and can be revised during computation if is later discovered not to be sufficiently large.

$$\alpha_{max} \geq \alpha \geq \alpha_{min} \qquad \Rightarrow \qquad 0 \leq \alpha \leq 20000 \qquad\qquad (7.17b)$$

7.4.4 **Method Formulation**

The differential algebraic equation (DAE) vector describing the state functions given by equation (7.15) was discretised using a two-point Radau quadrature. Discretisation is carried out forward in time, not backwards in time as in the conventional methods (Cuthrell and Biegler, 1989). The two collocation points for Radau quadrature used in this formulation, as scaled on element length, are 1/3 and 1, allowing the end of an element to be a collocation point. Continuity is emphasised for all state and co-state functions by enforcing the end of an element to be equal to the beginning of the next element.

The problem was solved using 100 finite elements and was assumed to remain fully singular for the entire residence time interval of $[0, 10^9]$.

The objective is to maximise the conversion of CO. The objective function was then formulated as follows;

$$\min_{\alpha} \sum_{i=1}^{N} \left(1 - X(i)\right) \qquad i = 1, 2, \ldots, N \tag{7.18}$$

Where N is the number of finite elements.

The formulation was implemented in AMPL® using IPOPT® solver and the obtained solution is discussed in the next session.

7.4.5 **Results**

The control profile obtained from the solution is shown in Figure 7.1. The profile appears to form a singular arc throughout the entire time interval. However, there are small perturbations towards each end of the arc that are not visible in the scale Figure 7.1 is presented in. Figure 7.2 shows such a bend for the upper residence time end. These perturbations occur at the maximum and minimum temperature bounds and indicate a transition to isothermal operation.

The bend shown in Figure 7.2 is calculated at the temperature of 500K, where the main arc (Figure 7.1) changes to the isothermal arc. Figure 7.3 shows how CO conversion changes along the singular control arc. The different segments representing isothermal and non-isothermal control arcs are not distinguishable in this figure as the profile is fully convex. This convexity is necessary for an optimal solution (Section 7.3).
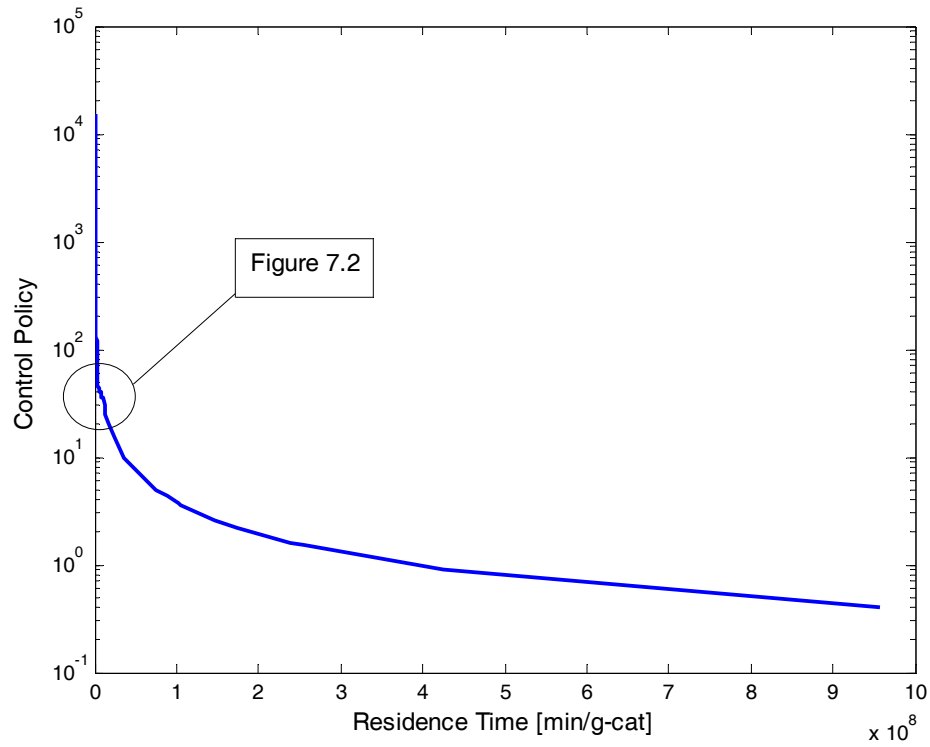
Figure 7.1: The Main Control Profile for Reaction and Mixing
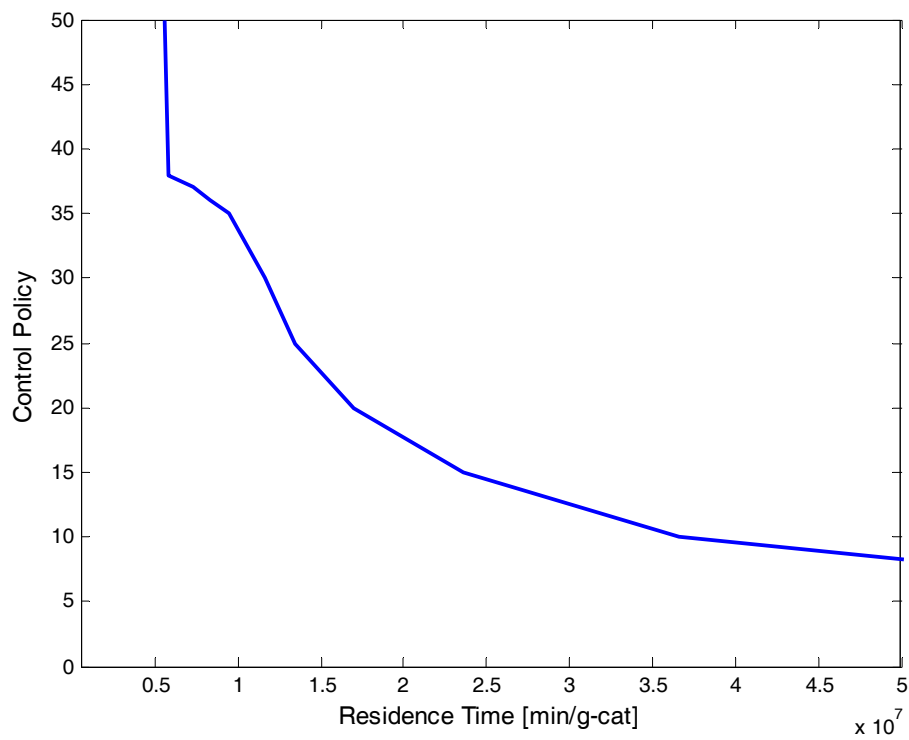
Figure 7.2: The Isothermal Control Profile (T = 500K)
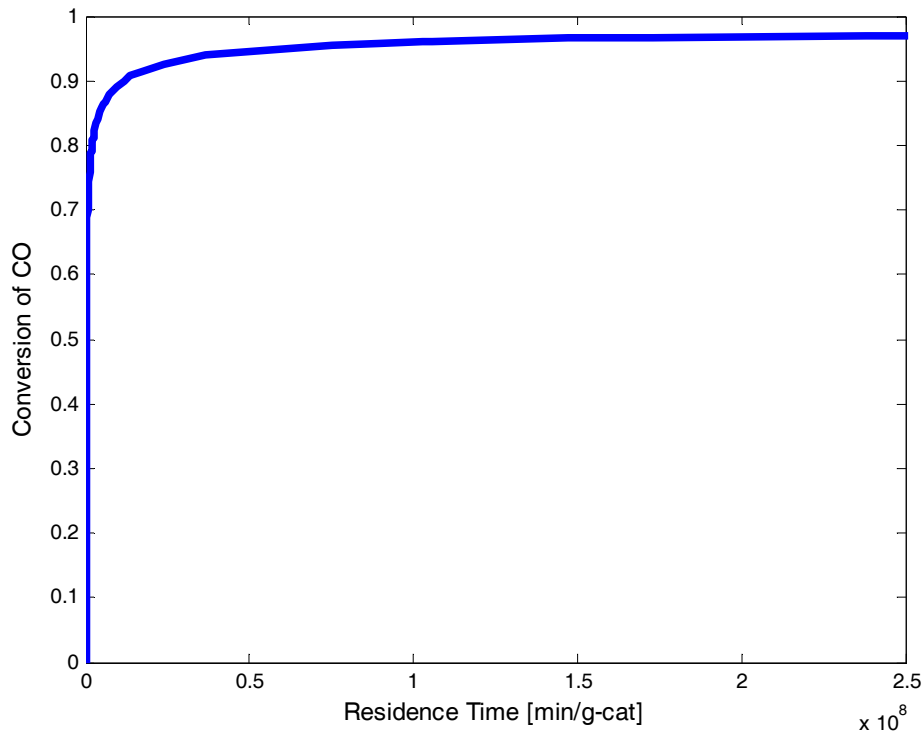
Figure 7.3: Variation of Conversion along the Control Profile

As stated, the singular control arcs represent the optimal combination of reaction and mixing which is a DSR profile on the attainable regions boundary. The boundary of the attainable regions can then be completed using plug flow reactor trajectories and mixing lines that emanate from the optimal DSR profile. The completed candidate attainable region for the WGS reaction is shown on a two-dimensional temperature-conversion projection in Figure 7.4 and three-dimensional structure is shown in Figure 7.5.

The general process sequence and its interpretation as a network of operations unit is given by;
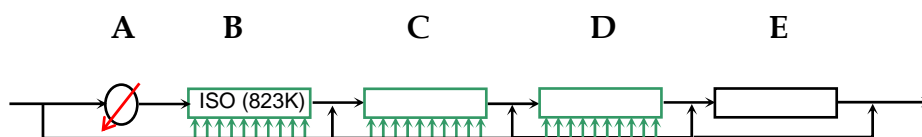
Preheating of the feed is carried from 300K to 823K (**A**), followed by an isothermal DSR (**B**) operating at a fixed temperature of 823K. The isothermal DSR then switches to a non-isothermal DSR (**C**), which navigates along the AR^C boundary from 823K to 500K. At 500K the non-isothermal DSR switches to an isothermal DSR (**D**) which operates at a fixed temperature of 500K. Plug flow reactor profiles (**E**) completes the AR^C boundary.
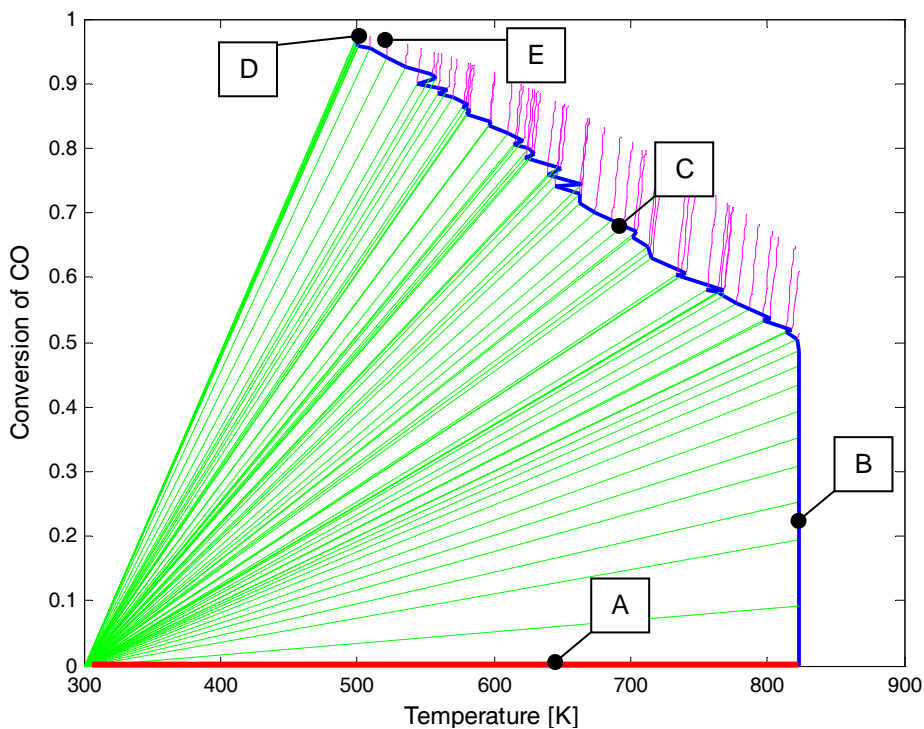
Figure 7.4: 2D AR^C Projection for the WGS System

The boundary of the AR^C, together with the sequence of reactors that occur on it, agrees with the results obtained by Kauchali *et al.,* (2004a & b) using the Iso-state algorithm (Rooney *et al.*, 2000) and the RCC algorithm.
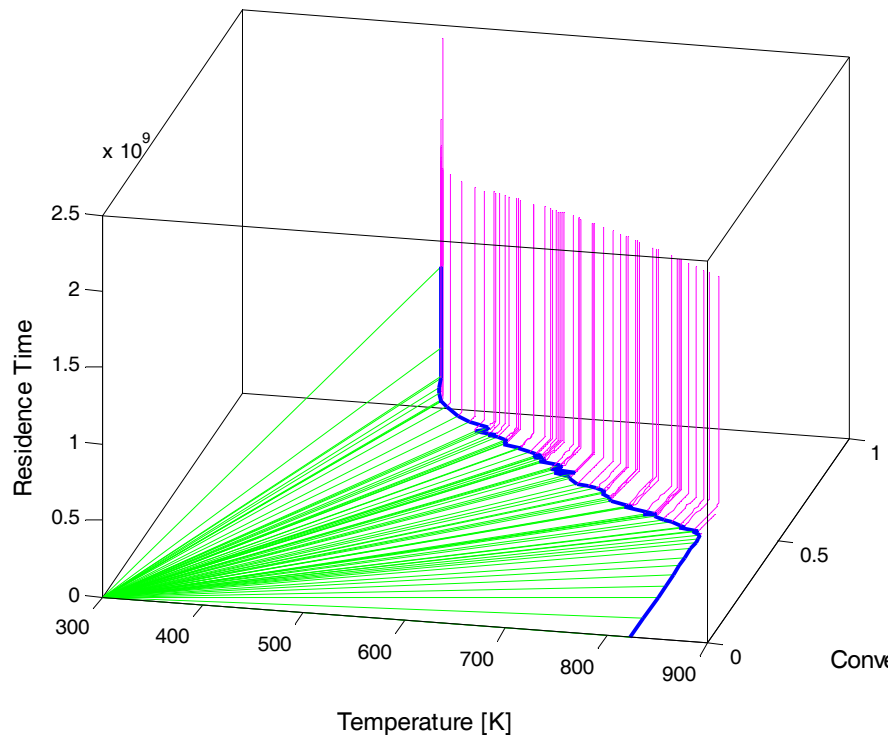
Figure 7.5: 3D AR^C Boundary for WGS System

Figures 7.4 and 7.5, show a non-smooth and 'wiggly' projections of the optimal control profile or DSR profile. This condition is due to the fact that the DSR is a very ill-conditioned singular control problem and some sort of regularization should be used to smooth-out the profile and remove the wiggles. Shivakumar Kameswaran's work focuses of addressing ill-conditioned singular optimal control problems.

7.5   Discussion

We have demonstrated a relationship between the maximum principle and attainable region analysis by solving a candidate AR using optimal singular control techniques that are based on Pontryagin's maximum principle theory. As McGregor (1998) has shown from analytical derivations, the attainable regions analysis conforms to the requirements of Pontryagin's maximum principle. This was confirmed by the AR^C generated using optimal control applications being in concurrence with the candidates generated by Kauchali *et al.*, (2004 a & b) using AR analysis tools.

A useful outcome of this demonstration is the formulation of singular optimal control technique as systematic tools for identifying candidate attainable regions. This adds up to the assembly of AR analysis tools that can be used to synthesise optimal chemical processes.

7.6   References

Aly, G. M., (1978), The computation of optimal singular control, *Int. J. Control*, **28** (5), pp. 681-688

Brenan, K. E., Campbell, S. L., Petzold, L. R., (1989), *Numerical Solution Of Initial-value Problems In Differential-Algebraic Equations*, North-Holland, New York, USA

Bryson, A. E., and Ho, Y. C., (1975), *Applied Optimal Control*, Hemisphere, Washington, D.C.

Cuthrell, J. E., Biegler T. T., (1989), Simultaneous Optimisation and Solution Methods for Batch Reactor Control Profiles, *Comp. Chem. Eng*. **13** (1/2), pp. 49-62

Glasser, B., Hildebrandt D., Glasser, D., (1992), Optimal mixing for Exothermic Reversible Reactions. *I&EC Research*, 1992, **31**, pp. 1541-1549

Jackson, R., (1968), Optimal Use of Mixed Catalysts for Two Successive Chemical Reactions, *J. Opt. Theor. Appl.*, **2** (1), pp. 27-39

Jackson, R., and Senior M. G., (1968), The optimization of chemical reactors by the delayed addition of reactant, *J. Opt. Theor. Appl.*, **2** (1), pp. 27-39

Jackson, R., Obando, R., Senior, M. G., (1971), On the control of competing chemical reactions, *Chem. Eng. Sci.*, 26, pp. 853-865

Kauchali, S., Hausberger, B., Hildebrandt, D., Glasser, D., Biegler, L. T., (2004a), Automating reactor network synthesis: finding a candidate attainable region for the water-gas shift (WGS) reaction, *Comp. Chem. Eng.*, **28**, pp. 149-160

Kauchali, S., Seodigeng T., Hausberger, B., Hildebrandt, D., (2004b), A Comparison of Automated Techniques in Determining Candidate Attainable Regions: Water Gas Shift Case Study, *Escape 14*, Lisbon, Portugal

Kelley, H. J., Kopp, R. E., Moyer, H. G., (1967), *Topics in Optimization*, Edited by Leitmann, Academic Press, New York, USA

King, R. P., Glasser, D., Stone S. L., (1972), Optimal Catalyst Concentration Profile for Bi-functional Catalysts, *J. Opt. Theor. Appl.*, **10**, pp. 94-108

Glasser, D., and King, R. P., (1973), Optimal catalyst concentration profile for bi-functional catalysts: Langmuirian kinetics, *Chem. Eng. Sci.*, 28, pp. 1685-1689

Ko, D. Y. C., and Stevens, W. F., (1971 a), Studies of Singular Solutions in Dynamic Optimization I: Theoretical Aspects and Methods of Solution, *AIChE J.*, **17**, pp. 249-252

Ko, D. Y. C., and Stevens, W. F., (1971 a), Studies of Singular Solutions in Dynamic Optimization I: Optimal Singular Design of a Plug-Flow Tubular Reactor, *AIChE J.*, **17**, pp. 160-166

Hermes, H., Lasalle, J., P., (1969), *Functional Analysis and Time Optimal Control,* Academic Press, New York, U.S.A.

McGregor, C. (1998). *Choosing the optimal system structure using the attainable region approach for systems involving reaction and separation*, Ph.D thesis, Republic of South Africa: University of the Witwatersrand.

Modak, J. M., Bonte, P., Lim, H. C., (1989), An improved computational algorithm for singular control problems in chemical reaction engineering, *Chem. Eng. Comm.*, 86, pp. 165-183

Podolski, W. F., and Kim, Y. G., Modelling the water-gas shift reaction, *Ind. Eng. Chem. Proc. Des. Dev.*, 13 (4), pp. 415

Pontryagin, L .S., Boltyanskii, V. G., Gamkrelidze, R. V., and Mishchenko, E. F., (1962), *The Mathematical Theory of Optimal Processes*, John Wiley, New York, USA.

Rooney, W. C., Hausberger, B. P., Biegler, L. T., Glasser, D., (2000), Convex attainable region projections for reactor network synthesis, *Comp. & Chem. Eng.*, **24**, no. 2-7, pp. 225 – 229

Siebenthal, C. D., Aris, R., (1964), The Application of Pontryagin's Methods to the Control of a Stirred Reactor, *Chem. Eng. Sci.*, **19**, pp. 729-746

Siebenthal, C. D., Aris, R., (1964), The Application of Pontryagin's Methods to the Control of Batch and Tubular Reactor, *Chem. Eng. Sci.*, **19**, pp. 747-761

7.7   List of Symbols

Abbreviations

AR	Attainable Regions
AR^C	Candidate Attainable Regions
CFSTR	Continuous Flow Stirred Tank Reactors
DAE	Differential Algebraic Equations
DCR	Differentially Cooled Reactor
DSR	Differential Side-stream Reactor
PFR	Plug Flow Reactor
RCC	Recursive Constant Control Policy
WGS	Water-Gas Shift Reaction

Symbols

α	Combination control policy for fundamental processes (mixing)
c	State variable of the system
c_o	State variable of the system at the feeding point
c_m	Mixing state variable of the system
f	Some time dependent vector function
f_0	Initial state of the vector function, at $t = 0$
g	Some time dependent vector function
g_0	Initial state of the vector function, at $t = 0$
$g(c)$	General process vector defined at c
H	The constrained Hamiltonian
H_u	Partial derivative of the constrained Hamiltonian with respect to control u
ΔH_{rxn}	Enthalpy of the reaction
k	Rate constant of reaction
K_i	Adsorption equilibrium constant of species i

K_p	Chemical equilibrium constant of reaction based on partial pressure
λ	Lagrange multiplier of the system state equations
λ^T	Co-state vector of the system state equations
μ_1, μ_2	Lagrange multipliers for the control path constraints
P_i	Partial pressure of the reacting component i
R	Universal Gas constant
$r(c)$	Reaction rate vector defined at c
r_i	Rate of reaction of species i [mol.s^{-1}.kg-cat^{-1}]
ΔS	Change in entropy
t	time
T	Temperature of reaction [K]
T_{ad}	Adiabatic temperature gradient
T_m	Mixing material temperature [K]
T_o	Feed temperature [K]
τ	Residence time
u	A time measurable scalar control
v	Mixing vector, mixing c with c^*
V_{min}	Lower bound of the constrained variable V
V_{max}	Upper bound of the constrained variable V
x	Some time dependent vector equation
x_0	Initial state of the vector equation, at $t = 0$
$\dot{x}$	Some differential of a time dependent vector equation x
X	Conversion of the limiting reagent

CHAPTER 8

SOLVING UNSTEADY STATE PROBLEMS

8.1 Introduction

In the previous chapters we have demonstrated how the convex control policy technique can be applied to identify solutions for conventional steady state AR problems. The solution to these problems were all characterised by the necessary conditions of the AR boundary such that

- *All variables used to characterise the AR boundary should obey linear mixing*
- *The AR boundary is always convex*

In this chapter we apply the RCC technique to solve unsteady state optimisation problems that are not essentially characterised by the necessary conditions of the AR boundary stated above. We focus on the Differential Algebraic Optimisation Problems (DAOP) that have previously been solved using computational optimisation algorithms (Jackson and Senior 1968; Lim *et al.* 1986; Modak *et al.* 1986; Cuthrell and Biegler 1989). These solution methods are known to be problem specific and numerically intense.

8.2 Background Literature

The set of problems this study focuses on, generally comprise of a number of DAE that describe a given system, similar to the generic time optimal control problem given by equation (7.1) in chapter 7. The aim is, in most cases to optimise the objective function described in a performance index equation by varying the control policy, *U(t)*. The final time at which the objective is optimised can, depending on a problem, be specified or open ended. An example of these DAOP's that is commonly encountered in chemical engineering is the feed profile optimisation problem. Feed profile optimisation problems involve finding optimal feed profiles that maximise the production of a product via some reaction. These problems are, in many cases, batch reactors with slow rates of production and/or low yield of high valued product. This class of problems known as the fed-batch reactor problem uses the controlled feed over time as a control policy to maximise the product yield at final time.

Over the past years, a number of publications appeared in the literature that proposes numerical techniques that can be applied to identify optimal feed profiles of fed-batch reactors. Jackson and Senior (1968) used Pontryagin's Maximum Principle (Pontryagin *et al.*, 1962) to derive an optimum reactant addition policy for a batch reactor with delayed reactant addition. Using theoretical mass action kinetics as a study case, the authors identified singular and bang-bang segments that form an optimum control policy profile. The difficulty in their methods was in finding bounds for the singular segments. San and Stephanopoulos (1981) identified an optimal feed addition policy for substrate inhibited kinetics with enzyme deactivation. The optimum feed addition policy was approximated using a quasi-steady state solution. Hong (1986) derived analytical solutions for the fed-batch fermentation reactor. The control

profile comprised of mixed singular and non-singular (bang-bang) arcs. The conjunction points between control arcs were determined using Kelley's transformation theory (Kelly *et al.*, 1967).

Modak *et al.* (1986) studied the general characteristics of optimal feed profiles for various fed-batch fermentation processes. The authors deduced that for fed batch processes, the most general optimal control sequence comprises; an interval of maximum feed rate segment, an interval of minimum feed rate segment (batch period), an interval of singular feed rate segment, and an interval of minimum feed rate segment (batch). Depending on the optimisation objective, Modak *et al.* (1986) proposed two control modes. If maximisation of the product yield is critical and the fermentation time not the key issue, the singular control can be utilised to achieve maximum net yields. Only when the fermentation time becomes important that the trade-offs between fermentation duration and product yield are balanced by a sequence of singular, maximum feed and minimum feed control segments.

Lim *et al.* (1986) derived somewhat generalised computational methods based upon the general characteristics proposed by Modak *et al.* (1986). These methods were illustrated using the penicillin fermentation and bacterial cell mass case studies. The authors placed emphasis on the fact that once the sequencing of segments of an optimal control is known, the determination of an optimal feed rate profile gets reduced to a problem of identifying switching times between segments.

Cuthrell and Biegler (1989) developed a simultaneous optimization and solution method based on successive quadratic programming and orthogonal collocation on finite elements. Their method showed improved solution accuracy and stability when illustrated by solving the penicillin

fermentation problem studied by Modak *et al.,* (1986).

This work proposes the use of the recursive convex control policy (RCC) formulations to approximate the solution of a fed-batch reactor problem. This solution is approximated by satisfying only the necessary of convexity as required by the Hamiltonian equation (Chapter 7, Pontryagin, 1962).

8.3 Optimal Substrate Feeding Policy for a Fed-Batch Fermentation Process

For a case study, we will consider a problem of finding an optimal time-varying control strategy for a fed-batch reactor involving the biosynthesis of penicillin as studied in a series of publications by Modak *et al.* (1986), Lim et al. (1986) and Cuthrell and Biegler (1989). We start by stating the problem and outlining some of its features. The RCC technique will then be applied to identify an optimal control strategy of the problem. We will provide an analytical based solution for a specific case study (Lim *et al.* 1986) and apply the convex control policy formulations to compute the numerical solution. This will permit comparison of the solution with previous results.

8.3.1 The Fed-Batch Fermenter Problem

The kinetic model and associated parameters for the Batch Fermenter Problem (BFP) were taken from Lim *et al.* (1986) and Cuthrell and Biegler (1989). The fermenter of hold-up volume (V in l) is considered to contain biomass (X), substrate (S) and product (P) at concentrations given in (g/l). The mass of product, M_P at time, t can be related to the reactor hold-up

volume and product penicillin concentration as;

$$M_P(t) = P(t) \cdot V(t) \tag{8.1}$$

The objective is to maximize the mass of product penicillin at final time (t_f) by manipulating the control policy (U in *g/hr*), which is the substrate feed rate. The set of differential algebraic equations describing the mass balance of species over time can be stated as follows.

The rate of change of the biomass concentration in the reactor is related to the biomass growth rate, $\mu(X, S)$ and the dilution factor due to substrate feed addition as;

$$\frac{dX}{dt} = \mu(X,S)X - \left(\frac{X}{S_F V}\right)U$$

(8.2)

The rate of change of penicillin concentration in the reactor is given by the net effect of production rate $\rho(S)$, degradation rate due to hydrolysis K_{degr} and dilution rate due to substrate addition as;

$$\frac{dP}{dt} = \rho(S)X - K_{\deg r}P - \left(\frac{P}{S_F V}\right)U \tag{8.3}$$

The concentration of substrate in the reactor is governed by the differential equation relating biomass growth rate, penicillin production and dilution rate as;

$$\frac{dS}{dt} = -\mu(X,S)\left(\frac{X}{Y_{X/S}}\right) - \rho(S)\left(\frac{X}{Y_{P/S}}\right) - \left(\frac{m_s S}{K_m + S}\right)X + \left(1 - \frac{S}{S_F}\right)\frac{U}{V} \quad (8.4)$$

The rate of change of hold-up volume is related to substrate addition as follows;

$$\frac{dV}{dt} = \frac{U}{S_F}$$

(8.5)

The biomass growth rate (h^{-1}) is defined by

$$\mu(X, S) = \mu_{max}\left(\frac{S}{K_X X + S}\right) \tag{8.6}$$

The penicillin production rate ($g\text{-}P/(g\text{-}X\,h)$) is given by

$$\rho(S) = \rho_{max}\left(\frac{S}{K_P + S(1 + S/K_{in})}\right)$$

$$\tag{8.7}$$

Lim *et al.*, (1986) detailed the rate constants, initial conditions and substrate concentration for this case study as listed below;

μ_{max} = 0.11 h-1 ρ_{max} = 0.0055 g-P/(g-X h) K_X = 0.006 g-S/(g-X)

K_P = 0.0001 g-S/l K_{in} = 0.1 g-S/l   Kdegr = 0.01 h-1

K_m = 0.0001 g-S/l m_s= 0.029 g-S/(g-X h) $Y_{X/S}$ = 0.47 g-X/g-s

$Y_{P/S}$ = 1.2 g-X/g-s S_F=500 g-S/l

$$\tag{8.8}$$

This type of problem is a numerically complex DAOP because of the bounds on the state and control profile as well as the linear appearance of the control policy in the state equations and objective function. For problems with linear response to the control, the optimal control profile is either bang-bang in nature or contains singular control arcs (Chapter 7).

8.3.2 Numerical Solutions for the BFP

The RCC algorithm was applied to the problem to obtain the numerical approximation of the solution. In this case an optimal time-varying feed profile that optimises the product yield at an unspecified final time, t_f is solved. This requires that the optimal feed rate to yield the maximum amount of product at the end of the batch period must be determined. The product yield can be calculated using,

$$M_P(t) = P(t) \cdot V(t) \qquad\qquad (8.1)$$

The objective function in this case can be expressed as

$$\max_{u(t), t_f} \Phi = P(t_f) \times V(t_f) \qquad\qquad (8.9)$$

The problem is solved for the maximum amount of product at an unspecified final time, t_f given initial conditions as

$$X(0) = 1.5 \ g/l \ ; \qquad P(0) = \ 0.0 \ g/l;$$

$$S(0) = 0.0 \ g/l; \qquad V(0) = 7 \ l \qquad\qquad (8.10)$$

and boundary conditions

$$0 \le X(t) \le 40 \ g/l \qquad 0 \le S(t) \le 100 \ g/l \qquad 0 \le V(t) \le 10 \ l$$
$$0 \le U(t) \le 50 \ g\text{-}S/h \qquad 72 \le t_f \le 200 \ h,$$

$$(8.11)$$

The RCC formulation for computing the optimal control sequence for a fed-batch penicillin reactor is written as follows;

u = [u$_{min}$…u$_{max}$] discretised over five hundred points

Maximise, for all u$_i$'s

$$\Phi_i = P(t) \times V(t)$$

subject to differential equations set (8.2) to (8.5)

*initial conditions (8.10) and boundary conditions (8.11)*

The problem was first solved for the analytically-based control profile as presented by Lim *et al.* (1986). The authors stated that the analytical computations of the optimal feed profile comprises sequentially, a 11.21 *hr* (t_1) period of maximum flow rate (100 *g/hr*), a batch period of 17.58 *hr* (t_2 = 28.79) and a singular flow rate period of 95.11 hr (t_3 = 124.9).

8.3.3 Results

The convex control policy formulation was implemented to solve the problem using MATLAB®. The tenth iteration solution profiles are obtained and presented together with the analytical solutions in Figures 8.1 – Figures 8.5.

The values for points of control profile discontinuity, final time and optimal time value of the objective functions agree closely with the analytical computations. Figure 8.1 shows that the control policy *U*, remains fixed at the upper bound for the first time segment. In the second segment the control policy switches to zero indicating full batch with no feed. The third segment is a singular profile showing a linear dependence of the control policy on time.
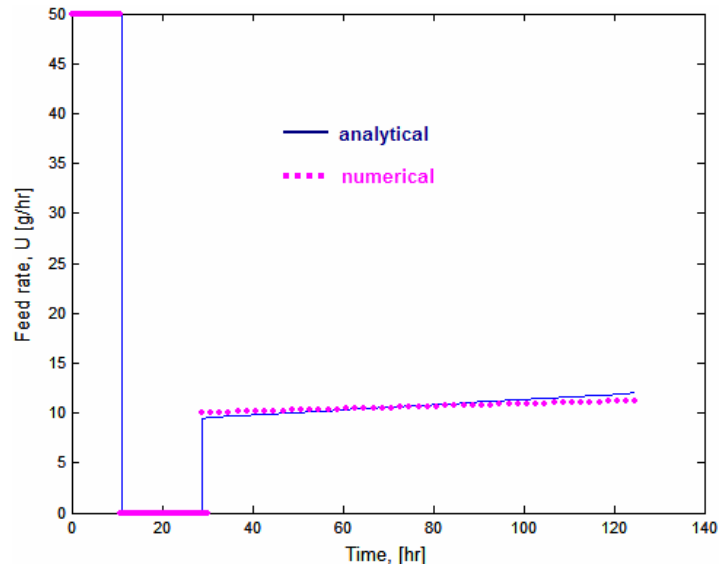
Figure 8.1: Analytically-Based and Numerically Solved Control Profile

The singular arc approximation accuracy improves as the number of iteration increases. However, as for most singular control problems, more and more iterations are needed as the computation gets closer to the solution and therefore achieving the exact profile becomes impractical.
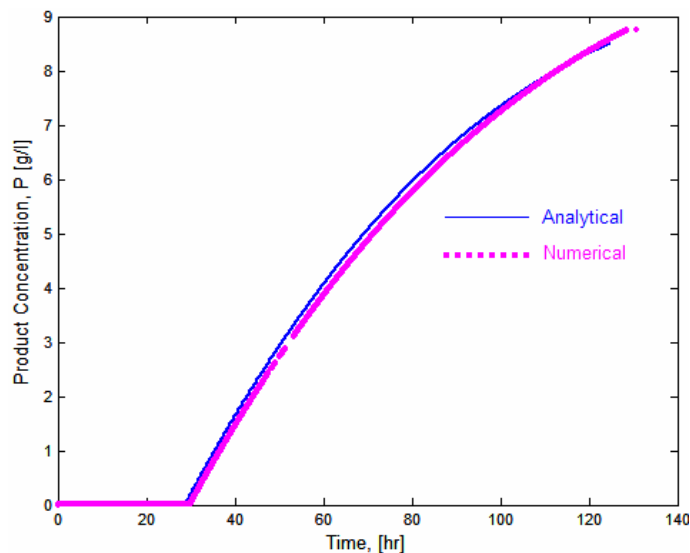
Figure 8.2: Product Concentration Profiles

Figure 8.2 shows how the penicillin production changes with time. In the first time segments of the problem control, the production rate of

penicillin remains passive and starts to increase in the third time segment. The initial delay in production awaits the biomass build-up to a threshold level at which penicillin production becomes active as shown in figure 8.3.

The inaccuracies in the approximation of optimal control profile along the singular segment are more visible in Figure 8.2 and 8.3.
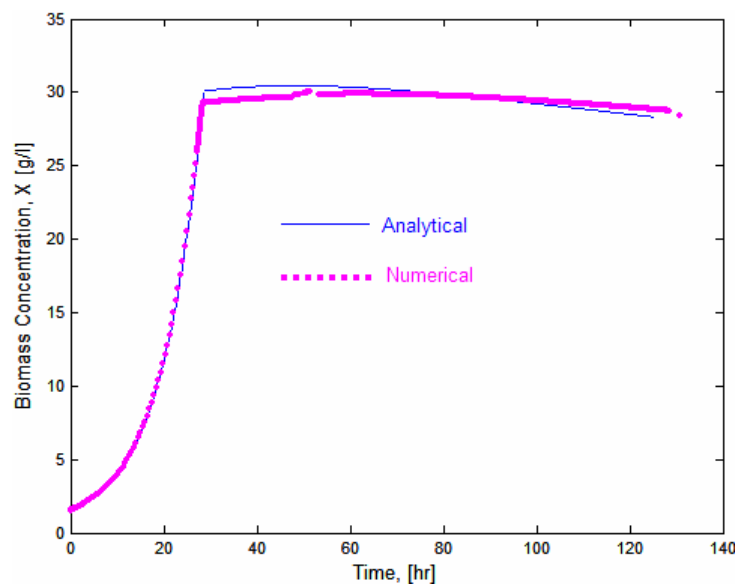
Figure 8.3: Biomass Concentration Profiles
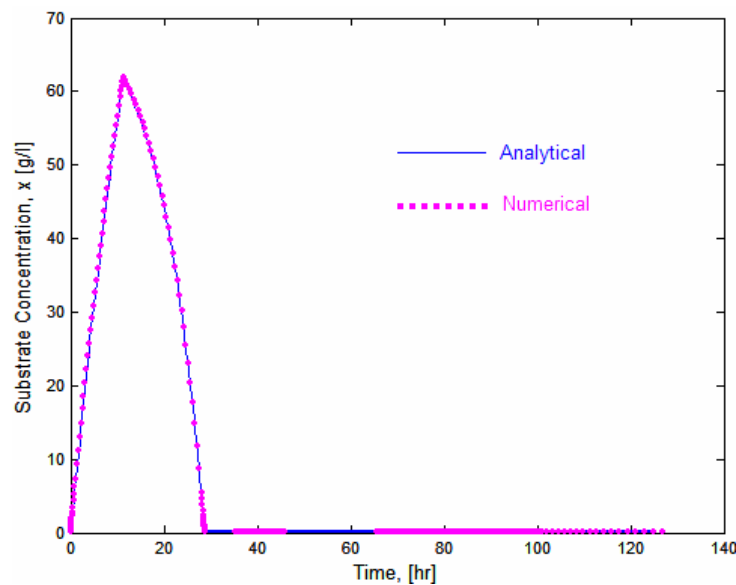
Figure 8.4: Substrate Concentration Profiles

Figure 8.4 shows how the substrate concentration increases in the reactor due to the controlled addition.
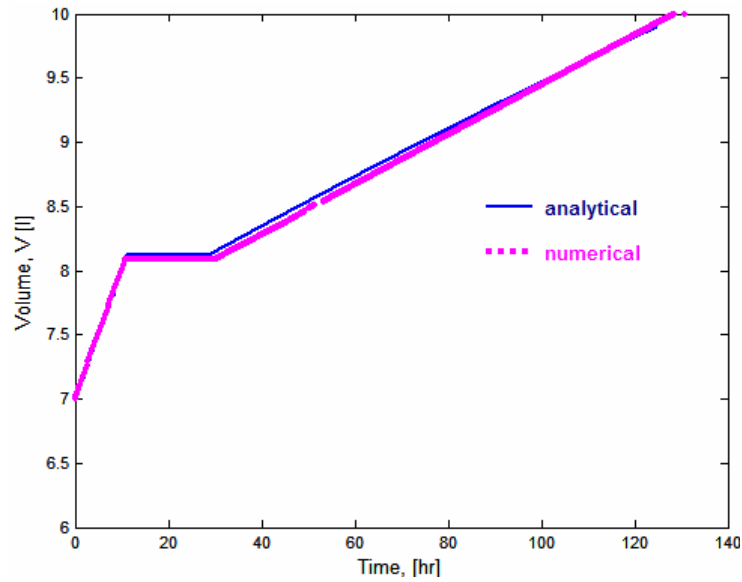
Figure 8.5: Reactor Contents Volume Profiles

The change in the volume hold-up depends only on the substrate addition as Figure 8.5 shows. During the full batch segment the hold-up volume remains unchanged and only increases during substrate feed addition.

8.4   Discussion and Conclusion

We have shown how the convex control policy algorithm can be used to solve problems that are not conventional attainable regions problems. Although we have not emphasised the computational aspects of the case study, such as computational time comparison we have demonstrated that by simply including the objective function and problem bounds, the algorithm can be transformed into an optimisation tool. The example used in the study was solved in an easy plug and play fashion without complex mathematics in the preparation.

It should be emphasised that the RCC algorithm does not satisfy any of the conditions of optimality as it assures only the requirements for convexity. The solution obtained herein will therefore only serve as an approximation as neither the maximum principle nor the Legendre-Clebcsh condition could be affirmed (Aly, 1978). However, the application of this technique as a simple optimal control sequence calculator should be acknowledged. As it was shown in chapter 3, the results of the computation closely approximate the conditions of optimality as the number of iterations in the computation is increased.

8.5 References

Aly, G. M., (1978), The computation of optimal singular control, *Int. J. Control*, **28** (5), pp. 681-688

Cuthrell, J. E., Biegler T. T., (1989), Simultaneous Optimisation and Solution Methods for Batch Reactor Control Profiles, *Comp. Chem. Eng*. **13** (1/2), pp. 49-62

Hong, J., (1986), Optimal Substrate Feeding Policy for a Fed Batch Fermentation with Substrate and Product Inhibition Kinetics, *Biotechnol. Bioeng.*, **28**, pp. 1421-1431

Jackson, R., and Senior M. G., (1968), The optimization of chemical reactors by the delayed addition of reactant, *J. Opt. Theor. Appl.*, **2** (1), pp. 27-39

Kelley, H. J., Kopp, R. E., Moyer, H. G., (1967), *Topics in Optimization*, Edited by Leitmann, Academic Press, New York, USA

Lim H. C., Tayeb, J. M., Modak J. M., Bonte, P., (1986), Computational Algorithms for Optimal Feed Rates for a Class of Fed-Batch Fermentation: Numerical Results for Penicillin and Cell Mass Production, *Biotechnol. Bioeng.*, **28**, pp. 1408-1420

Modak J. M., Lim H. C., Tayeb, J. M., (1986), General Characteristics of Optimal Feed Rate Profiles for Various Fed-Batch Fermentation Processes, *Biotechnol. Bioeng.*, **28**, pp. 1396-1407

Pontryagin, L .S., Boltyanskii, V. G., Gamkrelidze, R. V., and Mishchenko, E. F., (1962), *The Mathematical Theory of Optimal Processes*, John Wiley, New York, USA.

San, K. Y., and Stephanopoulos, G., (1983), Optimal Control Policy for Substrate Inhibited Kinetics with Enzyme Deactivation in an Isothermal CSTR, *AIChE J.*, **29**, pp. 417-424

8.6 List of Symbols

Abbreviations

AR	Attainable Regions
BFP	Batch Fomenter Problem
DAE	Differential Algebraic Equations
DAOP	Differential Algebraic Optimisation Problem
RCC	Recursive Constant Control Policy

Symbols

K_{degr}	Penicillin hydrolysis rate constant
K_{in}	Substrate inhibition rate constant
K_m	Substrate- Biomass inhibition rate constant
K_P	Substrate- Product inhibition rate constant
m_s	Biomass -Substrate inhibition rate constant
μ	Biomass growth rate (h^{-1})
P	Product penicillin concentration (g/l)
Φ	Objective function
ρ	Penicillin production rate (g-P (g-X $h)^{-1}$)
S	Substrate concentration (g/l)
S_F	Substrate concentration in feed (g/l)
t	time (hr)
t_f	Final time (hr)
U	Control policy, Substrate feed rate (g/h)
V	Reactor hold-up volume (l)
$Y_{P/S}$	Penicillin mass to substrate yield (g- Penicillin /g-Substrate)
$Y_{X/S}$	Biomass mass to substrate yield (g-Biomass/g-Substrate)

CHAPTER 9

CONCLUSIONS

The aim of the thesis was to contribute to the development of systematic attainable region analysis tools that are based on numerical formulations. These systematic tools would be implemented as computer algorithmic techniques to automate the procedure of reactor network synthesis using attainable region analysis.

The theory has been revised to illustrate the power of attainable regions as a process synthesis method. By use of a simple case study, a demonstration was carried out to show how analytical techniques of AR analysis can be applied to synthesise optimal reactor networks. The boundary of the candidate attainable region was interpreted in terms fundamental processes and/or combinations of fundamental processes which were in turn translated into process equipment network with flow configurations and design parameters. Although the procedure was straightforward, it required strong background knowledge in the theory of AR analysis. Also the studied simple theoretical example with ideal kinetic model resolved into an exhaustive algebraic exercise of deriving equations of optimal fundamental processes as required by the necessary conditions of attainable regions theory.

From the theory it was indicated that the boundary of the attainable regions, which is of the highest importance in generating candidate ARs, is outlined by optimal combinations of fundamental processes. These optimal process combination trajectories give pathway to extreme surfaces

of single process operation that shape the AR boundary, such as mixing planes and reaction surfaces. The algebraic complexity of attainable regions lies in identifying these optimal process combination trajectories from analytical methods.

A new systematic formulation for attainable regions called the recursive convex control policy has been developed to ease the complexity surrounding the application of AR analysis as a process synthesis technique. The recursive convex control policy applies iterative convex combinations of fundamental processes to approximate optimal combinations of fundamental processes that outline and provide access to extreme surfaces that complete the AR boundary. The RCC technique does not apply the necessary conditions in its method, and therefore does not limit the achieved solutions to the known necessary conditions.

A theoretical case study that has previously been studied using analytical methods was solved to demonstrate how the RCC formulations can be implemented as an algorithmic tool to simplify the procedure of identifying AR^{C}s. The RCC formulation proved to be clear cut in application as it required no specialised knowledge in the theory of AR analysis. The results were successfully verified to be consistent with the necessary conditions of optimality. The RCC technique proved to be the quickest automated AR technique known to date as it exhibited computational run-times in the order of 1/10th of previously known techniques.

A four-dimensional case study was studied to demonstrate the straightforward advancement of the RCC technique to solving multidimensional problems. The obtained results conformed to the necessary conditions derived from AR analysis theory. This demonstration

proved the RCC algorithm to be a breakthrough in the AR theory. Prior to this research work, higher dimensional implementation of AR analysis could only be speculated on due to the intricacy arising from the use of analytical methods. The previously developed systematic techniques fell short in attempting solution of multi-dimensional problems due to long computational runtimes.

The RCC technique is formulated from the necessary requirement for convexity and therefore is not pre-programmed to satisfy other necessary conditions of optimality. However, this is in no way a limitation as it was shown that by increasing the number of iterations the results converged to the optimal solution that satisfied all known necessary conditions. This remedial action was proven successful for both three and four-dimensional case studies considering only fundamental processes of reaction and mixing.

The ease of incorporating the attainable regions into process synthesis software packages was illustrated by assembling the RCC algorithm into a fully user-interfaced computer application. The application used a built-in theoretical example that allows the user to change reaction parameters and identify candidate ARs at a click of a button. The package displays a graphical output of the AR^C which can be manipulated by the user. Any point on the boundary of the AR^C can be translated into an optimal process flowsheet with flow configurations and key design parameters by a simple click with a mouse cursor. The easy interpretation of the boundary into process unit networks is facilitated by data tracking capability of the RCC algorithm. This is by far the most advanced and easy to use implementation of an automated AR^C technique to identify optimal reactor networks to enable use by non-specialists. This could have not been practical with the previously developed slow systematic techniques.

To consider more fundamental processes, a number of industrial type examples were demonstrated. The study used exothermic reversible reactions which over the years have been a challenge to process synthesis engineers due to their divergent need for high temperatures to promote fast kinetics and low temperatures to achieve high equilibrium conversions. The RCC algorithm was successfully applied to identify an optimal reactor configuration for a generic exothermic reversible system where the costs of cooling and reaction were compared. Numerous cases were considered where the two costs were contrasted and trends were identified. The results obtained were proven consistent with those obtained using analytical methods. In this study the RCC algorithm was used to handle systems with fundamental processes of reaction, mixing and cooling. A much more practical case study of ammonia synthesis was also studied to identify its optimal reactor networks.

The efficiency of the RCC algorithm was further demonstrated with a detailed study of a more complex methanol synthesis system. The reaction scheme of methanol synthesis comprises of three chemical reactions that exhibit a mixed endothermic-exothermic nature. The analytical methods cannot be used to solve this example as they require the case to be either fully exothermic or endothermic. With the aid of rate contour study, postulates were derived from which expectations on the behaviour of the optimal reactor network for this system were drawn. The reaction scheme was found to be endothermic at high temperatures and exothermic at low temperatures, an aspect that was identified to make the optimal reactor structure even more complex.

The RCC algorithm was applied to identify an optimal reactor network for methanol synthesis using attainable region analysis. Although the resulting reactor network was complex, the method of solution was easy

plug and play in nature. The interpretation of the AR boundary into process unit network was also straightforward due to the inherent data tracking capability of the RCC algorithm. In this case study the RCC algorithm was applied to handle a system considering fundamental processes of reaction, mixing, cooling and heating.

Another systematic technique to identify AR^Cs using singular optimal control tools was developed. As the RCC algorithm, the method relied on identifying the optimal combinations of processes that outline the AR boundary. The extreme surfaces and planes that shape the boundary of the attainable region originate from these optimal combinations of processes. In this technique the optimal combinations of processes are formulated and solved as singular optimal control problems. Singular optimal control solution methods apply Pontryagin's maximum principle to solve for optimal control of combinations of processes. This technique will therefore also serve as a check to guarantee that the attainable region analysis method is consistent with the maximum principle. The water-gas shift system was used to demonstrate the use of optimisation techniques in identifying candidate attainable regions. The obtained AR^C for the water-gas shift system was found to be consistent with that identified using RCC algorithm.

The application of the RCC algorithm was extended to solving unsteady state optimisation problems. The case study used in this demonstration was the fed batch penicillin fermentation reactor. Optimisation methods based on Pontryagin's maximum principle have previously been used to find the control sequence of the fed batch reactor problems. These methods require specialised optimisation knowledge and are known to be problem specific notwithstanding the fact that they are efficient and the most accurate. The RCC algorithm was shown to be very easy to apply in

approximating a control sequence for the fed penicillin fermentation reactor. Although the solution is known to satisfy the requirement for convexity only, the method proved to be efficient as a pre-calculator for the control sequence. The control profile identified using the RCC technique was not highly accurate; it however, showed a clear control sequence. This can be use to simplify the procedure of solving control sequences of fed batch reactor as it is known that, once the control sequence is known the optimisation problem reduces to a simple task of finding the switching times.

The two numerical methods have been successfully developed and demonstrated with the use a number of case studies. The main objective focused on the RCC algorithm as the core content of the thesis. A number of case studies that were solved using the RCC algorithm have proved the technique to be robust, reliable and consistent.

A future research area has been identified in which the RCC algorithm is coupled with other numerical techniques to compile a more powerful tool that will accurately identify candidate attainable regions boundaries. Currently, research is ongoing to incorporate the RCC algorithm with the Method of Bounding Hyperplanes to produce a tool that will guarantee quick and more accurate results by constructing the attainable regions from both the exterior and interior. In order to improve the stability and accuracy of the RCC algorithm, investigation of application of regularization methods to handle ill-conditioned problems is underway as the complete software package is being assembled.

In addition, a post doctoral research that investigates the application of the RCC algorithm to solving distillation synthesis problems has already been started and the preliminary stages show promising results. The success of

this implementation could lead to a powerful tool that can be used to solve reactive distillation problems.

In conclusion, we claim that the contribution of the RCC algorithm as the core content of the study and the number of case studies demonstrated as well as the singular optimal control technique developed, are a significant contribution to the development of numerical formulations for attainable region analysis. The title of this thesis promises the development of such formulations. This contribution is not only to the development of attainable region analysis as a process synthesis technique. The RCC algorithm does also contribute to the field of dynamic optimisation as it has been demonstrated to be applicable to the field of unsteady state optimisation.

The numerical formulations developed in this study will enable the inclusion of attainable region analysis in chemical process simulation and optimisation tools. This will help in the synthesising of new optimal chemical process and optimisation of existing ones and therefore be an invaluable tool to the filed of process synthesis and chemical engineering as a whole. This contribution gives easy access to the power of the attainable region analysis to the chemical engineering community without the need for specialised knowledge to help studying chemical processes of industrial significance. It can therefore be anticipated that this contribution will be important to chemical engineering research and industry for many years to come.

CHAPTER 10

PUBLICATIONS

Seodigeng T., Hausberger B., Hildebrandt D., Glasser D.,(2005), RCC Algorithm for Attainable Region Analysis: Addressing Four-dimensional Problems, *Comp. & Chem. Eng.*, Submitted for publication

Seodigeng T., Kauchali, S., Hausberger, B., Hildebrandt, D., (2004), A Comparison of Automated Techniques in Determining Candidate Attainable Regions: Water Gas Shift Case Study, *Escape 14*, Lisbon, Portugal

Seodigeng T., Hausberger B., Hildebrandt D., Glasser D.,(2003), DSR Algorithm for attainable regions analysis: Higher Dimensional Problems, *SAIChe Congress 2003*, Sun City, South Africa, Paper 2A-5.

Seodigeng T., Hausberger B., Hildebrandt D., Glasser D., Kauchali S., (2004), DSR Algorithm for Construction of Attainable Region Structures, *PSE 2003*, Kunming, China, Paper 396.

Seodigeng T., Hausberger B., Hildebrandt D., Glasser D., (2005), Attainable Regions for Methanol Synthesis, To be submitted for publication